Thermal-Mechanical Response To An Intruding Magma Chamber

A thesis presented to the Faculty

of the State University of New York

at Albany

in partial fulfillment of the requirements

for the degree of

Master of Science

Department of Geological Sciences

Christoph Arz

1992

Thermal-Mechanical Response To An Intruding Magma Chamber

Abstract of

a thesis presented to the Faculty

of the State University of New York

at Albany

in partial fulfillment of the requirements

for the degree of

Master of Science

Department of Geological Sciences

Christoph Arz

1992

Abstract

The thermal-mechanical response of rock at shallow to medium depth beneath the earth's surface has been modeled as a magma body ascends toward it. The overall stress field is calculated by considering the country rock as a viscous fluid, a thermal-elastic material, or as an elasto-plastic material that fractures when its strength is overcome.

The stress field within and around a spherical magma body surrounded by a homogeneous, Newtonian fluid has been evaluated and can be used at deeper levels in the earth's crust where the viscosity of the country rock is relatively low. With decreasing depth wall rock material becomes more viscous which results in diminishing stress magnitudes. In a highly viscous material shear stress and tangential stress have negligible magnitudes. They become more important by considering a spherical magma chamber rising within a bigger spherical container.

In the thermal-elastic model the current pressure inside the magma body and the stress field within the host rock are determined. A pressure increase of the magma chamber is induced by crystallization of anhydrous minerals associated with exsolution of an aqueous phase. This results in magma chamber expansion and pressure increase since the elastic deformability is limited.

Thermal stress due to heating of country rock material is the most important stress component and is sufficient to fracture brittle country rock. The temperature distribution within the wall rock has a fundamental influence on the fracturing process and its associated stress field. Four regions in the elasto-plastic host rock can be distinguished. From the magma outward, they are: (1) a cataclastic region with shear fractures more or less parallel to the chamber's margin, (2) a thermal-elastic zone with preexisting fractures, (3) a fractured region containing shear fractures with high angles to the interface between magma and host rock, and (4) an almost intact elastic outer region. The fluid pressure of a porous host rock enhances the fracturing process, but the fluid pressure of the magma hinders the development of the cataclastic region. Ascent of a magma body surrounded by a fractured material can occur by stoping, in which disengaged wall rock fragments sink in less dense magma.

State University of New York at Albany

College of Sciences and Mathematics

Department of Geological Sciences

The thesis for the master's degree submitted by

Christoph Arz

under the title

Thermal-Mechanical Response To An Intruding Magma Chamber

has been read by the undersigned. It is hereby recommended

for acceptance by the Faculty with credit to the amount of

six semester houres.

Dr. Brian M. Bayly Brian Bayly 4 Aug 1992

Dr. Winthrop D. Means W.D. Means Aug. 4 '92

Dr. John W. Delano John W. Delano 5 Aug. 1992

Recommendation accepted by the Dean of Graduate Studies for

the Graduate Academic Council.

_____

Acknowledgements

I would like to take this opportunity to show my appreciation to those individual who enabled me to complete my research on magma chamber processes.

I wish to thank my Graduate Committee, Drs. Winthrop Means, John Delano, and particularly Dr. Brian Bayly, for their guidance throughout my thesis research.

I am very appreciative for the help and knowledge received from the faculty of the Department of Geological Sciences of the State University of New York at Albany.

I should not forget the support I received from the graduate students; especially Rolf Herrmann, Susi Vogel, Young-do Park, Andreas Plesch, Ben Hanson, Volker Brüchert, and Chris Achong. Without them, Albany would have been a cold place to live and study at.

Final preparation of this thesis is due to a large part from Diana Paton who allowed me to establish a sense of order from the chaos created while writing this thesis.

But above all I must give thanks to my family, Mr. and Mrs. Alfred Arz, my brother Dominik, and Elke Wilharm whose belief in me enabled me to realize that if the dreams are indeed big enough, then the facts will not matter.

Finally, I must thank God for granting me the strength, knowledge, and wisdom for making my dream a reality.

Research was financially supported by a Teaching Assistantship from the State University of New York at Albany, the Exchange Program between the Bayerische Julius Maximilians Universität Würzburg and the State University of New York at Albany, and the Fulbright-Commission.

Table of Contents

List of Figures

List of Tables

Nomenclature

A	area of vertical walls of magma chamber (cylinder)	[m^2]
A_η	constant	[Pa s]
a	average grain radius	[m]
b	bulk modulus of magma	[Pa]
C	Carman constant	[m^{-1}]
C_o	uniaxial compressive strength	[Pa]
C_p	heat capacity	[J kg^{-1} K^{-1}]
C_1, C_2	constants	
c	concentration	[mol m^{-3}]
D	diffusion coefficient	[m^2 s^{-1}]
E	Young's modulus	[Pa]
E_a	activation energy	[J mol]
erf (x)	error function	
f	crystallization rate	[s^{-1}]
g	acceleration of gravity	[m s^{-2}]
H	magma chamber height	[m]
I_{max}	mush crystal nucleation rate	[m^{-3} s^{-1}]
j	mass flux	[kg m^{-2} s^{-1}]
J	mass accumulation rate	[kg s^{-1}]
K	permeability	
K_a	wall correction factor	
K_o	distribution coefficient	
K_R	constant	
k	thermal conductivity	[$Jm^{-1}s^{-1}K^{-1}$]
Le	Lewis number, κ / D	
M	mass of magma	[kg]
m	molar mass of water	[kg mol^{-1}]
N	mass of volatiles	[kg]
n	relative abundance of species; constant; mass fraction of exsolved water	
p	pressure	[Pa]
p_i	pressure inside magma chamber	[Pa]
p_o	pressure outside magma chamber	[Pa]
q	heat flux	[J m^{-2} s^{-1}]
R	universal gas constant	[J mol^{-1} K^{-1}]

Ra	Rayleigh number, $g\alpha_T\Delta TH^3 / \kappa\nu$	
R_b	radius of deformation layer	[m]
R_c	radius of boundary between fractured and not fractured zone	[m]
R_i	radius of magma chamber	[m]
$R\nu$	buoyancy ratio, $k\alpha_c j_w / \rho D\alpha_T q_w$	
Rq	flux thermal Rayleigh number, $g\alpha_T q_w H^4 / k\kappa\nu$	
$R\rho$	buoyancy ratio, $\alpha_c \Delta W / \alpha_T \Delta T$	
r,θ,ϕ	spherical coordinates	
S	fractional amount of magma chamber expansion	
S_o	shear strength	[Pa]
T_c	contact temperature at interface magma - host rock	[K]
T_h	initial temperature of host rock, ambient temperature	[K]
T_i	temperature of magma	[K]
T_m	initial temperature of magma	[K]
T_o	temperature of host rock	[K]
T_s	temperature of earth's surface	[K]
T^*_{Ro}	$\int_{Ri}^{r} Ro(\Delta T) r^2 \, dr$	
t	time	[s]
t_c	contamination time, equation 2-1.2.11	[s]
t_s	solidification time, equation 2-1.2.10	[s]
U	ascent velocity	[m s^{-1}]
u,v,w	orthogonal velocity components	[m s^{-1}]
u_r,v_θ,w_ϕ	spherical velocity components	[m s^{-1}]
u	radial displacement	[m]
V	volume ratio, V_{mi} / V_{li}	[m^3 s^{-1}]
V'	molar volume of water	[m^3 mol^{-1}]
V_a	activation volume	[m^3]
V_c	volume of expanded magma chamber	[m^3]
V_{ci}	initial volume of magma chamber	[m^3]
V_g	volume of exsolved gas	[m^3]
V_l	volume of supersaturated magma	[m^3]
V_{li}	initial volume of supersaturated magma	[m^3]
V_m	volume of undersaturated magma	[m^3]
V_{mi}	initial volume of undersaturated magma	[m^3]

W	mass fraction	
W_s	mass fraction of water in supersaturated magma	
x,y,z	orthogonal coordinates	
Y	yield strength	[Pa]
Y_{max}	mush crystal growth rate	[m s^{-1}]
z_{ini}	initial depth of diapir	[m]

Greek Symbols

α_c	chemical expansivity	
α_T	thermal expansivity	[K^{-1}]
β	$(1 + \sin \phi)/(1 - \sin \phi)$	
Δh_f	latent heat of crystallization	[J kg^{-1}]
Δp	overpressure in magma chamber	[Pa]
ΔT	temperature difference	[K]
ΔW	mass fraction difference across the chemical boundary layer	
$\Delta \rho$	density difference	[kg m^{-3}]
$\delta(t)$	boundary layer thickness as function of time	[m]
δ_c	chemical boundary layer thickness	[m]
δ_T	thermal boundary layer thickness	[m]
$\partial T_o/\partial z$	geothermal gradient	[K m^{-1}]
η	viscosity	[Pa s]
η_{eff}	viscosity ratio η_h/η_m	
η_h	viscosity of host rock	[Pa s]
η_m	magma viscosity	[Pa s]
ϑ	velocity of isotherms	[m s^{-1}]
κ	thermal diffusivity	[m^2 s^{-1}]
λ	ratio: R_i/R_o	
ν	Poisson's ratio	
ν_k	kinematic viscosity	[m^2 s^{-1}]
Φ	volume fraction	
Φ_f	fraction of fluid pressure	
ϕ	angle of internal friction of fractured rock	[°]
ϕ_i	angle of internal friction of intact rock	[°]
φ	porosity	
ρ	density	[kg m^{-3}]

ρ_h	density of host rock	[kg m^{-3}]
ρ_l	density of undersaturated magma	[kg m^{-3}]
ρ_{li}	density of initial undersaturated magma	[kg m^{-3}]
ρ_m	density of magma	[kg m^{-3}]
ρ_o	reference density	[kg m^{-3}]
σ	stress	[Pa]
$\sigma^{(i)}$	stress inside the magma chamber	[Pa]
$\sigma^{(o)}$	stress outside the magma chamber	[Pa]
$\sigma^{(tot)}$	overall stress	[Pa]
σ_{mean}	mean stress	[Pa]
σ_{rr}	radial normal stress	[Pa]
$\sigma_s^{(max)}$	maximum shear stress	[Pa]
$\sigma_s, \sigma_{r\theta}$	shear stress	[Pa]
$\sigma_{\theta\theta}$	tangential normal stress	[Pa]
σ_1	maximum principal stress	[Pa]
σ_3	minimum principal stress	[Pa]
T_o	tensile strength	[Pa]
τ	ratio of solidification and contamination times, equation 2-1.2.12	
υ	velocity ratio, U / ϑ	
ψ	stream function	

Subscripts and Superscripts

'	thermal-elastic zone
"	fractured zone
*	includes latent heat
bub	vapor bubble
c	chemical
h	host rock
i	inside magma chamber
m	magma
o	outside magma chamber
T	thermal
v	vapor
w	value at the magma chamber-country rock contact

Chapter I Introduction

1.1 Crustal Magmatic Ascent

It is well known that magma ascends buoyantly under the action of gravity. But in which manner it actually moves is still a mystery. This is mainly because of the complicated nature of the earth. At shallow depth crustal material is brittle and can fracture when its strength is overcome whereas at deeper levels the same material is ductile and flows at a certain state of stress. Between these cases there is a broad range in which flow and fracture take place simultaneously, for example in form of cataclastic flow (e.g. Mogi, 1971, Carter and Tsenn, 1987, Kirby, 1985). In the following, four major regions within the earth's crust are described in which magmatic ascent has different forms. From deep to shallower crust they are: (1) a ductile region, (2) a semi-brittle zone, (3) a brittle zone with stoping, and (4) a brittle region containing dikes. Each region is discussed separately, but keep in mind, that there is a diffuse transition between regions.

Ductile Region

In this region the country rock is assumed to be highly viscous; it is pushed aside by an ascending magma diapir. Ascent velocities of diapirs are controlled by the viscosity distribution of the wall rock (Marsh, 1982), the density contrast of magma and host rock, and the size of the diapir. A large diapir within less viscous host rock would have the highest velocity whereas the velocity of a small magma body in a highly viscous surroundings may become negligibly small.

A transition to the next region, the semi-brittle zone, is modelled by considering diapiric ascent within a thin thermal boundary layer. Here, wall rock is softened due to the heat transfer from the hot magma into the wall which is related to a temperature increase in the host rock. This kind of ascent can be simulated by considering a magma chamber rising within a bigger container (Marsh, 1982). Mahon et al. (1988) calculated ascent velocities of a granitoid diapir in a temperature varying medium and concluded that the ascent velocity is strongly dependent on the viscosity of the wall rock and the deformation layer width.

Semi-brittle Region

When a magma body gets into shallower depths the viscosity of its surroundings increases. The ascent velocity described above would approach zero. In the semi-brittle region magmatic ascent can only be possible when the surroundings fracture and pass the diapir in the manner of cataclastic flow. Cataclastic flow is a kind of motion in which material flows due to fracturing and healing. This region is not well understood and there is almost nothing written about the stress distribution around a diapir in this kind of environment.

One approach is to consider the adjacent rock as a power law fluid as reported in Mahon et al. (1988). They give a mathematical expression of a temperature and strain rate dependent effective viscosity of the wall rock. Another possibility is to describe the host rock as an elasto-plastic material that fractures or deforms permanently when its strength is overcome. An approximation of this kind of view can be found in references dealing with openings in rocks or tunnels (e.g. Obert and Duvall, 1967).

Brittle Region: Stoping

The process in which disengaged roof rock fragments sink through the magma is known as stoping and was first introduced by Daly (e.g. Daly, 1903). He suggested that stoping is caused by thermal stresses developed in the host rock due to sudden and uneven heating by the advancing, hot magma body. He called this process marginal shattering. Marsh (1982) discussed stoping in more detail and presents a stress description of an elastic wall rock heated by a hot magma. He pointed out that for a reasonable temperature gradient the thermal stress exceeds easily the strength of the wall rock. Furlong and Myers (1985) assumed a time varying temperature profile in the host rock. Failure patterns around cylindrical openings in rocks are reported in Ewy and Cook (1990). They observed cracks oriented parallel to the opening. This is in agreement with calculations from Marsh (1982) and Furlong and Myers (1985).

Another mechanism to fracture the wall rock is caused by expansion of the magma chamber as reported in Phillips (1974), Blake (1984), and Tait et al. (1989). Crystallization of anhydrous minerals produces a separation of volatiles. This second boiling reaction is linked to an increase of the chamber's volume associated with an increase in stress (Burnham, 1979). Fracture will appear when the strength of the surrounding wall is overcome.

Brittle Region: Dikes

The final mechanism that may take place in the brittle crust is the formation of dikes, in particular ring-dikes. Dikes follow structural planes of weakness by filling the cracks formed along such planes. There are the same kind of stresses

leading to fracture the host rock as in stoping: thermal stress, and stress due to rapid expansion of the magma body (e.g. Phillips, 1974).

1.2 Remaining Problems

Most work that has been done in modeling with diapirs has picked only a single piece out of a complicated system. For example, the stress calculations of a magma body within a brittle country rock include either heat transfer (Marsh, 1982, Furlong and Myers, 1985) or water exsolution due to crystallization of the magma body (Blake, 1984, Tait et al., 1989). But, both mechanisms need to be combined and this is attempted here; furthermore, all kinds of stresses need to be combined to get a unified picture of the total stress field including thermal stress, overpressure, stress due to buoyancy, fluid pressure within the host rock, and the weight of the overburden. Once the importance of each stress component is known some of them can probably be neglected.

Another important question arises when the stresses are higher than the strength of the rock. Host rock will fracture associated with a decrease in stress magnitude. The overall stress field is different in a fractured material than in an intact, elastic medium (Obert and Duvall, 1976). An attempt is made here to describe the stress field in a fractured rock adjacent to an ascending magma chamber. What is the stress history of a rock mass as a magma approaches?

1.3 Overview of this Study

This particular study deals with the thermal-mechanical response of the country rock when a magma body approaches. Three different materials describe the behavior of the country rock at two different levels in the earth's

crust: (i) a viscous material in the lower crust, (ii) a thermal-elastic and (iii) an elasto-plastic material in the middle to upper crust.

The study is differentiated into three parts: (1) Processes within and around a magma body, (2) stresses within and around this chamber, and (3) the response of the host rock.

Processes

The temperature distribution within the country rock is of fundamental importance to calculate thermal stresses and has a strong influence on the mechanical behavior of the wall rock. Several heat transfer processes are reviewed like convection, conduction, and stoping. Only conduction of heat is picked for calculating the temperature and stress field.

Water generation within a magma body is important in the development of the magma pressure. Here, boundary layer processes and volatile transfer within a mush region adjacent to the chamber are discussed.

Stress

The stress field is first calculated for two extreme cases. In one case, country rock is modelled as a material that deforms elastically when it is heated from the magma or when a certain force on it is applied. During crystallization of the magma a separation of an aqueous phase leads to overpressure. In this model, temperature, water solubility, and the elastic properties are the major parameters.

In another model country rock and magma are assumed as highly viscous Newtonian fluids. The density contrast between magma and host rock and the country rock's viscosity are the dominant variables.

Response of Host Rock

The overall stress field within a thermal-elastic host rock is presented including thermal stresses, overpressure of the magma chamber, stress due to buoyancy, weight of overburden and fluid pressure within host rock. Then, a more realistic model is discussed by considering host rock as an elasto-plastic material that fractures when its strength is overcome. In this model the stress distribution and a possible ascent mechanism is presented. Finally, a history of a rock mass at a particular location as a magma body approaches is described.

Chapter II: Processes within and around Magma Chambers

2.1 Heat Generation and Transfer

2.1.1 Introduction

As magma rises through the earth's crust the temperature distribution will become quite complex. This is due to the differing mechanism of heat transfer coupled with crystallization processes and the varying diapir and ambient temperatures. Four different heat processes are taken into account in this study: free convection within the magma, forced convection within a deformation layer adjacent to the diapir, heat conduction within the wall rock, and stoping. Each mechanism is discussed separately.

2.1.2 Free Convection

Free convection is the principal mechanism inside a magma chamber but it is assumed to be absent in the country rock. Inside a diapir many processes work together because several phases are involved (gas, crystals, liquid). There are three types of convection or circulation. One is thermal convection driven by temperature contrast. Another type is compositional convection driven by density contrast due to fractional crystallization and third, there are circulation processes due to the diapir ascent. The latter case is discussed in chapter III. A good summary about the interaction between convection and crystallization within a cooling magma chamber is given in Brandeis and Jaupart (1986). As magma cools, its density increases which results into convective instabilities. At the same time crystallization of magma effects an increase in its viscosity and tends to

stabilize the convective instability. Brandeis and Jaupart (1986) argued that thermal convection is weak in magmas with viscosities greater than 10^6 Pas and can be neglected compared to other processes such as compositional convection or crystal settling. In this study, only high viscosity magmas are taken into consideration, so that thermal convection does not have an influence on the contact temperature of magma and wall rock.

2.1.3 Forced Convection

Forced convection occurs when a fluid motion is caused by the imposition of external forces in form of pressure differences (e.g. Eckert and Drake, 1972). This kind of boundary layer flow takes place within a narrow zone between diapir and host rock. The phenomena of thermal boundary layer and its velocity field is discussed in paragraphs 2.2.2 (boundary layer mechanism) and 3.2.2 (deformation layer), respectively.

2.1.4 Heat Conduction

If host rock material is highly viscous or rigid and material flow can be neglected heat is transferred by conduction. This approach provides only a minimum estimate of the temperature rise in the country rock. Any convection would accelerate the heating of the host rock and cooling process of the magma. Assume magma and host rock have constant initial temperatures of T_m and T_h, respectively. In this model, we consider magma and host rock as two semi-infinite solids of different materials which brought together at some time $t = 0$ (Fig. 2-1.1). Suppose the magma does not ascend. The temperature field is then allowed to relax with time to its equilibrium condition. At the interface of both

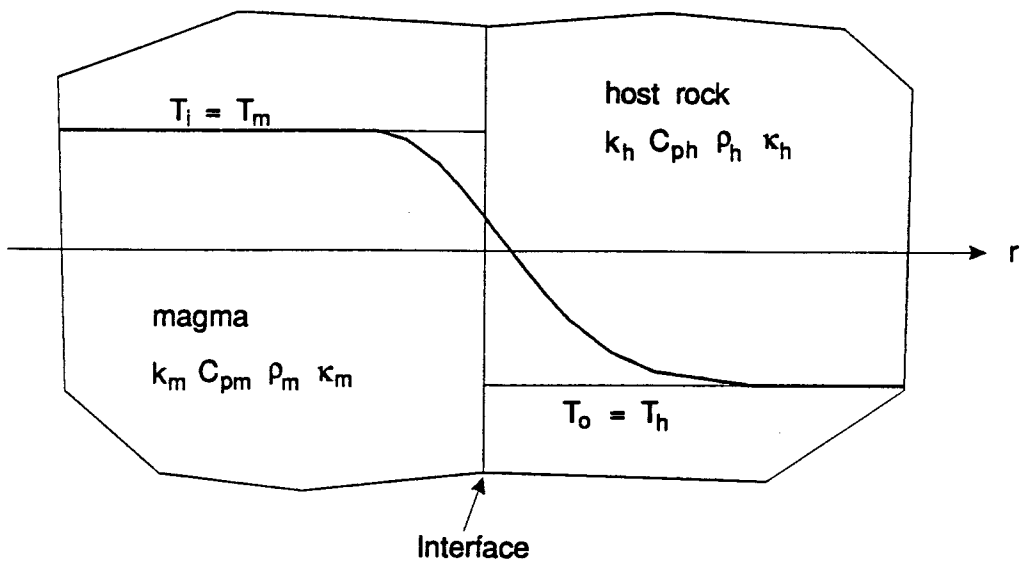

Fig. 2-1.1: Two semi-infinite bodies in contact.

materials a certain contact temperature, T_c, will adjust immediately and does not vary with time. This is so, because magma and host rock are considered as semi-infinite in extent. Any geometry of the magma chamber (e.g a spherical body) would result in a decrease of the contact temperature with time. But, in these calculations the effect of the geometry is neglected. The appropriate differential equations for the above system are

$$\frac{\partial T_i}{\partial t} = \kappa_m \frac{\partial^2 T_i}{\partial r^2} \qquad \text{magma chamber} \qquad (2\text{-}1.4.1a)$$

$$\frac{\partial T_o}{\partial t} = \kappa_h \frac{\partial^2 T_o}{\partial r^2} \qquad \text{host rock} \qquad (2\text{-}1.4.1b)$$

where r is the radius from the magma chamber center, t is the time after emplacement, κ is the thermal diffusivity defined as

$$\kappa = \frac{k}{\rho C_p} \qquad (2\text{-}1.4.2)$$

in which k is the thermal conductivity, ρ is the density, and C_p is the specific heat. The indices m and h stand for magma and host rock, respectively.

The initial conditions are for no contact:

$T_i = T_m$ if $t = 0$ and $r < R_i$,
$T_o = T_h$ if $t = 0$ and $r > R_i$

where T_i is the temperature of the magma, T_o is the temperature of the host rock, and R_i is the position of the interface. The boundary conditions must reflect two facts: (1) the temperature must be continuous across the interface, (2) the heat flow from the magma of higher temperature must be equal to the heat flow into the host rock of lower temperature. Mathematically, these conditions are:

$$T_i = T_o \qquad \text{if } t > 0 \text{ and } r = R_i,$$

$$k_m \frac{\partial T_m}{\partial r} = k_h \frac{\partial T_h}{\partial r} \qquad \text{if } t > 0 \text{ and } r = R_i.$$

Solving the differential equation system (2-1.4.1) with the above boundary conditions the temperature distribution for both magma and host rock can be obtained:

$$T_i = T_h + \frac{T_m - T_h}{1 + \chi} \left[1 + \chi \, \mathrm{erf} \frac{r - R_i}{\sqrt{4 \kappa_m t}} \right] \qquad (2\text{-}1.4.3a)$$

$$T_o = T_h + \frac{T_m - T_h}{1 + \chi} \left[1 + \mathrm{erf} \frac{R_i - r}{\sqrt{4 \kappa_h t}} \right] \qquad (2\text{-}1.4.3b)$$

with

$$\chi = \sqrt{\frac{k_h \rho_h C_{ph}}{k_m \rho_m C_{pm}}} \qquad (2\text{-}1.4.4)$$

and erf(x) is the error function defined as:

$$\mathrm{erf}(x) = \frac{2}{\sqrt{\pi}} \int_0^x \exp(-\xi^2) \, d\xi \qquad (2\text{-}1.4.5)$$

The contact temperature, T_c, at the interface is constant and is given by

$$T_c = T_h + \frac{T_m - T_h}{1 + \chi} \qquad (2\text{-}1.4.6)$$

This model assumes a fixed boundary between magma and host rock during crystallization and neglects the effect of latent heat of crystallization. An approximation to include the latter effect is given below. A more detailed study of

the temperature development within the host rock is reported in Brandeis et al. (1984).

2.1.5 Heat Generation

During ascent, heat will be generated within the magma chamber by the latent heat of crystallization, decay of radioactive isotopes, and conversion of potential energy to heat through viscous deformation mechanisms.

Latent heat will be released during crystallization of the magma body from the liquidus at which crystallization begins to the solidus where crystallization is completed. A simple reasonable approximation to incorporate latent heat to the temperature distribution is given by adding an equivalent specific heat to the heat capacity of the magma (Jaeger, 1968):

$$C^*_{pm} = C_{pm} + \frac{\Delta h_f}{\Delta T_{xx}} \qquad (2\text{-}1.5.1)$$

where Δh_f is the latent heat and ΔT_{xx} is the temperature difference of the crystallization interval. The thermal diffusivity of the magma becomes

$$\kappa^*_m = \frac{k_m}{\rho_m C_{pm}^*} \qquad (2\text{-}1.5.2)$$

In all calculations the liquidus and solidus temperatures are taken to be 1073 K and 923 K, respectively (Wyllie et al., 1976). Note, that these values may change with depth and time. Typical values of the latent heat are given by Trial

and Spera (1990) with $\Delta h_f = 4.2 \times 10^5$ J kg^{-1} and Brandeis et al. (1984) with $\Delta h_f = 3.6 \times 10^5$ J kg^{-1}. For values for the specific heat, C_p, see paragraph 2.3 (physical properties).

Loss of potential energy produces heat by viscous dissipation in the wall rock. The equivalent temperature is estimated to be about 1.5 K/km of ascent for most magma bodies (Marsh, 1982). A total ascent of 5 km would result in 7.5 K added to the system.

The conversion of potential energy to heat and the heat added by radioactive decay of isotopes ($\approx$2 K, Harrison and McDougall, 1980) are small compared to the latent heat of crystallization and can be neglected.

As an geological example consider a spherical magma reservoir with a radius, R_i, of 5 km and initial temperature, T_m = 1073 K. Let the chamber's top be fixed at 8 km depth. The ambient temperature at 8 km depth becomes 483 K by using a geothermal gradient of 25 K km^{-1} and a surface temperature of 283 K. The thermal parameters are:

	magma	host rock	equation
ρ [kg m^{-3}]	2425	2500	2-3.2.1
k [J m^{-1} s^{-1} K^{-1}]	2.59	2	2-3.3.2
C_p [J kg^{-1} K^{-1}]	1234	993	2-3.3.3
Δh_f [J kg^{-1}]	3.6x10^5	-	
ΔT_{xx} [K]	150	-	
C^*_p [J kg^{-1} K^{-1}]	3634	-	2-1.5.1
κ [m^2 s^{-1}]	8.7x10^{-7}	8.1x10^{-7}	2-1.4.2
κ^* [m^2 s^{-1}]	2.9x10^{-7}	-	2-1.5.2

The contact temperature is 885 K. The temperature distribution is shown in Figs. 2-1.2 and 2-1.3 evaluated from equation (2-.1.4.3).

2-1.6 Ascending Magma Chamber

Ambient Temperature

If magma rises through the continental crust the ambient temperature, T_h, changes with time as the diapir becomes closer to the earth's surface. For a constant ascent velocity the time dependent ambient temperature becomes

$$T_h(t) = \int_{U\,t}^{z_{ini}} \frac{\partial T_h}{\partial z}\, dz + T_s \qquad (2\text{-}1.6.1)$$

where z_{ini} is the initial depth of the diapir, $\partial T_h/\partial z$ is the geothermal gradient, U is the ascent velocity (see equations 3-2.1.5 or 3-2.2.1), T_h is the initial ambient temperature at t = 0, $T_h(t)$ is the temperature of the host rock at infinity at a time, t, after emplacement, and T_s is the temperature of the earth's surface (T_s = 283 K). A realistic orogenic geothermal gradient, within the crust, of 25 K/km (Clark, 1966) is used in this study.

As an example consider a magma chamber initially at 8 km depth (chamber's top). Suppose, the chamber ascends with an average velocity of 0.5 m per year. At t = 0, the ambient temperature at 8 km depth becomes 483 K; After 1000 years the chamber's top is at 7500 m depth and the ambient temperature reduces to 470.5 K.

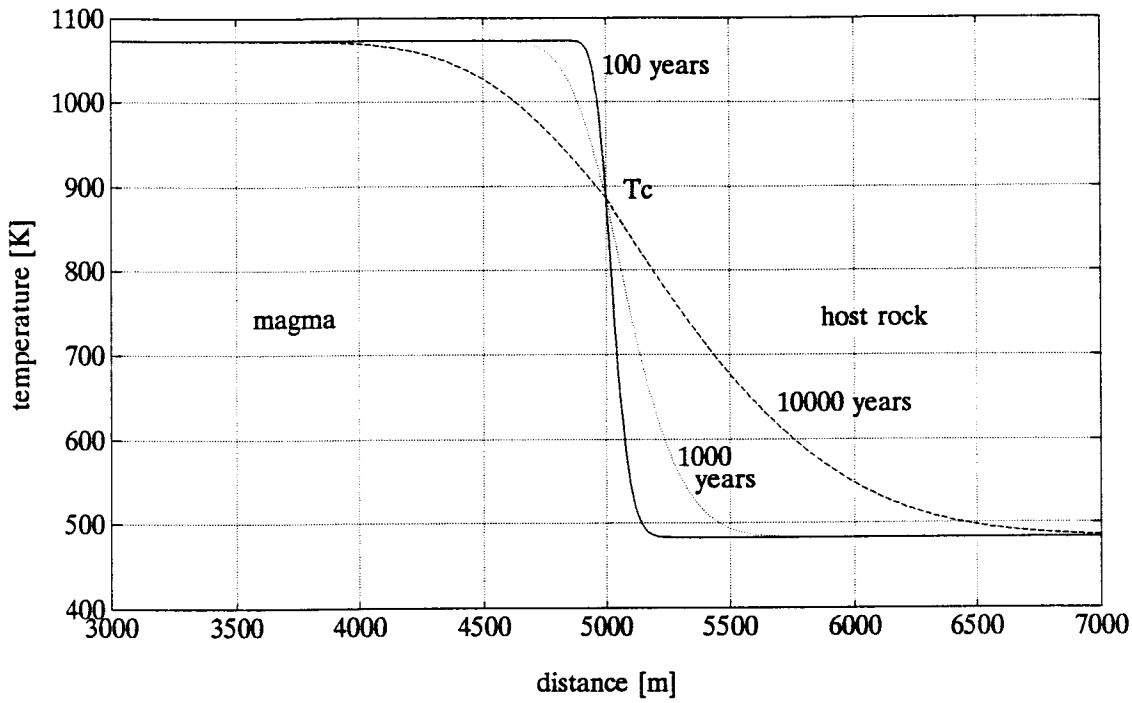

Fig. 2-1.2 : Temperature distribution around a cooling magma chamber at 8 km depth (chamber's top) with a radius of 5 km. Numbers labeling curves are times in years after intrusion. The interface magma - host rock is indicated at 5000 m distance. For variables, see text. T_C indicates the contact temperature.

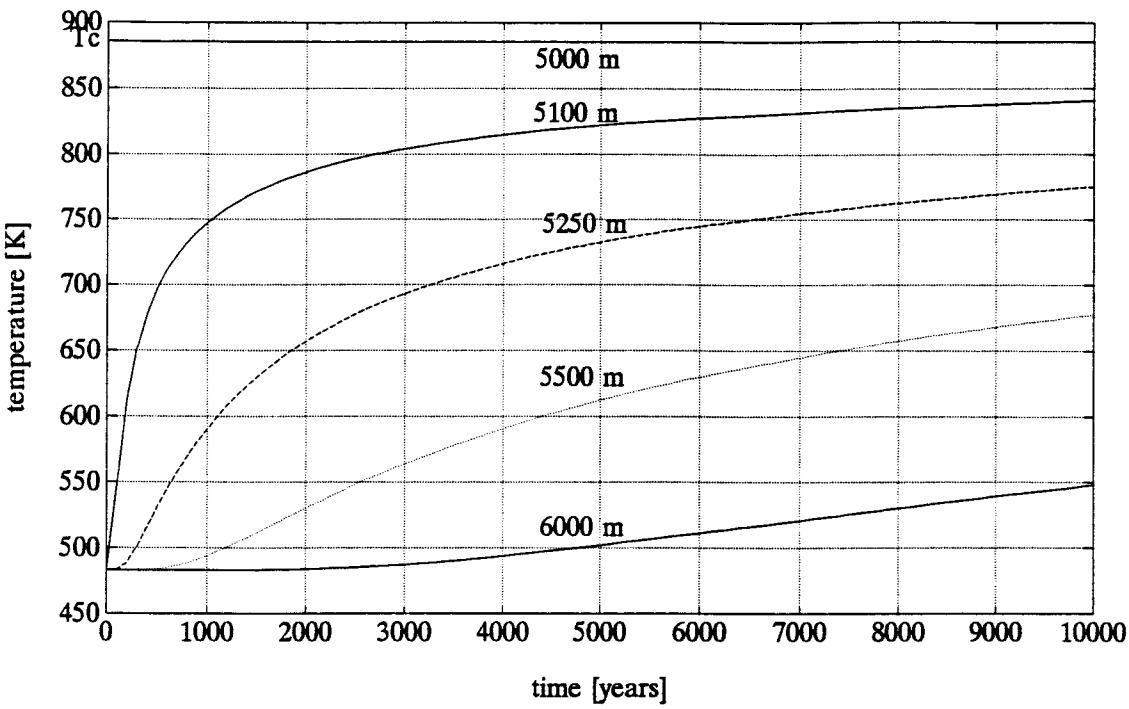

Fig. 2-1.3 : Temperature-time developments for different distances. The time is equal to zero at the interface of magma and host rock (distance = 5000 m). For variables, see text. T_c indicates the contact temperature.

Temperature Field

The temperature field described above is calculated under the assumption of a magma chamber at a fixed location within the earth's crust. Its isotherms are parallel to the magma - host rock interface. An ascending chamber would create isotherms which are closer to one another in the direction of ascent and wider apart in the opposite direction (Fig. 2-1.4). The slope of the temperature profile in Fig. 2-1.2 would become steeper.

As an example, we assume a constant ascent velocity, U, of 0.5 m per year. In Fig. 2-1.5 there is a plot of temperature versus distance for t = 100, 300 and 500 years. By considering the isotherms at 550 K and 600 K in direction of magma ascent the following information can be obtained:

Isotherm at 550 K:

time	distance	velocity of isotherm	velocity ratio of magma and isotherm
t [a]	$r - R_i$ [m]	$\vartheta = (r - R_i) / t$ [m a^{-1}]	$\upsilon = U / \vartheta$
100	100	1.00	0.50
300	170	0.57	0.88
500	220	0.44	1.13

Isotherm at 600 K:

time	distance	velocity of isotherm	velocity ratio
t [a]	$r - R_i$ [m]	$\vartheta = (r - R_i) / t$ [m a^{-1}]	$\upsilon = U / \vartheta$
100	75	0.75	0.67
300	130	0.43	1.16
500	170	0.34	1.47

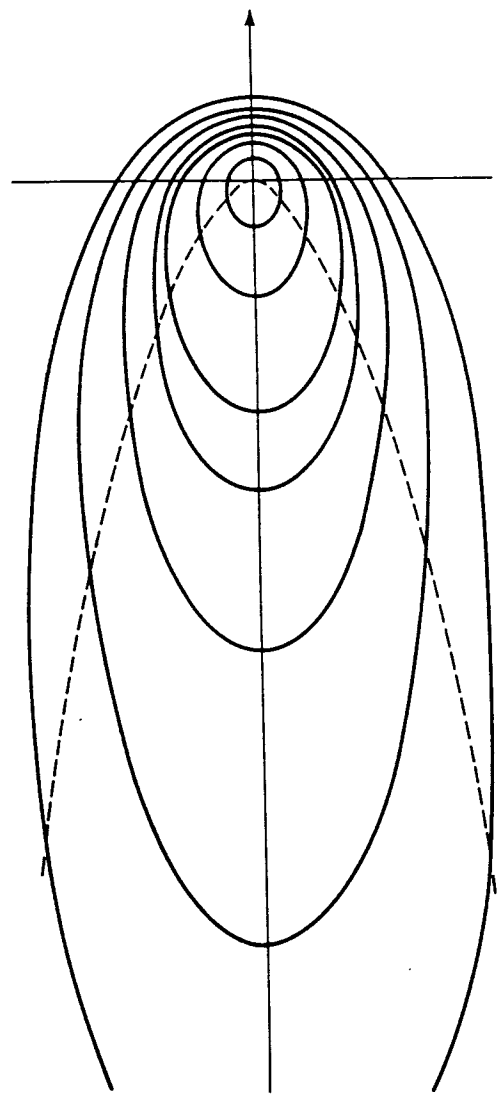

Fig. 2-1.4: Lines constant temperature describing the temperature field created by a moving point source (after Eckert and Drake, 1972).

When the velocity ratio, υ, equals 1, the isotherms and the magma chamber ascend with the same rate. When this conditions is reached both velocities are in equilibrium. At this equilibrium temperature the temperature field within the host rock is independent of time. For a velocity ratio bigger than one the isotherms are slower then the magma chamber. This ratio decreases with time until it becomes 1. Then, the equilibrium condition is reached. In the above example the equilibrium temperature after 300 years must be between 550 K and 600 K.

In Fig. 2-1.5 the equilibrium temperature can graphically be found at the intersection of a temperature - distance curve at a particular time and a vertical line representing the equivalent distance due to the ascent velocity after the same time. In the example of U = 0.5 m a^{-1}, we find the distance from the chamber's center at initial depth to its crest after a particular time, t:

time [years]	distance [m]
100	5050
300	5150
500	5250

Each pair of intersection represents the state where a particular temperature and the magma chamber have equal velocities. A higher equilibrium temperature is reached earlier than a lower temperature. This effects a steeper slope of the temperature profile within the host rock.

In Fig. 2-1.6 there is a plot of temperature versus distance connecting the equilibrium points. The resulting curve is the temperature profile within the host rock at the chamber's crest that rises up with a constant velocity of 0.5 meter per

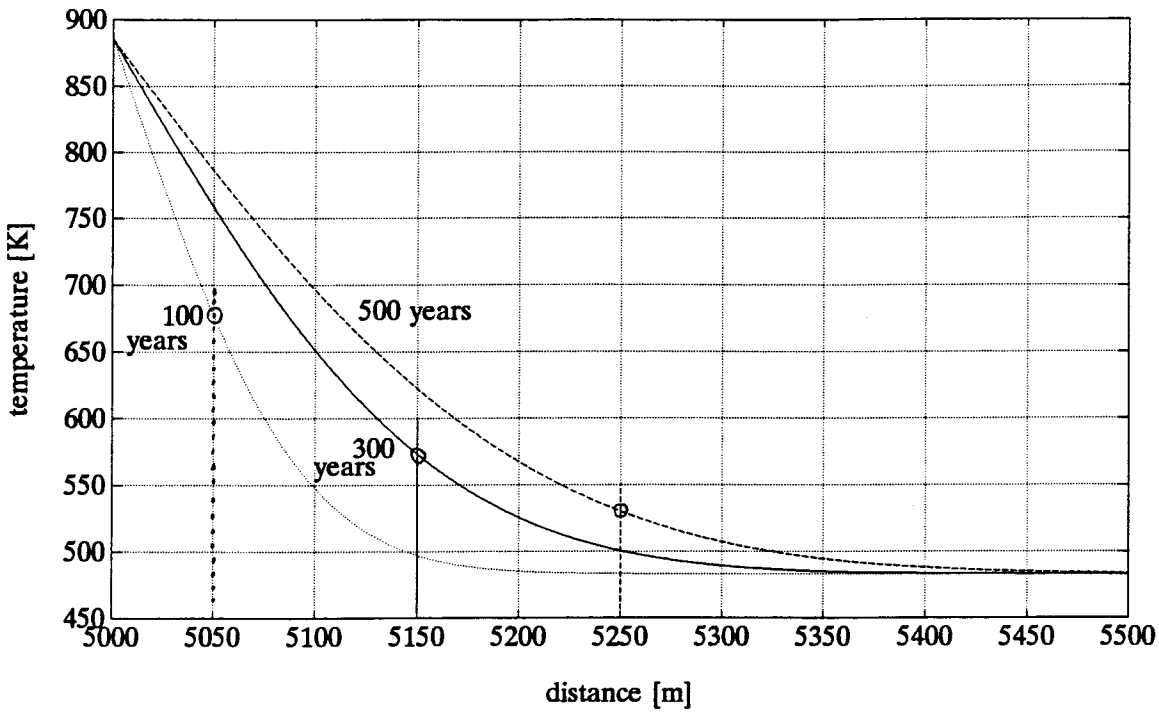

Fig. 2-1.5: Temperature field within the country rock at 100, 300, and 500 years after emplacement of a magma reservoir. 5000 m indicates the interface between magma and host rock. The vertical lines represent the distances of the magma chamber's crest that rises with a constant velocity of 0.5 m a^{-1}. The intersection of a pair of lines indicates the state where a particular temperature migrates with the same velocity as the magma chamber.

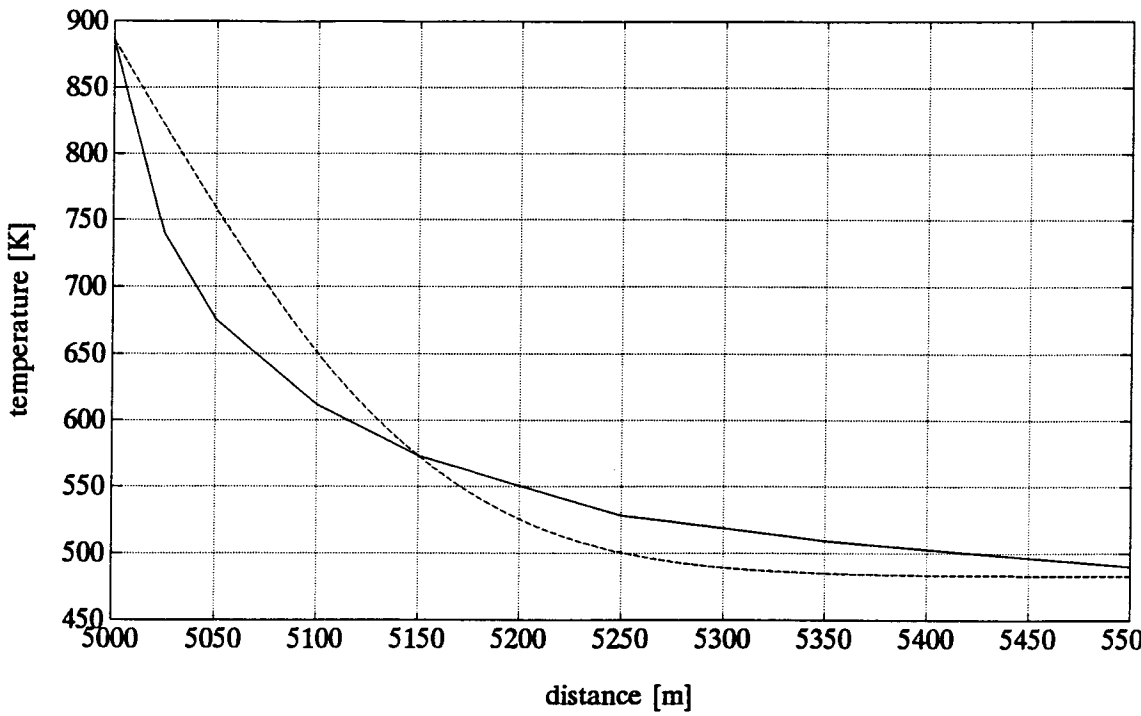

Fig. 2-1.6: Temperature distribution within the host rock. The dashed line represents the temperature field after 300 years after emplacement of a magma chamber at a particular location in the earth's crust. The solid line represent the temperature profile above the crest of an ascending magma chamber with a constant velocity of 0.5 m a^{-1}.

year. Note, that this temperature profile is not a rigorous profile but it leads to a correction of the right kind. In reality, the ascent velocity is not constant and decreases as the chamber becomes closer to the earth's surface. More about this is written in chapter 3.2.

2.1.7 Stoping

Magmatic stoping is defined as the process in which rock fragments from a fractured host rock sink into the magma on account of their greater gravity (Daly, 1903). During their way downward heat is delivered from warmer magma into the colder wall rock fragments. This effects partial melting of wall rock fragments and contamination of the magma. In this process, magma cools faster because the total area of cold wall rock has increased. In the same way that latent heat gives an effect like a material with larger specific heat stoping gives the opposite effect.

2.2 Water Generation and Transfer

2.2.1 Introduction

There are three principal types of processes by which magma heterogeneities can arise. Chemical heterogeneities can develop (i) during segregation of a magma body (ab initio, before rise begins), (ii) during magma ascent, and (iii) during solidification or after magma ascent ends (in situ). A schematic diagram is shown in Fig. 2-2.1.

Ab initio processes are anatexis and roof melting. When magma moves through a conduit, heat will be delivered to the country rock so that contamination with the surrounding walls may result in partial fusion associated with formation of a small magma chamber (e.g. Huppert and Sparks, 1988).

For the in situ processes two major mechanisms are responsible: (i) transfer of material, especially volatiles, within a mush of crystals and melt adjacent to the magma body and (ii) boundary layer mechanism within the chamber.

A necessary condition for volatile transfer is supersaturation of melt with respect to volatiles (H_2O for example). H_2O-rich fluids can produce chemical gradients especially in highly charged trace elements (Taylor et al., 1981). This process becomes more important after a significant portion of magma has crystallized (Candela, 1986).

A boundary layer is defined as a thin region adjacent to the magma chamber margin which accommodates the temperature and composition anomalies due to the country rock (Fig. 2-2.2). Magma outside of the boundary

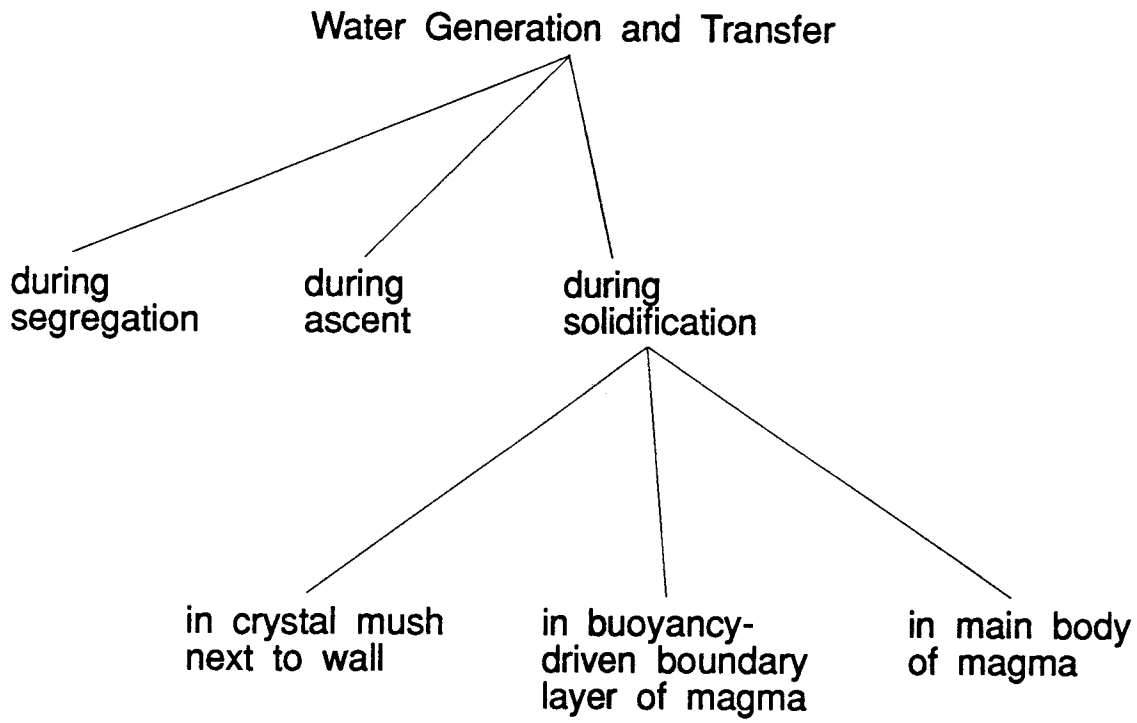

Fig. 2-2.1: Water generation and transfer near the interface of magma and host rock.

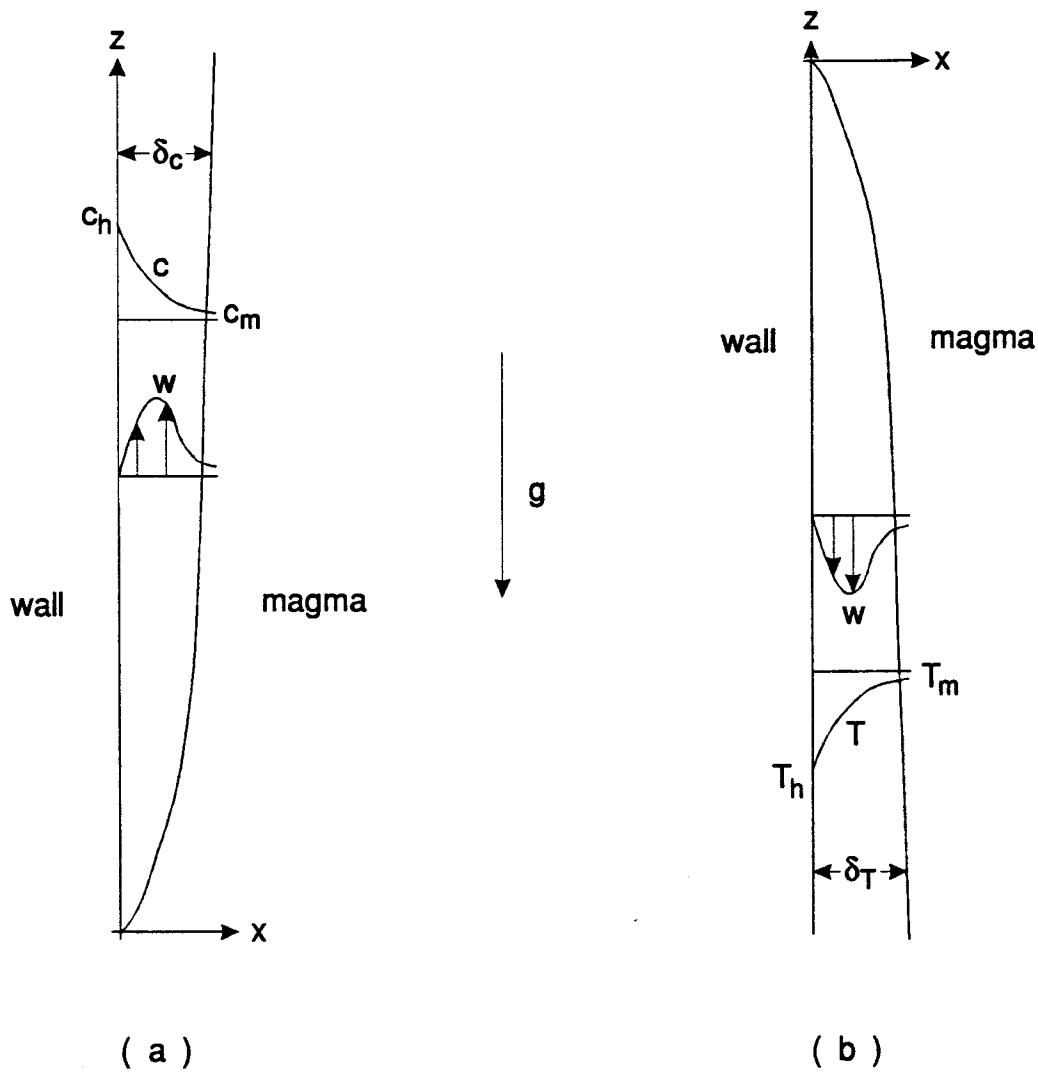

Fig. 2-2.2 : Schematic sketches for (a) compositional boundary layer, (b) free convection boundary layer on a cold vertical plate. Symbols are explained in text.

layer is essentially isothermal and iso-compositional (Trial and Spera, 1990). Boundary layer mechanisms play an important role in liquid fractionation (McBirney et al., 1985, see Fig. 2-2.3).

2.2.2 Boundary Layer Mechanisms

General concept of Boundary Layers

To understand flow in a boundary layer we consider the interface of magma and host rock as a vertical plate, shown schematically in Fig. 2-2.2a. Assume, there is a constant concentration difference of component f across the boundary between magma and host rock. If the concentration of this component is uniform along the z-direction and varies only along the x-direction dc/dx is the only concentration gradient. Hence, diffusion along x is the only flux and vertical flow is not possible. But for example, if gravity operates and several components have different densities, the flow parallel to z driven by gravity interacts with the flow along x driven by diffusion. This kind of flow is known as a chemically driven boundary layer flow. If component f is less dense and its concentration in the boundary layer is higher than the bulk magma the boundary layer flow is upward.

As another example, consider a hot, fluid magma at temperature T_m that is in contact with a cold, solid wall (T_h). Here, magma is cooled by thermal conduction in horizontal direction. The resulting denser and colder fluid flows downward close to the boundary. Heat is advected in vertical direction before it has penetrated far in the horizontal direction. The convection occurs within a thin boundary layer. Outside this film the fluid remains at rest at temperature T_m. The vertical velocity at the wall and outside the boundary layer is zero. The velocity

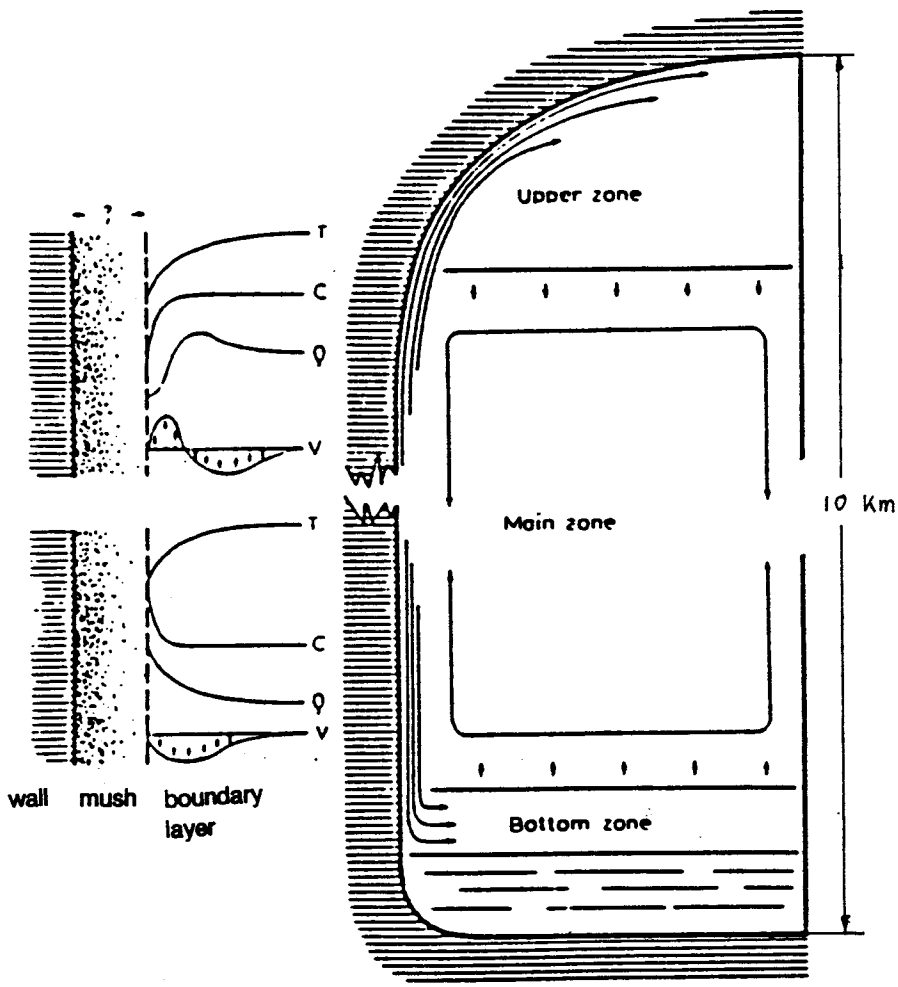

Fig. 2-2.3 : Boundary layers next to the steep wall of a crystallizing magma may have one of two possible relations, depending on whether the chemical variations reinforce or oppose the effects of thermal contraction. The lower part of the diagram illustrate the case of a tholeiitic magma that becomes denser at it evolves. The dense boundary layer descends and ponds on the floor to form a stable bottom zone. In case of a calc-alkaline magma, however, the compositional boundary layer close to the wall becomes lighter and rises to accumulate as a separate upper zone even though the thermal effect on density causes the magma to descend in the region farther from the wall. The diagram on the left illustrates the profile of temperature (T), concentration of heavy components (C), density (ρ) and velocity (v) (McBirney et al., 1985).

profile within the layer is shown in Fig. 2-2.2b (velocity = w). The maximum velocity of the fluid and the boundary layer thickness (δ_T) vary with z, whereas the temperature difference across the boundary layer is fixed at (T_m - T_h) (Tritton, 1989). Such flow within a boundary layer due to a horizontal temperature gradient is called a thermally driven boundary flow.

Principles of Liquid Fractionation

Liquid fractionation is a process by which segregation of distinct magmas occurs in the liquid ± crystals state (McBirney et al., 1985). The process of liquid fractionation is mainly the result of density differences produced by compositional and thermal gradients. During crystallization or melting these gradients determine whether material flows up- or downward depending on the sign of the buoyancy. In this model, called double-diffusive convection, a differentiated liquid will be delivered within a thin boundary layer adjacent to the wall to form a stratified gravitationally stable zone under the roof and on the floor of the magma reservoir.

Calc-alkaline magmas, for example, that crystallize relatively large amounts of phases rich in heavy components, such as iron, becomes less dense with progressive differentiation. The density of an andesitic magma at a typical temperature of 1100°C is close to 2450 kg/m^3, while that of rhyolite at 900°C is around 2200kg/m^3 (Fig. 2-2.4).

Tholeiitic magmas become progressively enriched in iron over much of their range of solidification and therefore get denser (Fig. 2-2.4). This compositional effect reinforces that of thermal contraction, and beyond a certain maximum level of enrichment, however, this trend is reversed (McBirney et al.,

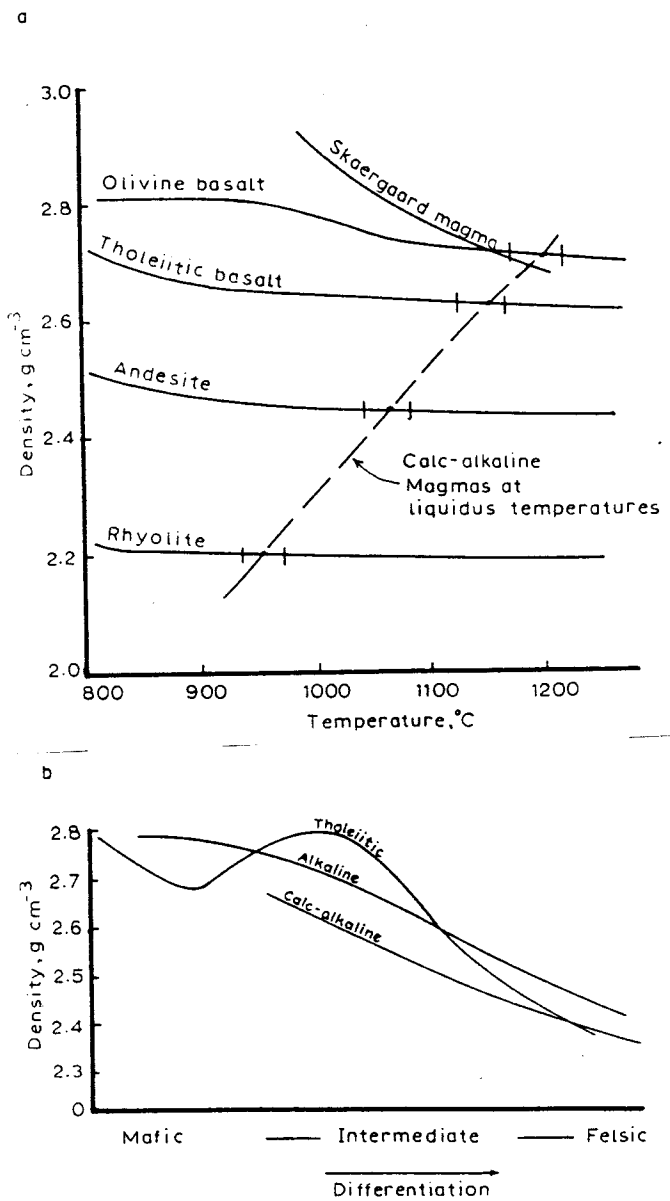

Fig. 2-2.4 : (a) The dependence of density on temperature for common igneous rocks. The dashed line is drawn through the liquidus temperatures of the calc alkaline series to illustrate how much greater is the effect of changing composition than the effect of falling temperature at constant composition. (b) Variations of density with differentiation of the major types of igneous series. The calc-alkaline series is based on average rocks of the Cascade Range. The tholeiitic series is for rocks of the Galapagos Islands, and the alkaline one for the phonolithic series of Tahiti (after McBirney et al. 1985).

1985). The result is that subsequent liquids become lighter. Lighter liquid can accumulate under the magma chamber's roof and form a gravitationally stable zone.

Kinetic Effects on Crystal-Liquid Fractionation

Consider a case of diffusion-controlled crystallization in a static liquid in a closed system. Baker and McBirney (1985) state that the steady state concentration (c_x) of a dispersed component at a distance x from a crystal-liquid interface is determined by its abundance in the bulk liquid far from the interface (c_∞), its equilibrium distribution coefficient (K_o), its molecular diffusivity (D), and the linear crystallization rate (f) in the form of

$$c_x / c_\infty = 1 + [(1 + K_o) / K_o] \exp(- f x / D) \qquad (2\text{-}2.2.1).$$

The ratio f/D is a measure of the steepness of the concentration gradient in the chemical boundary layer (Lasaga, 1981). Both distribution and diffusion coefficient are a function of the magnitude of enrichment or depletion. In Fig. 2-2.5 there is a plot of distance x versus concentration ratio c_x/c_∞ for an incompatible element (upper curves, K_o = 0.1) and a compatible element (lower curves, K_o = 10). For constant crystallization rate, each set of curves demonstrate the effect of differing diffusivities on the concentration profile of elements with the same distribution coefficient. If there is enough time, and if the liquid is not stirred by convection or turbulence, the chemical boundary layer width (δ_c) can extend tens of centimeter into the liquid. For high crystallization rates, compatible elements cannot diffuse to the crystals fast enough and they become depleted; incompatible elements cannot diffuse away from the crystals fast enough and they become enriched.

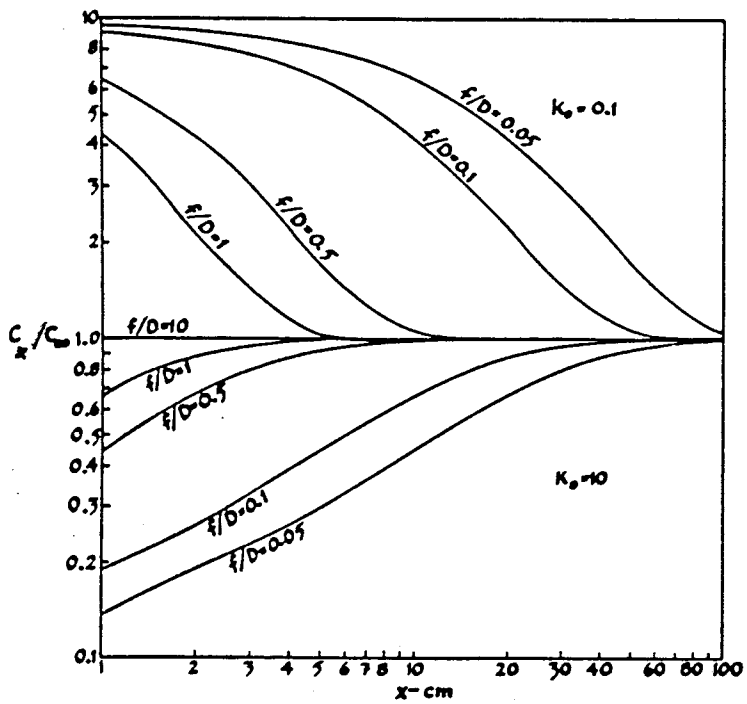

Fig. 2-2.5 : Enrichments and depletions of incompatible and compatible trace elements due to crystallization in a static liquid. The curves with varying f/D ratios show the effect of varying diffusivities but constant rate on abundances across the compositional boundary layer (after Baker and McBirney, 1985).

Consider a simple boundary-layer liquid formed by wall-rock melting. For trace elements, which do not affect liquid densities, their diffusivities determine the concentrations across the boundary layer (Baker and McBirney, 1985). Faster diffusing elements become enriched relative to the slower one.

Effect of Horizontal Thermal and Compositional Gradients

It can be imagined that liquid fractionation happens preferentially at the wall-magma interface because the melt there gets in contact with material of different temperature and composition. We define a composition difference ΔW and a temperature difference ΔT across the interface of magma and host rock. Because of the different temperature and composition of magma and wall, thermal and chemical boundary layers can develop next to the wall (see above). So, it is important to consider how differing rates of thermal and chemical boundary diffusion would be reflected in the forms of thermal and chemical boundary layers next to the wall. In the following, the wall is visualized as a well-defined boundary between a moving fluid and a rigid solid, but in reality, it is an interface between moving and static liquids of differing viscosities and crystal contents (McBirney et al. 1985). It is also assumed that, except for the small temperature drop and composition jump at the margin and the associated flow, the whole magma and wall rock is standing still. But in reality, there are convection within magma and host rock due to temperature and composition gradients (see paragraph 2.1.2) and due to the ascending chamber (see paragraph 3.2.1).

One important factor is whether the flow within a boundary layer is driven by thermal or chemical buoyancy. This is important because only in a chemically

driven regime the marginal flow is upwelling and leads to a chemically stratified cap (calc-alkaline magmas). In a thermally driven regime, the cold walls produce such an enormous negative thermal buoyancy force that the flow is downwards everywhere in the boundary layer, (tholeiitic magmas) and light species cannot flow roofward (Trial and Spera, 1990). Nevertheless, upwelling boundary layers may also occur when the flow is transitional between thermal and chemical dominance. If the flow in both a thermal and chemical boundary layer is downwards, then they reinforce one another. Spera et al. (1982) pointed out that significant chemical fractionation can also occur due to coupling of rapid convection flow and slow horizontal Soret diffusion within a thermal boundary layer. Soret diffusion is a spontaneous flow of mass due to a temperature gradient. McBirney et al. (1985) reported that the thickness of the boundary layer in the thermally driven case is much larger than in the chemically driven case : $(\delta_c)_T >> (\delta_c)_C$. The reason is that thermal diffusion (conduction), usually between $3x10^{-3}$ and $5x10^{-3}$ $cm^2\ s^{-1}$, is relatively rapid compared to chemical diffusion (normally 10^{-5} - 10^{-10} $cm^2\ s^{-1}$). Typical values are calculated by Trial and Spera (1990) : thermally driven boundary layers have values within a range of meters whereas chemical driven boundary layers have a thickness of only a few centimeters.

For a constant wall temperature and a constant mass fraction at the magma chamber-country rock contact the flow is chemically driven if :

$$R\rho > 1.2\ Le^{1/3} \qquad (2\text{-}2.2.2)$$

with :

$R\rho = \alpha_c \Delta W / \alpha_T \Delta T$: buoyancy ratio

$Le = \kappa / D$: Lewis number,

where α_c is the expansivity in the chemical regime, α_T is the thermal expansivity, ΔW is the difference in composition or the mass fraction across the chemical boundary layer, ΔT is the temperature difference across the thermal boundary layer, κ is the thermal diffusivity and D is the diffusion coefficient (Trial and Spera, 1990).

For a constant mass flux (j_w) and a constant heat flux (q_w) at the magma chamber-country rock contact a chemically driven flow is possible if :

$$R\nu > 0.22\ Le^{2/3} \qquad (2\text{-}2.2.3)$$

with :

$R\nu = k\alpha_c j_w / \rho D \alpha_T q_w$: buoyancy ratio

where k is the thermal conductivity and ρ is the density of the melt (Trial and Spera, 1990). Table 2-1 gives a scaling relationship to obtain order-of-magnitude estimates of heat and chemical transport rates, boundary layer thicknesses, flow rates for a variety of boundary conditions (Trial and Spera, 1990).

One example illustrates the application to a geological problem. Consider a magma chamber of intermediate composition, for example 55 wt% SiO_2 and 0.1 wt% H_2O. H = 10^4 m, ρ_m = 2400 kg m^3, η_m = 9.6×10^5 Pas, κ = 10^{-6} m^2s^{-1}, k = 3 $Jm^{-1}s^{-1}K^{-1}$, C_p = 1200 $Jkg^{-1}K^{-1}$, α_T = 5×10^{-5} K^{-1}, Δh_f = 3.6×10^5 Jkg^{-1}. Let the temperature difference from magma to solidus be ΔT_s = 150 K and the temperature difference across the boundary layer be ΔT = 10K. The properties for H_20 are: α_{c1} = 2, D_1 = $10^{-11}m^2s^{-1}$, ΔW_1 = 0.05; and for SiO_2 they are: α_{c2} = 0.5, D_2 = 10^{-16} m^2s^{-1}, ΔW_2 = 0.2. The subscripts 1 and 2 indicate water and silica, respectively.

TABLE 2-1 : Scaling relationships: Thermal and compositional boundary conditions are the same type

	compositionally driven		thermally driven	
	Constant T_w, W_w	Constant q_w, j_w	Constant T_w, W_w	Constant q_w, j_w
	($R\rho >> Le^{1/3}$)	($R\nu >> Le^{1/3}$)	($R\rho << Le^{1/3}$)	($R\nu << Le^{2/3}$)
w	$\frac{4\kappa}{9H}(Ra\,R\rho)^{1/2}\,Le^{-1/2}$	$\frac{1\kappa}{9H}(Rq\,R\nu)^{2/5}\,Le^{-3/5}$	$\frac{4\kappa}{9H}Ra^{1/2}$	$\frac{1\kappa}{9H}Rq^{2/5}$
δ_T	$\frac{3}{2}H\,Le^{1/4}\,(Ra\,R\rho)^{-1/4}$	$3H\,(Rq\,R\nu)^{-1/5}\,Le^{3/10}$	$\frac{3}{2}H\,Ra^{-1/4}$	$3H\,Rq^{-1/5}$
δ_c	$\frac{3}{2}H\,(Ra\,R\rho\,Le)^{-1/4}$	$3H\,(Rq\,R\nu\,Le)^{-1/5}$	$\frac{3}{2}H\,Ra^{-1/4}\,Le^{-1/3}$	$3H\,Rq^{-1/5}\,Le^{-1/3}$
q_w	$\frac{2}{3}\frac{k\,\Delta T}{H}(Ra\,R\rho)^{1/4}\,Le^{-1/4}$	constant	$\frac{2}{3}\frac{k\,\Delta T}{H}Ra^{1/4}$	constant
j_w	$\frac{2}{3}\frac{k\,\Delta W}{C_p\,H}(Ra\,R\rho)^{1/4}\,Le^{-3/4}$	constant	$\frac{2}{3}\frac{k\,\Delta W}{C_p\,H}Ra^{1/4}\,Le^{-2/3}$	constant
ΔT	constant	$3\frac{q_w\,H}{k}(Rq\,R\nu)^{-1/5}\,Le^{3/10}$	constant	$3\frac{q_w\,H}{k}Rq^{-1/5}$
ΔW	constant	$3\frac{C_p\,j_w\,H}{k}(RqR\nu)^{-1/5}\,Le^{4/5}$	constant	$3\frac{C_p\,j_w\,H}{k}Rq^{-1/5}\,Le^{2/3}$

From Trial and Spera (1990)

The first step is determining the driving buoyancy forces. The thermal Rayleigh number is defined as

$$Ra = \frac{g\,\alpha_T\,\Delta T\,H^3}{\kappa\,\nu_k} = 1.25\text{x}10^{13} \qquad (2\text{-}2.2.3)$$

where ν_k is the kinematic viscosity of the magma, ν_k is defined as: $\nu_k = \eta_m/\rho_m$. For H_2O: $R\rho$ = 200, Le = 10^5, and for SiO_2: $R\rho$ = 200, Le = 10^{10}. Using equation (2-2.2.2) the flow type can be decided. For this example, the flow of H_2O is chemically driven and the flow of SiO_2 is thermally driven. Referring to table 2-1 the flow characteristics can be calculated :

	H_2O	SiO_2
w [m a^{-1}]	222	4959
δ_T [m]	37.7	7.8
δ_C [m]	0.2	0.004
q_w [$Jm^{-2}a^{-1}$]	2.5x10^7	11.9x10^7
j_w [$kgm^{-2}a^{-1}$]	0.331	0.0004

In case of water, marginal flow will be upward, in case of silica, flow will be downward.

The next question that has to be cleared up is whether the magma body will be contaminated before chemical stratification can develop. Trial and Spera (1990) reported that in a thermally driven regime, the magma body may be significantly contaminated even though it does not stratify, while in a chemically driven case stratification may be slow compared to solidification of the magma reservoir. Defining a solidification time (t_s) as the time interval required for cooling the body from the initial temperature to the solidus, and a contamination time (t_c)

as the time required to increase the mass of the contaminating component in the chamber by 10% of the amount initially present,

$$t_s \approx \frac{\text{total supersolidus heat}}{\text{rate of heat removal}} = \frac{\rho_m H^3 (C_p \Delta T_s + \Delta h_f)}{4 q_w H^2} \qquad (2\text{-}2.2.4)$$

where ρ_m is the magma density, H is the magma chambers height (with its volume of approximately H^3), C_p is the heat capacity, ΔT_s is the initial to solidus temperature interval, Δh_f is the heat of crystallization, and q_w is the heat flux across the margins of the magma body. Cooling is supposed to be along all four sidewalls of the body. For H_2O the contamination time is :

$$t_c \approx \frac{1}{10} \frac{\text{initial } H_2O \text{ content of magma}}{\text{rate of } H_2O \text{ input}} = \frac{\rho_m H^3 W_{H2O}}{40 j_w H^2} \qquad (2\text{-}2.2.5)$$

where W_{H2O} is the initial H2O concentration of the uncontaminated melt. Then the ratio

$$\tau = \frac{t_s}{t_c} \approx \frac{10 (C_p \Delta T + \Delta h_f) j_w}{W_{H2O} q_w} \qquad (2\text{-}2.2.6)$$

can be an argument whether melt contamination occurs or not. When $\tau > 1$, the magma chamber will be strongly contaminated in a time t_c (Trial and Spera, 1990). Calculation from Trial and Spera (1990) indicates that chemical zonation develops only for highly mobile species such as H_2O. Zonation of species like SiO_2 cannot develop because their contamination time is extremely long.

As an example we calculate t_s, t_c, and τ for the example described above:

	H_2O	SiO_2
t_s [a]	$13x10^4$	$3x10^4$
t_c [a]	$9.1x10^4$	$3x10^8$
t	1.43	0.0001

In case of water, significant enrichment at the top of the magma chamber will occur in a time of $13x10^4$ years. No SiO_2-enriched magma will accumulate roofward because the ratio of thermal to compositional buoyancy is greater than one. Although the mass fraction of SiO_2 in the chamber increases with time, most silica will be crystallized before it would have reached the chamber's roof. Trial and Spera (1990) reported that diffusive cross-coupling can significantly increase the transport of a slow diffusing species such as silica. If water is bound on the silicate network it may rise in form of hydroxyl groups together with silica to the topmost layer of the magma chamber and is not able to diffuse in molecular form through the melt.

Finally, another important quantity in a chemically dominated regime is the rate, J, at which liquid from the wallrocks is delivered to the roof of the magma chamber:

$$J = j_w A \qquad (2\text{-}2.2.7)$$

where A is the area of the vertical walls and j_w is the mass flux of the component. For a cylindrical magma chamber with a circumference of 30 km and a height, H, of 10 km, the area, A becomes $300x10^6$ m^2.

Using the example above, the mass rate is equal to $9.93x10^7$ kg a^{-1} (J = 0.331 kg $m^{-2}a^{-1}$ * $300x10^6$ m^2). Within 10^4 years there is $9.93x10^{11}$ kg water accumulated under the roof of the chamber. The mass of the magma chamber is

$\cong 1.72 \times 10^{15}$ kg (density * volume). Assume that the topmost layer which contains the accumulated water is 1% of the total chamber (= 1.7×10^{13} kg), then there is 5.8 wt% water present after 10^4 years.

Vapor Saturation in Boundary Layers

In the previous paragraph water was diffusing only in molecular form or as a cluster of a few molecules dissolved within the magma. As soon as melt becomes saturated with water or other volatiles a separate phase forms. Where saturation is the result of crystallization of anhydrous phases this effect is known as second or resurgent boiling. In a cooling magma that is in homogeneous equilibrium, the separation of a vapor phase can also be the result of a pressure decrease (first boiling). More about the water solubility is written in paragraph 2.2.5.

When crystals nucleate at the wall of a magma chamber, water bubbles either rise separately or in plumes of water + liquid ± crystals. According to Candela (1991) the rising velocities for either a single vapor bubble or a plume containing vapor can be calculated by using a Stokes-like formula. The velocity of a single vapor bubble is given by:

$$U_{bub} = \frac{R^2_{bub}\, g\, \Delta\rho_v}{3\, \eta_m} \qquad (2\text{-}1.2.8)$$

where R_{bub} is the radius of the bubble, g is the acceleration due to gravity, $\Delta\rho_v$ is the density difference of magma and water bubble, and η_m is the viscosity of the magma. The above equation gives an expression of the maximum velocity because thermal convective counter-flow decelerates the bubble velocity.

In the other model, vapor bubbles accumulate in a boundary layer until a certain volume of melt ± crystals becomes light enough to rise as a single, plume-like unit of liquid + gas. The resulting ascent velocity of this bubble-laden plume is

$$U_{plume} = \frac{8\, g\, \Phi_V\, \Delta\rho_V\, D_{H2O}\, t}{9\, \eta_m} \qquad (2\text{-}1.2.9)$$

where $\Phi_V \Delta\rho_V$ is the density contrast between the bubble-laden liquid and the bulk melt, Φ_V is the volume fraction of the vapor, D_{H2O} is the diffusion coefficient of water, and t is the time. In this case, the boundary layer thickness is given by the diffusion distance for water on the time scale for plume rise: $\delta^2 \approx 4 D_{H2O}\, t$.

2.2.3 Volatile Transfer within the Mush Region

A model of volatile transfer moving through the mush region adjacent to the magma chamber is adapted from Candela (1991, Fig. 2-2.6). During crystallization of a magma chamber more and more magma crystallizes at the wall and the solidified boundary migrates towards the center of the chamber. Define a variable F to describe the crystallization process where F varies from 1 (100% liquid) to 0 (100% solid). At some time, the water content becomes saturated in the remaining liquid. As this critical fraction of remaining liquid is reached he defines another variable, Z, the vapor exsolution progress variable. Z is set to unity at the initiation of vapor exsolution and progresses toward zero as vapor is exsolved. The Z = 1 front follows behind the F = 1 front as crystallization proceeds. An immobile mush will develop as a result of increasing viscosity of the crystal + liquid mixture. Vapor bubbles will probably be trapped and can only escape from the site of bubble nucleation through a three dimensional critical

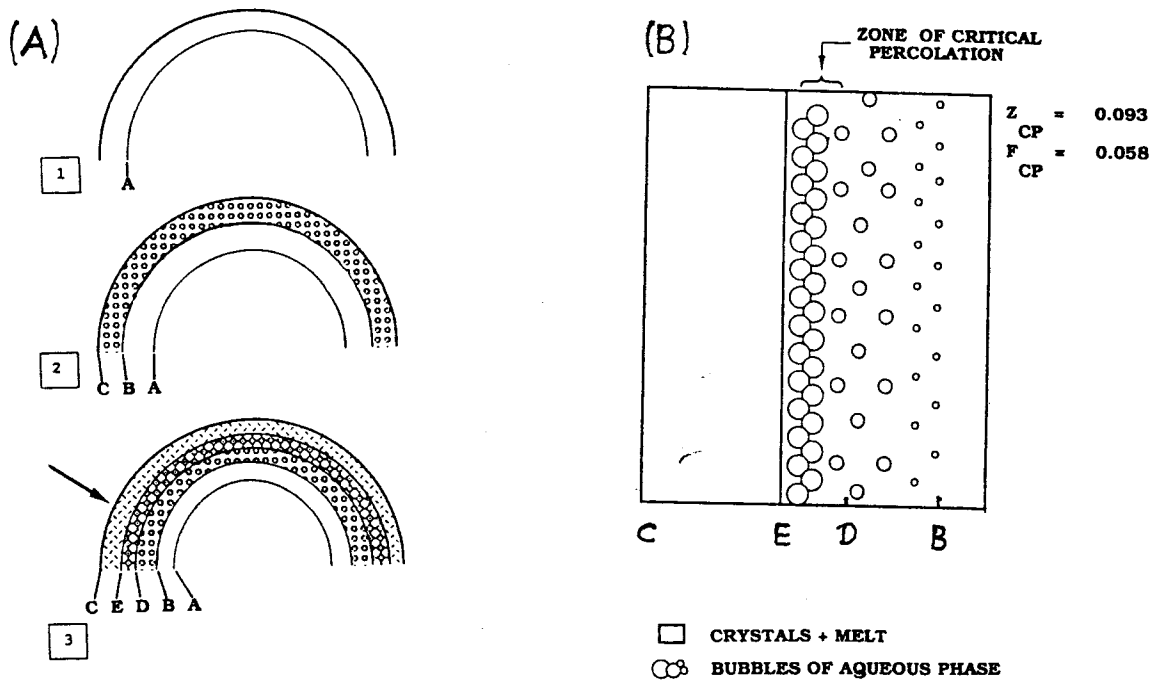

Fig. 2-2.6 : (A) Three stages in the formation of a crystallization interval upon intrusion are shown: A is the leading edge of the crystallization interval, B is the leading edge of the zone of aqueous phase saturation, C is the magma to country rock contact, D is the leading edge of the zone of percolation, and E is the solidus. (B) Sketch to illustrate the production of a spanning cluster of vapor bubbles at critical percolation. Initial H_2O concentration = 2.5%, H_2O saturation = 4%. Under these conditions the critical progress variable of the exsolution of water, Z_{cp}, is 0.093, and the progress variable of crystallization, F_{cp}, is 0.058 (after Candela, 1991).

percolation network or it can be advected through a cracking front that may be formed a few degree below the solidus. Advection of fluid can be possible if the volume fraction of the aqueous phase in the crystallization interval reaches $\approx$ 0.31. Critical percolation is limited in a region between the solidus and a surface characterized by a critical value of Z, the vapor exsolution variable.

Migration of the aqueous phase can be considered as a flow through a porous medium following Darcy's law:

$$w = \frac{K g \Delta\rho_V}{\eta_V} \qquad (2\text{-}2.3.1)$$

where K is the permeability of the matrix, g is the acceleration due to gravity, $\Delta\rho_V$ is the density difference of solidified magma and vapor, and η_V is the viscosity of water. Following Trial and Spera (1990) the average permeability, K, can be expressed as :

$$K = \frac{\varphi^3 a^2}{C (1 - \varphi)^2} \qquad (2\text{-}2.3.2)$$

where C, the Carman constant, represents the tortuosity of the mush, φ is the porosity, and a is the average grain radius within the mush. Here, the porosity φ is equal to Φ_V, the volume fraction of water in the crystallization interval.

The width of the percolation zone is time dependent and given by Brandeis and Jaupart (1986):

$$\delta(t) = 0.3\ \kappa^{1/2}\ Y_{max}^{-9/64}\ I_{max}^{-3/64}\ t^{5/16} \qquad (2\text{-}2.3.3)$$

where κ is the thermal diffusivity, t is the time, Y_{max} and I_{max} represent the maximum intra-mush crystal growth and nucleation rates, respectively.

Knowing the thickness of the critical percolation zone (δ_{CP}) the total volume of percolating water can be calculated by:

$$V = \pi H \int_0^t w\,\delta(t)\,dt \qquad (2\text{-}2.3.4)$$

As an example we use the same variables as above but a few more variables have to be determined: $\Phi_V = \varphi = 0.31$, a = 0.5 mm, η_V = 1000 Pa s, $\Delta\rho_V$ = 1400, $Y_{max} = 10^{-9}$ m s^{-1}, $I_{max} = 10^6$ m^{-3} s^{-1}, C = 1000 m^{-1}. K, the permeability, can be calculated using eqn. (2-2.3.2): $K = 1.56 \times 10^{-11}$. The percolation velocity is 0.64 m a^{-1} (eqn. 2-2.3.1), the thickness of the percolation zone after 10^4 years becomes 11.3 m. Using equation (2-2.3.4), then multiplying with the water's density of 1000 kg m^{-3} the total mass of water accumulated under the roof is 3×10^{12} kg or 15.8wt% by assuming the entire water is present in 1% of the total mass of the magma body.

2.2.4 Water solubility in Magmas

The solubility of water in many natural magmatic systems is limited. McMillan et al. (1986), for example, record water solubilities in a calcium aluminosilicate melt of 1.04 wt% at 25.8 MPa and 9.25 wt% at 513 MPa. In both cases the temperature is about 1180°C. Usually, the solubility of water increases with increasing pressure but decreases with increasing temperature (see e.g. Hamilton et al., 1964, Burnham, 1975 and 1979, Maaløe and Wyllie, 1975, Whitney, 1975, McMillan et al., 1986, and Anderson et al., 1989). The pressure dependence of water solubility for several magmas is shown in Fig. 2-2.7.

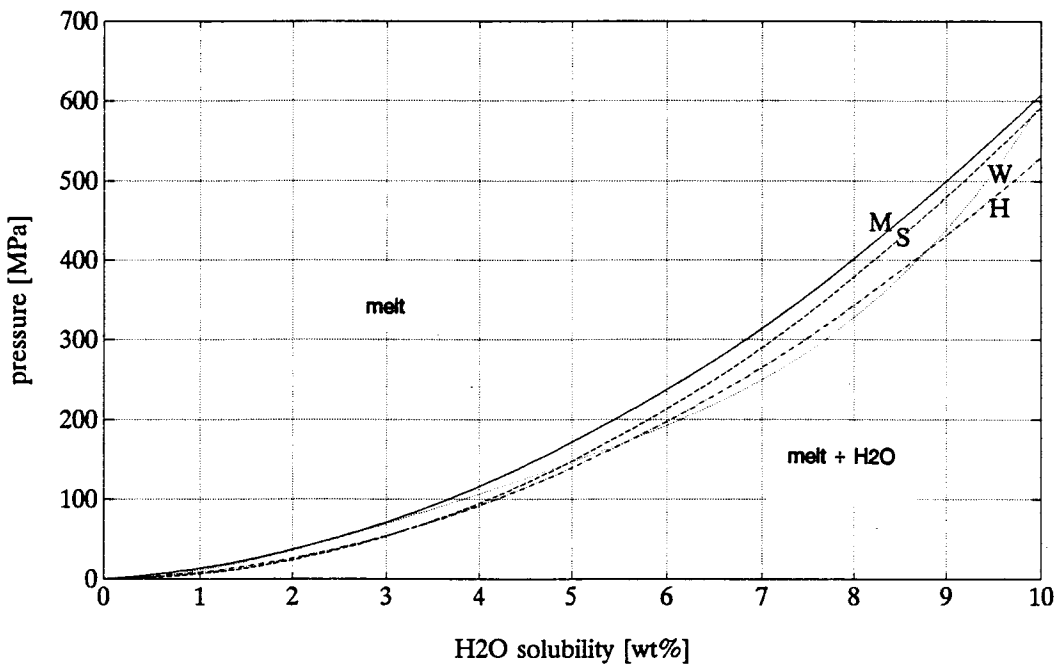

Fig. 2-2.7 : Water solubility in dependance of pressure for several magma types. M: Calcium aluminosilicate melt, 64.6 wt% SiO_2, 1181°C (McMillan et al., 1986), H: Andesite, 58.4 wt% SiO_2, 1100°C, Hamilton (1964), S: Rhyolite, 825°C (Sparks, 1978), W: Quartz monzonite, 71 wt% SiO_2, 900°C (Whitney, 1975). Curves M, H, M are best fit polynomials of data sets.

Keep in mind that a small weight per cent of water represents a large mole fraction because its molecular weight is much smaller than that of other major element oxides. Therefore, the solubility is large enough to change significantly the structure of the melt compared to that under dry conditions. The responsible process that changes the melt structure is linked to bridging oxygens of the silicate network according to the equation:

$$H_2O + \equiv Si-O-Si\equiv \leftrightarrow 2(\equiv Si-OH).$$

Jambon (1982) proposed a model in which the first 2 wt% water content was associated with a dramatic increase in the concentration of hydroxyl groups. In this case most of the molecular water had combined with bridging oxygens to produce OH complexes. This results in a less polymerized melt and an increase in the case of transport of cations. Beyond 2 wt%, water remains in molecular form which does not significantly affect the structure of the melt (Jambon, 1982). Webster (1990) pointed out that the water solubility of water-saturated haplogranite melt varies strongly with melt composition, decreasing from peralkaline melt to quartz-orthoclase melt. A total water content between 5 and 6.4 wt% in melt inclusions in Plinian Bishop rhyolite (California) were measured by Anderson et al. (1989). Rutherford et al. (1985) reported 4.6 (± 1.1) wt% volatiles in rhyodacitic pumice from Mount St. Helens glass inclusions. Sommer (1977) measured between 3.9 and 7.0 wt% water in melt inclusions of quartz phenocrysts from rhyolitic Bandelier tuffs. Melt inclusions of phenocrysts from Taupo rhyolitic tephra yield 4.5 (± 0.8) wt% water (Herwig et al., 1989). This agrees with Dunbar et al. (1989) who reported 4.3, 4.3 and 5.9 wt% water from Taupo magmas as well.

2.2.5 Summary

The most effective process to store water in the uppermost layer of a hot magma chamber which is still in a liquid state is the boundary layer mechanism. This process is based on buoyancy of a lighter melt segregated from the initial magma and accumulated under the roof of the magma body. The differentiated melt at the upper zone is gravitational stable. The development of such a lighter liquid occurs preferentially in a very small zone adjacent to the immobile mush region adjacent to the wall rock. Within such a boundary layer, chemical gradients exist because of different temperature and composition of magma and country rock. The temperature difference leads to melt starting to crystallize at the wall-magma interface. In a calc-alkaline magma, heavy incompatible elements such as iron crystallize first. The resulting lighter residual melt can stream upward. Water with a high diffusivity is enriched in the boundary layer and can be transported to the roof. The boundary layer process is possible if the fluidity of the magma is maintained. Water in an oversaturated melt is transported as a separate phase in form of bubbles or within a plume of crystals, melt and water bubbles. An increase of the magma's viscosity, due to crystallization and cooling, subsequently decelerates the water flow within the boundary layer. Volatile transfer within a percolation network then becomes more important in generating water to the topmost layer of a magma reservoir. The above mechanisms operate simultaneously; boundary layers can develop where the magma is in the liquid state. In addition, water ascent in form of bubbles takes place in a region where magma has crystallized sufficiently to form a separate phase. Transport of water within a percolation network occurs in a more or less immobile mush region adjacent to the country rock.

2.3 Physical Properties of Magmas

2.3.1 Viscosity

In a Newtonian fluid, the shear viscosity, η, is defined as the ratio of shear stress, σ_s, and shear strain rate. Usually magmas are non-Newtonian fluids which have a non-linear relationship between strain rate and shear stress and there can be a certain yield stress, Y, to initiate permanent deformation. The momentum equation for the general case can be written as

$$\sigma_s = Y + \eta \left[\frac{\partial u}{\partial y}\right]^n \qquad (2\text{-}3.1.1)$$

where σ_s is the shear stress parallel to the plane of flow (direction x), $\partial u/\partial y$ is the velocity gradient perpendicular to the plane of shear (shear strain rate), and n is a constant with a value of one or less. The viscosity is dependant on pressure, temperature, composition, volatile content, and crystal content. A good summary of these effects on the viscosities of magmas is given by McBirney and Murase (1984) and in this study only briefly discussed.

The viscosity of silicate melts above their liquidus temperature can be expressed by an Arrhenius type of equation

$$\eta = A_\eta \exp(E_a/RT) \qquad (2\text{-}3.1.2)$$

where A_η is a constant, E_a is the activation energy of viscous flow, R is the universal gas constant, and T is the absolute temperature. In this study $A_\eta = 10^{-4}$ Pa s and $E_a = 293 \times 10^3$ J mol^{-1}.

The viscosity is a reflection of the magma's degree of polymerization. Bottinga and Weill (1972) distinguished between chain formers (Si, Al) which polymerize the melt, and network modifying elements (Ca, K, Na, Mg, Fe, Ti, Al) which tend to depolymerize the melt and therefore reduce its viscosity. Plots of viscosity versus temperature for different types of magma are shown in Fig. 2-3.1. Magmas containing crystals have higher viscosities than crystal-free magmas (McBirney and Murase, 1984).

Water depolymerizes the melt resulting in a decrease in viscosity (Jambon, 1982) whereas CO_2 tends to increase the polymerization. Fig. 2-3.2 shows the effect of water on the viscosity of a basaltic liquid.

Load pressure reduces the viscosity (Kushiro, 1980) and with increasing time the melt becomes more viscous (McBirney and Murase, 1984).

2.3.2 Density

The density depends on composition, pressure, and temperature. In Fig. 2-2.4a the temperature relationship is shown for different magma types. Marsh (1984) gives a mathematical expression for the density variation due to a temperature variation:

$$\rho = \rho_0 \exp(-\alpha_T \Delta T) \qquad (2\text{-}3.2.1)$$

in which ρ_0 is the reference density, α_T is the thermal expansion, and ΔT is the temperature difference. The variation of the density during magma differentiation is demonstrated in Fig. 2-2.4b and is discussed in more detail in chapter 2.2.2. In this study $\rho_0 = 2500$ kg m^3 and $\alpha_T = 5 \times 10^{-5}$ K^{-1}.

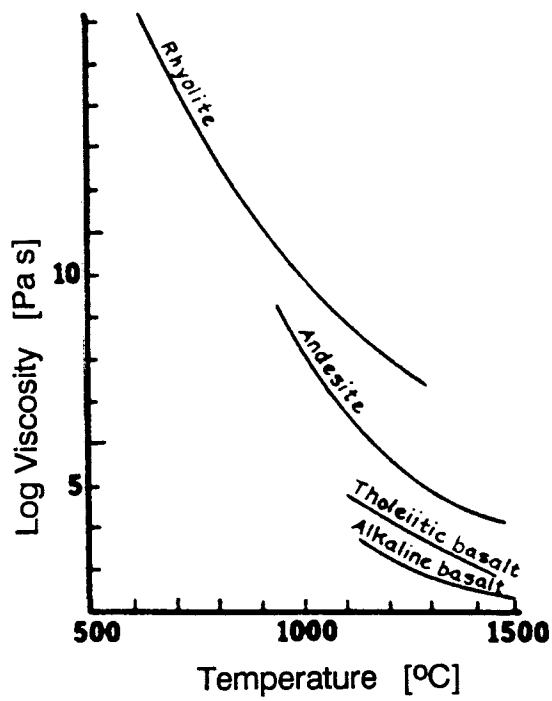

Fig. 2-3.1 : The effect of temperature on the viscosities of some igneous rocks (after McBirney and Murase 1984).

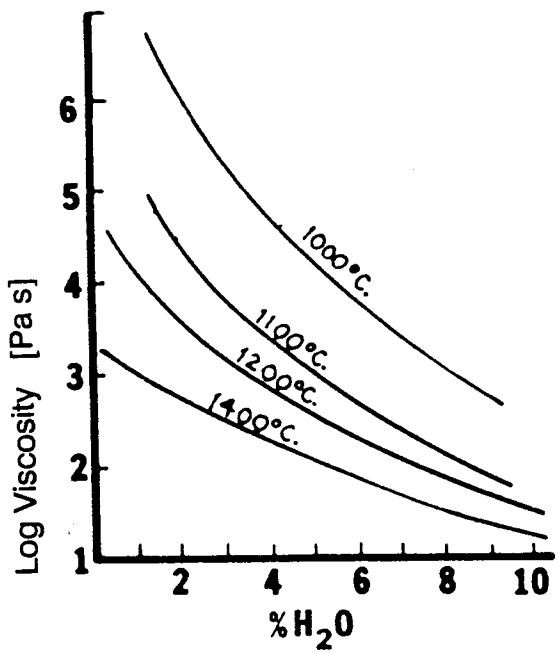

Fig. 2-3.2 : Variation of the viscosity of basaltic liquids with their water contents (after McBirney and Murase, 1984).

2.3.3 Thermal Variables

The thermal variables used in this study are heat capacity, C_p, temperature diffusivity, κ, and heat conductivity, k, which are related in the following way

$$\kappa = k / \rho C_p \qquad (2\text{-}3.3.1)$$

where ρ is the density. The thermal conductivity and specific heat for magma and host rock can be determined from the equations used by Wells (1980).

$$k = (0.311 + 1.72\text{x}10^{-4} T)^{-1} + 2.1\text{x}10^{-3} (T - 800) \qquad (2\text{-}3.3.2)$$

$$C_p = 753 + 0.46 T - 1.45\text{x}10^{7} / T^2 \qquad (2\text{-}3.3.3)$$

where T is the absolute temperature in Kelvin. Typical values of viscosity, thermal conductivity and heat capacity for different temperatures are:

T [K]	η [Pa s]	k [J m^{-1} s^{-1}]	C_p [J kg^{-1} K^{-1}]
1273	$1.05\text{x}10^{8}$	2.88	1330
1073	$1.83\text{x}10^{10}$	2.59	1234
873	$3.40\text{x}10^{13}$	2.32	1136
673	$5.51\text{x}10^{18}$	2.08	1031

Chapter III: Stresses within and around Magma Chambers

3.0 Introduction

The purpose of this chapter is to describe the stress field within and around a magma chamber. Stresses are important in understanding the behavior of a material. In this study, it is of particular interest to know the stress distribution within the rock surrounding an intruding magma. There are two principal processes that can induce stresses. First, magma can rise up to the earth's surface and second, material can be expanded. Buoyancy is the driving force for magma ascent. In this case the host rock is considered as a highly viscous material that descends past the magma body. Expansion can be both the magma body itself and the surrounding material can expand. The latter case is caused by heat conduction from the hot magma into the host rock. If material is heated it expands, but if expansion is limited by any kind of confinement the stress inside this material will increase. This kind of stress is known as thermal stress. In the former case the magma chamber itself can expand if melt becomes oversaturated with volatiles. At this condition vapor-bubbles appear and occupy more space than when the volatiles were dissolved. The amount of bubble's expansion is limited by the response of the host rock.

3.1 Magma Chamber Expansion

The processes in view are, of course, continuous but for the purpose of developing qualitative relations we fix on some particular location for the magma chamber and consider its state at that location. At least initially, the mechanical ideas used apply to just this location and are drawn from statics.

Key quantities are (i) the volume of the chamber, (ii) the amount of volatiles that have exsolved into the vapor state, and (iii), the excess pressure above the lithostatic pressure for the depth considered. These are three interrelated unknowns; to estimate magnitudes we write three equations involving them, by considering three different aspects of the geological situation,

(i) the pressure-volume relations for magma chamber contents (magma + water bubbles);

(ii) the solubility-pressure relation for volatiles dissolved in magma;

(iii) the mechanical relation between strain in the host rock, the excess pressure in the chamber and the chamber's volume.

3.1.1 Volume Development of the Magma Chamber

Consider a silicic magma that undergoes progressive hydration due to liquid fractionation and crystallization (see chapter 2). Water-rich magma accumulates under the roof because it is less dense than underlying magma. When the maximum solubility of water is reached, magma becomes oversaturated and H_2O will form a separate phase. This second-boiling reaction where melt → crystals and H_2O takes place with an increase in volume and requires the surroundings to move aside (Burnham, 1979). This is achieved by compression of the underlying magma (Blake, 1984). If the surrounding rock is less compressible than the melt, host rock cannot deform as much as the volume of the gas would require which leads to an increase in magma pressure. Let V_{li} be the initial volume of supersaturated magma at a lithostatic pressure p_o at the topmost region of a magma chamber and V_{mi} be the remaining initial undersaturated part of magma below this layer (Fig. 3-1.1). When the magma becomes oversaturated the following volume balance has to be satisfied:

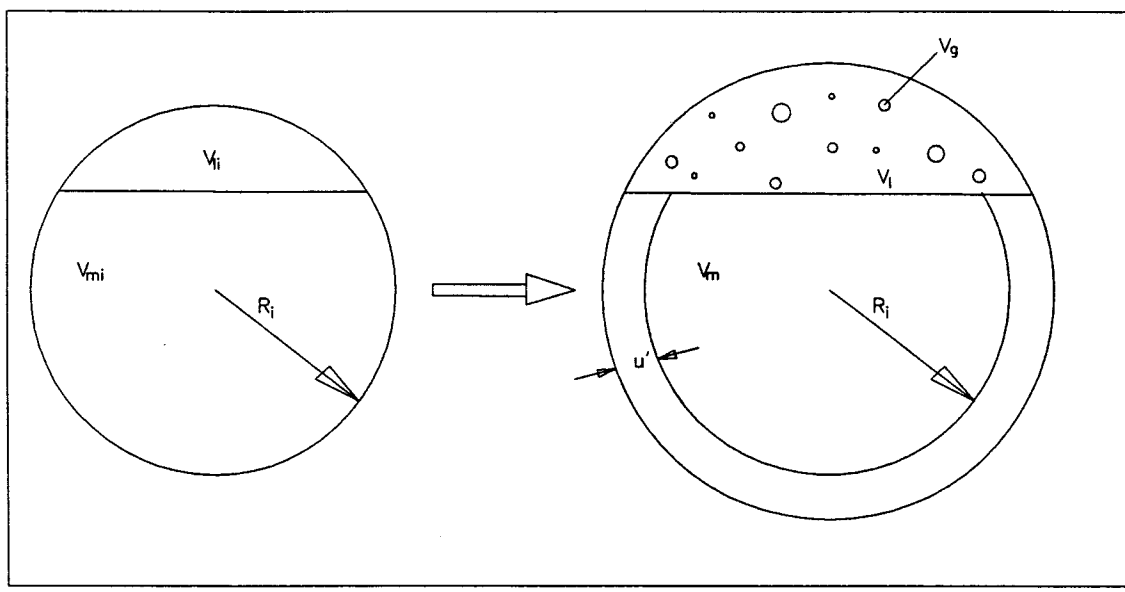

Fig. 3-1.1: Sketch of a magma chamber with an initial volume, V_{ci}, equal to $V_{li} + V_{mi}$ where V_{li} is the volume of the upper supersaturated layer, and V_{mi} is the remaining undersaturated volume. On vesiculation, this chamber evolves into a state where the upper region has become saturated containing both, gas (V_g) and melt (V_m), in an expanded chamber of volume $V_c = (V_{li} + V_{mi})(1 + S)$. u is the radial displacement. The separation of the supersaturated magma into two phases causes a pressure increase and compression of the undersaturated part of the chamber (V_m).

$$V_g + V_l + V_m = (V_{li} + V_{mi})(1 + S) \qquad (3\text{-}1.1.1)$$

where V_g and V_l are the volumes of water and coexisting silicate liquid, V_m is the volume of the remaining, undersaturated, magma at pressure p, and S is the volume strain or the fractional amount of chamber expansion (Blake, 1984).

Assume a silicic magma as a compressible fluid with constant bulk modulus b and mass M. Note that the bulk modulus is the inverse of the compressibility. The pressure dependence of its density is given by

$$\rho_l = M / V_l = \rho_{li} \exp(\Delta p/b) \qquad (3\text{-}1.1.2)$$

where ρ_{li} is the density of the initial undersaturated magma, and Δp is the pressure difference of the current pressure inside, (p_i), and the pressure outside, (p_o), the magma chamber. In the present situation, pressure rises because of vesiculation of the magma. If the mass of supersaturated magma remains constant during vesiculation it follows that

$$V_l = V_{li} \exp(-\Delta p/b) \qquad (3\text{-}1.1.3)$$

and similarly,

$$V_m = V_{mi} \exp(-\Delta p/b) \qquad (3\text{-}1.1.4)$$

Usually the ratio $\Delta p/b$ is very small, so that V_l and V_m are approximately

$$V_l = V_{li} (1 - \Delta p/b) \qquad (3\text{-}1.1.5)$$

$$V_m = V_{mi} (1 - \Delta p/b) \qquad (3\text{-}1.1.6)$$

Murase and McBirney (1973) showed that the bulk modulus is more or less constant if the temperature is ≤ 800 °C. For rhyolite, b is about 30 GPa.

The density of the gas is defined as

$$\rho_g = N / V_g = m / V' \qquad (3\text{-}1.1.7)$$

where N is the mass, V' is the molar volume and m is the molar mass (0.018 kg/mol for water) of the gas. The molar volume V' is pressure and temperature dependant. Assuming water as an ideal gas then

$$V' = RT / p_i \qquad (3\text{-}1.1.8)$$

where R is the universal gas constant (8.31433 J mol^{-1} K^{-1}), T is the absolute temperature, and p_i is the current pressure inside the magma chamber. Table 3-1 shows the molar volume of water as an ideal - and a non-ideal gas as it varies with pressure. Between 0 and 300 MPa there is less than 13% deviation from the ideal behavior. Therefore, calculations are accurate enough taking water as an ideal gas.

The mass fraction of exsolved water can be expressed as

$$n = N / (N + M) \qquad (3\text{-}1.1.9)$$

where N and M are the mass of gas and upper magma, respectively. Using equation (3-1.1.7), (3-1.1.8), (3-1.1.9), and with $M = \rho_{li} V_{li}$ the volume of the gas in the topmost region of the chamber can be expressed as

$$V_g = \frac{n}{(1 - n)} \frac{(\rho_{li} V_{li} R T)}{m p_i} \qquad (3\text{-}1.1.10)$$

Substituting equations (3-1.1.5), (3-1.1.6), and (3-1.1.10) into (3-1.1.1) gives the first equation with the three unknown p_i, S and n:

$$p_i^2 + p_i (p_o - S b) - \frac{n}{(1 - n)} \frac{\rho_{li} R T b}{(1 + V) m} = 0 \qquad (3\text{-}1.1.11)$$

Table 3-1

pressure [MPa]	V of H2O [cm3] * 800 C	V ideal [cm3] 800 C
10	873.729	892.128
20	428.135	446.064
30	280.026	297.376
40	206.345	223.032
50	162.478	178.426
100	77.881	89.213
200	42.315	44.606
300	32.770	29.738
400	28.335	22.303
500	25.699	17.843
600	23.910	14.869

* Data taken from Halbach and Chatterjee (1982)

with

$$V = V_{mi} / V_{li}$$

3.1.2 Solubility Relation

The total mass fraction of water in the upper magma can be expressed as

$$W = n + (1 - n)W_s \qquad (3\text{-}1.2.1)$$

where W is the total amount of water in the oversaturated melt (as mass fraction), and W_s is the maximum mass fraction of water dissolved within the magma at equilibrium. In Fig. 2-2.7 the solubility of several magma types at different temperatures are shown as a function of pressure. One approximation of W_s for rhyolitic melts at 825°C is given by Sparks (1978):

$$W_s = 4.11 \times 10^{-6} \sqrt{p_i} \qquad (3\text{-}1.2.2)$$

If we are willing to assume some possible values for W, then for any single assumed value, equations (3-1.2.1) and (3-1.2.2) together provide a second relation between n and p_i (S is not involved).

3.1.3 Volume Strain and Thermal-Elastic Response

The magma chamber expansion is a function of temperature and pressure. Consider a magma reservoir as a hollow sphere with an internal radius R_i embedded in a thick shell with an outer radius R_o (Fig. 3-1.2). Let the total volume of the sphere be

$$V_{ci} = \frac{4}{3} \pi R_i^3 \qquad (3\text{-}1.3.1)$$

Suppose the surrounding material is isotropic and deforms elastically when the sphere expands. If the pressure inside the sphere is hydrostatic it will expand equally in radial distance. The total volume of the expanded chamber then becomes

$$V_c = \frac{4}{3}\pi (R_i + u')^3 \qquad (3\text{-}1.3.2)$$

where u' is the radial displacement of the interface of magma and host rock. The volume strain, S, is defined as

$$S = \frac{\Delta V}{V_{ci}} = \frac{(V_c - V_{ci})}{V_{ci}} \qquad (3\text{-}1.3.3)$$

or

$$S = \frac{3u'}{R_i} + \frac{u'^2}{R_i^2} + \frac{u'^3}{R_i^3} \qquad (3\text{-}1.3.4)$$

if $u' << R_i$ then S reduces to

$$S = 3u'/R_i \qquad (3\text{-}1.3.5)$$

For the following discussion of mechanics, we work with u' rather than with S. To calculate the radial displacement, u', consider the magma chamber as a sphere in which the temperature distribution is symmetrical with respect to the center and is therefore a function of r, the radial distance, alone. Since the body forces are neglected the thermal-elastic stress-strain formulation in spherical coordinates is used (Saada, 1974):

$$\frac{d}{dr}\left[\frac{1}{r^2}\frac{d}{dr}(r^2 u)\right] = \frac{1+\nu}{1-\nu}\alpha_T \frac{d}{dr}(\Delta T) \qquad (3\text{-}1.3.6)$$

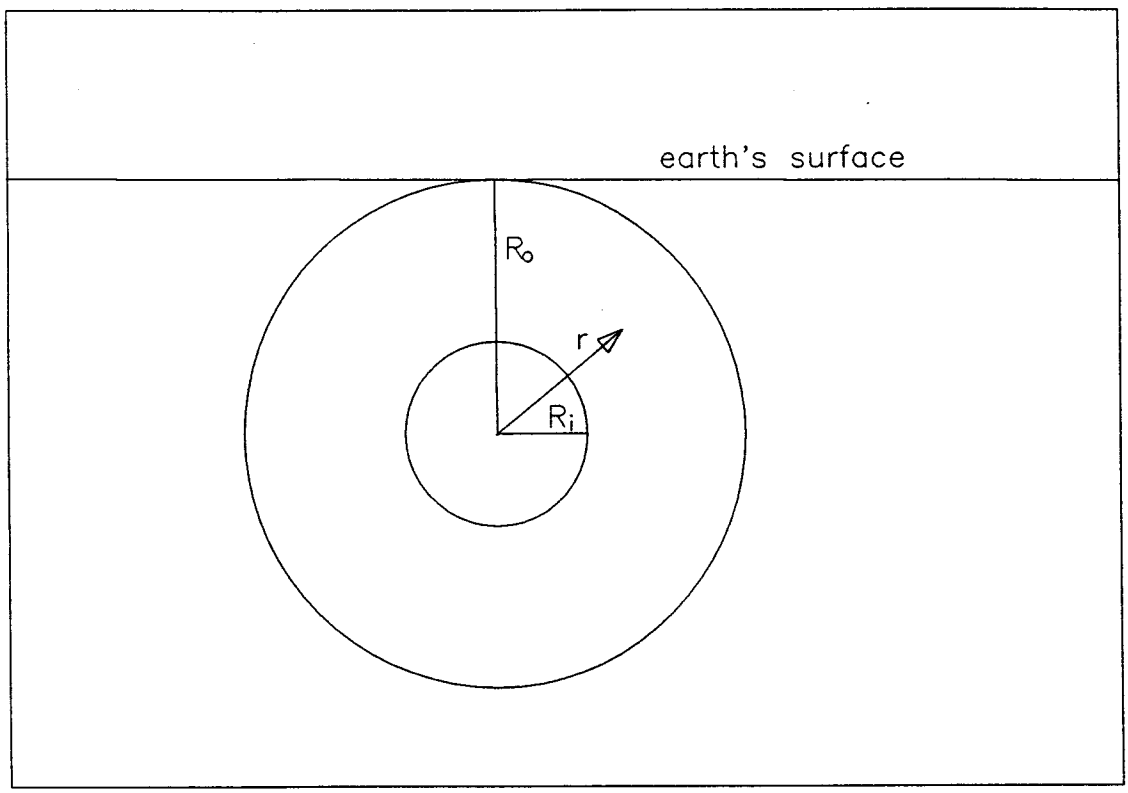

Fig. 3-1.2: Schematic representation of a silicic magma chamber with radius R_i embedded in a thick shell with an outer radius R_o. The position vector, r, describes any point within the shell. A real magma chamber is confined not by a spherical shell but by the whole of the earth. Let h be the distance from the center of the chamber to the earth's surface at its nearest point. By choosing R_o equal to h as shown in the figure, we make the confinement provided by the sphere approximately equal to the confinement that would be provided by the earth. To represent a magma ascending, R_o would be decrease with time.

where u is the radial displacement of a point at distance r, ν is the Poisson's ratio, α_T is the linear thermal expansion, and ΔT, the temperature difference of magma and host rock, is a function of time and distance. The general solution of equation (3-1.3.6) is given by

$$u = \frac{(1+\nu)\,\alpha_T}{(1-\nu)\,r^2}\int_{R_i}^{R_o}(\Delta T)r^2\,dr + C_1 r + \frac{C_2}{r^2} \qquad (3\text{-}1.3.7)$$

where C_1 and C_2 are the constants of integration. R_i and R_o are the inner and outer radius of the hollow sphere, respectively. From Hooke's Law, the non-zero stress components are directly obtained from the stress-strain relations. They are:

$$\sigma_{rr} = \left[-\frac{2\alpha_T E}{(1-\nu)r^3}\int_{R_i}^{r}(\Delta T)r^2\,dr\right] + \frac{E\,C_1}{(1-2\nu)} - \frac{2\,E\,C_2}{(1+\nu)r^3} \qquad (3\text{-}1.3.8a)$$

$$\sigma_{\theta\theta} = \left[\frac{\alpha_T E}{(1-\nu)r^3}\int_{R_i}^{r}(\Delta T)r^2\,dr\right] + \frac{E\,C_1}{(1-2\nu)} + \frac{E\,C_2}{(1+\nu)r^3} - \frac{\alpha_T E\,(\Delta T)}{(1-\nu)} \qquad (3\text{-}1.3.8b)$$

where E is the Young's modulus. For a hollow sphere with inner radius R_i, the boundary conditions are:

$\sigma_{rr} = -\Delta p$ at $r = R_i$

$\sigma_{rr} = 0$ at $r = R_o$

Therefore

$$\frac{E\,C_1}{(1-2\nu)} - \frac{2\,E\,C_2}{(1+\nu)R_i^3} = -\Delta p$$

and

$$-\frac{2\alpha_T E}{(1-\nu)R_o^3}\int_{R_i}^{R_o}(\Delta T)r^2\,dr + \frac{E\,C_1}{(1-2\nu)} - \frac{2\,E\,C_2}{(1+\nu)R_o^3} = 0$$

Solving for C_1 and C_2, and substituting the results into equations (3-1.3.8a,b), the stress components are:

$$\sigma_{rr} = -\frac{2\alpha_T E}{(1-\nu)\,r^3}\left[T^*_r - T^*_{Ro}\,\mathcal{A}\right] - \Delta p\,\frac{R_i^3}{r^3}\,\mathcal{B} \qquad (3\text{-}1.3.9a)$$

$$\sigma_{\theta\theta} = \frac{\alpha_T E}{(1-\nu)\,r^3}\left[T^*_r + 2T^*_{Ro}\,\mathcal{C}\right] + \frac{1}{2}\Delta p\,\frac{R_i^3}{r^3}\,\mathcal{D} - \frac{\alpha_T E\,(\Delta T)}{(1-\nu)} \qquad (3\text{-}1.3.9b)$$

with:

$$T^*_r = \int_{R_i}^{r}(\Delta T)r^2\,dr \qquad T^*_{Ro} = \int_{R_i}^{Ro}(\Delta T)r^2\,dr$$

$$\mathcal{A} = \frac{r^3 - R_i^3}{R_o^3 - R_i^3} \qquad \mathcal{B} = \frac{R_o^3 - r^3}{R_o^3 - R_i^3}$$

$$\mathcal{C} = \frac{r^3 + R_i^3}{R_o^3 - R_i^3} \qquad \mathcal{D} = \frac{R_o^3 + 2r^3}{R_o^3 - R_i^3}$$

Tensile stresses have a positive sign and compressive stress components are negative. For an infinite surrounding medium the results simplify to:

$$\sigma_{rr} = -\frac{2\alpha_T E}{(1-\nu)\,r^3}\,T^*_r - \Delta p\,\frac{R_i^3}{r^3} \qquad (3\text{-}1.3.10a)$$

$$\sigma_{\theta\theta} = \frac{\alpha_T E}{(1-\nu)\,r^3}\,T^*_r + \frac{1}{2}\Delta p\,\frac{R_i^3}{r^3} - \frac{\alpha_T E\,(\Delta T)}{(1-\nu)} \qquad (3\text{-}1.3.10b)$$

The radial displacement becomes

$$u = \frac{(1 + \nu)\,\alpha_T}{(1 - \nu)\,r^2}\left[T^*_r + \frac{T^*_{Ro}\,\mathcal{M}}{(1 + \nu)}\right] + \frac{\Delta p\,\mathcal{N}}{2E\,r^2} \qquad (3\text{-}1.3.11)$$

with

$$\mathcal{M} = \frac{2(1 - 2\nu)\,r^3 + (1 + \nu)\,R_i^3}{R_o^3 - R_i^3}$$

$$\mathcal{N} = \frac{2(1 - 2\nu)R_i^3\,r^3 + (1 + \nu)\,R_i^3\,R_o^3}{R_o^3 - R_i^3}$$

Lastly, the volume strain or the fractional amount of magma chamber expansion at the interface magma - host rock has to be calculated by inserting equation (3-1.3.11) into (3-1.3.5) at $r = R_i$:

$$S = \frac{9\,\alpha_T\,T^*_{Ro}}{R_o^3 - R_i^3} + \frac{3\,\Delta p\,K_m}{2\,E} \qquad (3\text{-}1.3.12)$$

with:

$$K_m = \frac{R_o^3(1 + \nu) + 2R_i^3(1 - 2\nu)}{R_o^3 - R_i^3}$$

Equation (3-1.3.12) is the third of the equations we need for finding p_i, n, and S. If the outer radius of the hollow sphere, R_o, goes to infinity equation (3-1.3.12) simply reduces to

$$S = \Delta p\,\frac{3(1 + \nu)}{2E} \qquad (3\text{-}1.3.13)$$

3.1.4 Pressure inside the Magma Chamber

The current pressure within the magma chamber can be calculated by combining thermal-elastic displacements of host rock with magma chamber expansion. The equations to uses are (3-1.3.12) and (3-1.1.11). Solving for p_i yields

$$p_i = \frac{p_o}{2} - \frac{\alpha_T T^*_{Ro}}{2D(R_o^3 - R_i^3)} + \sqrt{\left[\frac{p_o}{2} - \frac{\alpha_T T^*_{Ro}}{2D(R_o^3 - R_i^3)}\right]^2 + \frac{n \rho_{li} R T_m}{(1 - n) m (1 + V)D}} \qquad (3\text{-}1.4.1)$$

with:

$$D = \left[\frac{1}{b} + \frac{3 K_m}{2 E}\right]$$

To calculate the current pressure inside the magma chamber at different levels in the earth's crust, equations (3-1.4.1), (3-1.2.1), and (3-1.2.2) have to be solved simultaneously. This can be done numerically with an iteration procedure. In an environment without tectonic activity the difference of lithostatic (p_o) and magma pressure (p_i) is the excess pressure responsible to deform or fracture the surrounding material, which we write as Δp.

3.1.5 Example and Discussion

As a typical geological example for calculating the pressure development inside a magma reservoir with radius R_i = 5 km, the following variables are kept constant: ρ_h = 2500 kg m^{-3}, b = 3×10^{10} Pa, E = 5×10^{10} Pa, ν = 0.25, m = 0.018 kg mol^{-1}, R = 8.3143 J $mol^{-1}K^{-1}$, T_m = 1073 K, T_h = 473 K, α_T = 5×10^{-5} K^{-1}, κ = 1×10^{-6} $m^2 s^{-1}$. Suppose a chemically identical host rock and magma body, then

the magmas density, ρ_m, can be calculated by using equation. (2-3.2.1): ρ_m = 2425 kg m^{-3}.

The next step is to calculate the integral

$$T^*_{Ro} = \int_{R_i}^{R_o} \Delta T\, r^2\, dr$$

As a first approximation this value is kept constant by assuming a temperature distribution within the country rock that is constant in time (Fig. 2-1.5). T^*_{Ro} = 10^{12} K m^3 after 300 years, for example.

Fig. 3-1.3 shows the variation of Δp with depth to the crest of the chamber. The ratio of undersaturated to supersaturated volume, V, is assumed to be 100 in all calculations. If 6% of total water is present in the supersaturated layer of the magma chamber there exists only a tiny overpressure of about 2 MPa at 8 km depth. The depth is calculated from the lithostatic pressure in the following way:

$$\text{depth} = \frac{p_o}{g\,\rho_h} \qquad (3\text{-}1.5.1)$$

where g is the acceleration due to gravity (g = 10 m s^{-2}). For example, the depth = 8 km if p_o = 200 MPa (see point a). Rising of the magma chamber with lowering the lithostatic pressure effects an increase in magma pressure with a maximum of $\approx$34 MPa at about 1 km depth (point b). If during magma ascent the water content increases Δp would increase more rapidly.

In all the calculations for this figure, the same temperature profile has been assumed (with T^*_{Ro} = 1×10^{12} K m^3 as above) and the same volume ratio V of undersaturated magma to supersaturated. In a real situation, the temperature

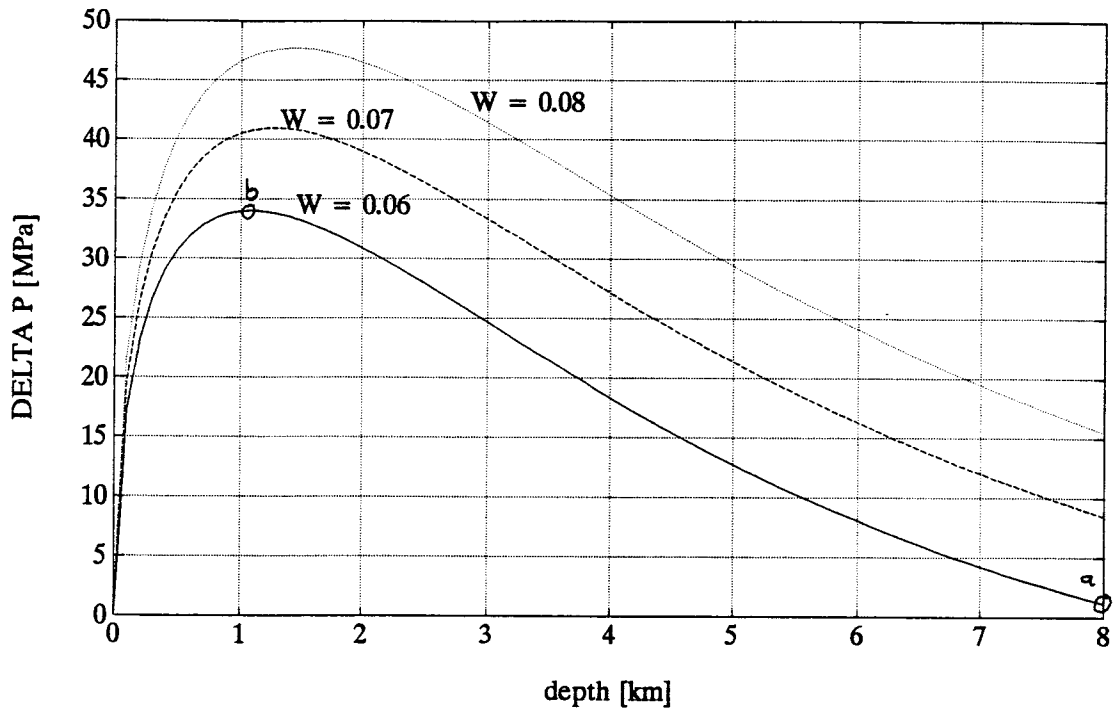

Fig. 3-1.3: Overpressure (Δp) versus depth. Lines are plotted for chamber's inside the earth's crust that contain different amounts of total water (W = 6,7, and 8 wt%). V = 100; for other variables see text. Because the depth scale runs from left to right, the process of an ascending magma can be followed by reading the diagram from right to left.

profile and the ratio V would both change as the magma rose to shallower depths, with effects as described next.

The effect of the volume of the topmost region containing supersaturated magma (V_{li} in Fig. 3.1.1) is demonstrated in Fig. 3-1.4. A small layer of magma (V = 200) with 6% water effects only a small overpressure. If a larger amount of magma contains the same percentage of total water (V = 50) the current magma pressure is much higher. During differentiation and stratification, the ratio V (volume undersaturated / volume saturated) could diminish e.g. V = 200 when depth = 8 km but V = 50 when depth = 3 km; the increase of Δp as magma ascends would then be steeper than the profiles in Fig. 3.1.4.

In Fig. 3-1.5 the excess pressure Δp is calculated for different T^*_{Ro} values plotted against depth. A T^*_{Ro} value of 0 K m^3 results in a distinct maximum of 36 MPa at 1 km depth whereas a higher T^*_{Ro} value (10×10^{12} K m^3) produces a maximum of 22 MPa at 1.5 km depth. The highest pressure is reached when the temperature effect is least (top curve, $T^*_{Ro} = 0$); Δp becomes negative at the right-hand side of the diagram. Both of these features result from the same fact, that heating the host rock produces outward displacement and an increase in volume of the chamber. This is so at least under the assumption of ideal elastic behavior which we are currently using, with $\nu = 0.25$; see first term on the right-hand side of the equation (3-1.3.12) for the expansion factor, S. The essential point is the strong heating of the host rock close to the magma chamber. The expansion of this hot shell is best accommodated by the whole shell moving outward to larger radius. This contrast with the behavior one would see if the entire host region were heated uniformly; in this case, its thermal expansion would lead to the cavity getting smaller. With strong local heating of just the innermost

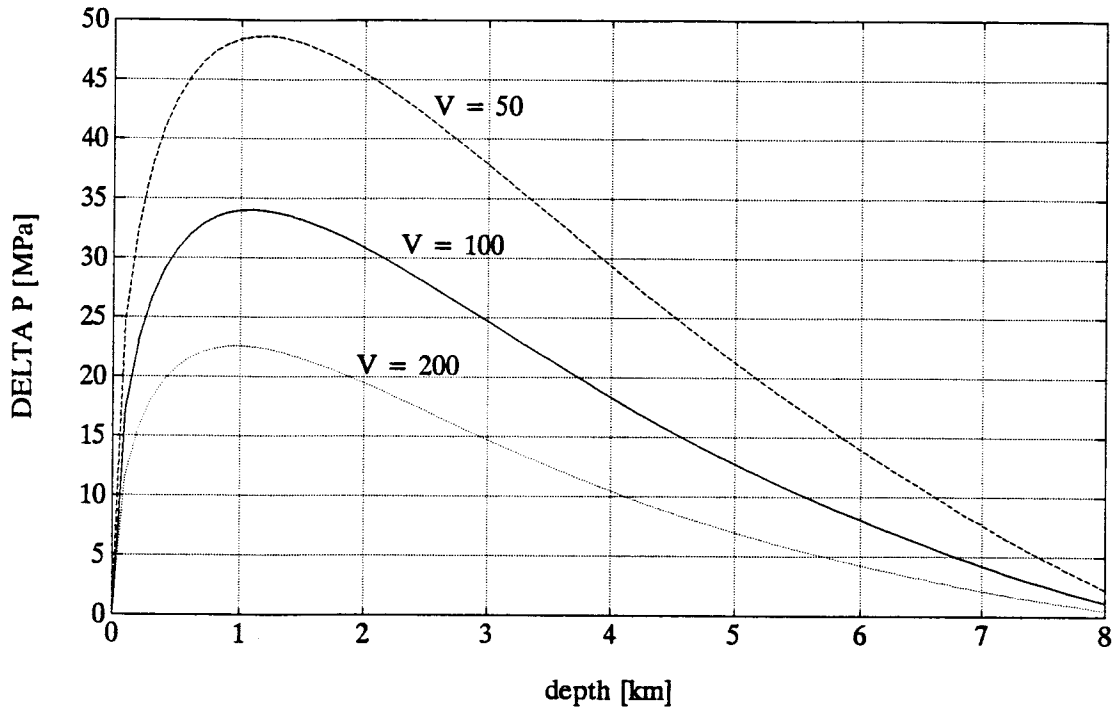

Fig. 3-1.4: A plot of overpressure (Δp) versus depth for different ratios of undersaturated to supersaturated magma volumes. W, the total water content, is fixed at 6%. For other variables see text.

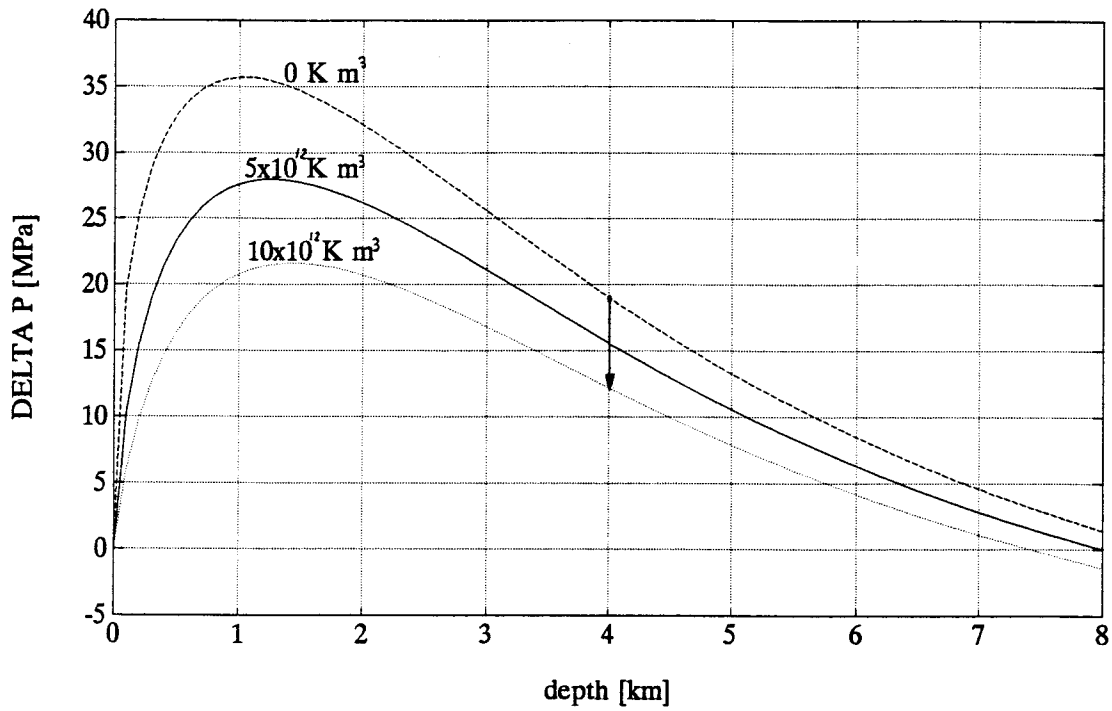

Fig. 3-1.5: Variation of Δp versus depth calculated for different values of T^*_{Ro}. V and W are kept constant at 100 and 0.06, respectively. For other variables see text.

shell, this shell expands outward despite the fact that host rock farther out is also heating up and expanding. As equation (3-1.3.11) shows, the effect is governed by the sign of $\mathcal{M}$, which is governed in turn by Poisson's ratio ν; at least for large ν, heating the host produces outward displacement of the host and so diminishes the pressure build-up due to vesiculation.

Now, we follow the history of a magma chamber fixed at a particular location at 4 km depth. With time the magma cools down and the host rock becomes heated. At a time, t, equals zero the integral T^*_{Ro} = 0 K m^3. This results in an overpressure of 18 MPa (Fig. 3-1.5). As time goes on T^*_{Ro} gets bigger but Δp decreases with time (see arrow in Fig. 3-1.5). $T^*_{Ro} \cong 10 \times 10^{12}$ K m^3 after 20×10^3 years and Δp = 12 MPa. If the chamber ascends Δp decreases more slowly or increases slowly because the chamber gets into shallower depth.

To get a first impression of the stress state of the host rock, we go back to considering a stationary magma chamber and use equation (3-1.3.9). The stress distribution in the host rock is calculated for two different times, 10^3 and 10^4 years after intrusion. The depth of the magma reservoir is fixed at 8 km and the overpressure, Δp, is kept constant at 5 MPa but the temperature changes with time according to equation (2-1.4.3b). All other variables are taken from above. The radial and tangential stress components are shown in Fig. 3-1.6. At the interface magma - host rock the radial stresses are compressive and their magnitudes are equal to the excess pressure Δp. With increasing distance away from the interface they increase to a maximum at about 200 m and 800 m distance at t = 10^3 and 10^4 years, respectively; then decrease to zero at the earth's surface. The tangential stress components are also compressive at the interface with -1.326 GPa and -1.294 GPa for t = 10^3 years and t = 10^4 years,

respectively. Then, their magnitudes decrease dramatically with increasing distance and become tensile at about 500 m (10^3 years) and 1200 (10^4 years) m distance and reach a maximum in tensile stress at 600 m and 2000 m for t = 10^3 and 10^3, respectively. From this distance their magnitudes decrease and reach 8 MPa for t = 10^3 years and 36 MPa for t = 10^4 years at the earth's surface. We continue to assume ideal elastic behavior without interfering effects such as fractures which such stresses could readily produce in less idealized materials.

The Young's modulus, E, and the thermal expansion, α_T, of the host rock have strong influence on the stress distribution which is shown in Fig. 3-1.7 for the radial and tangential stress components. The stress magnitude is the less the more elastic the material behaves and the less it expands during heating. The Poisson's ratio has not such a strong influence on the stress magnitudes.

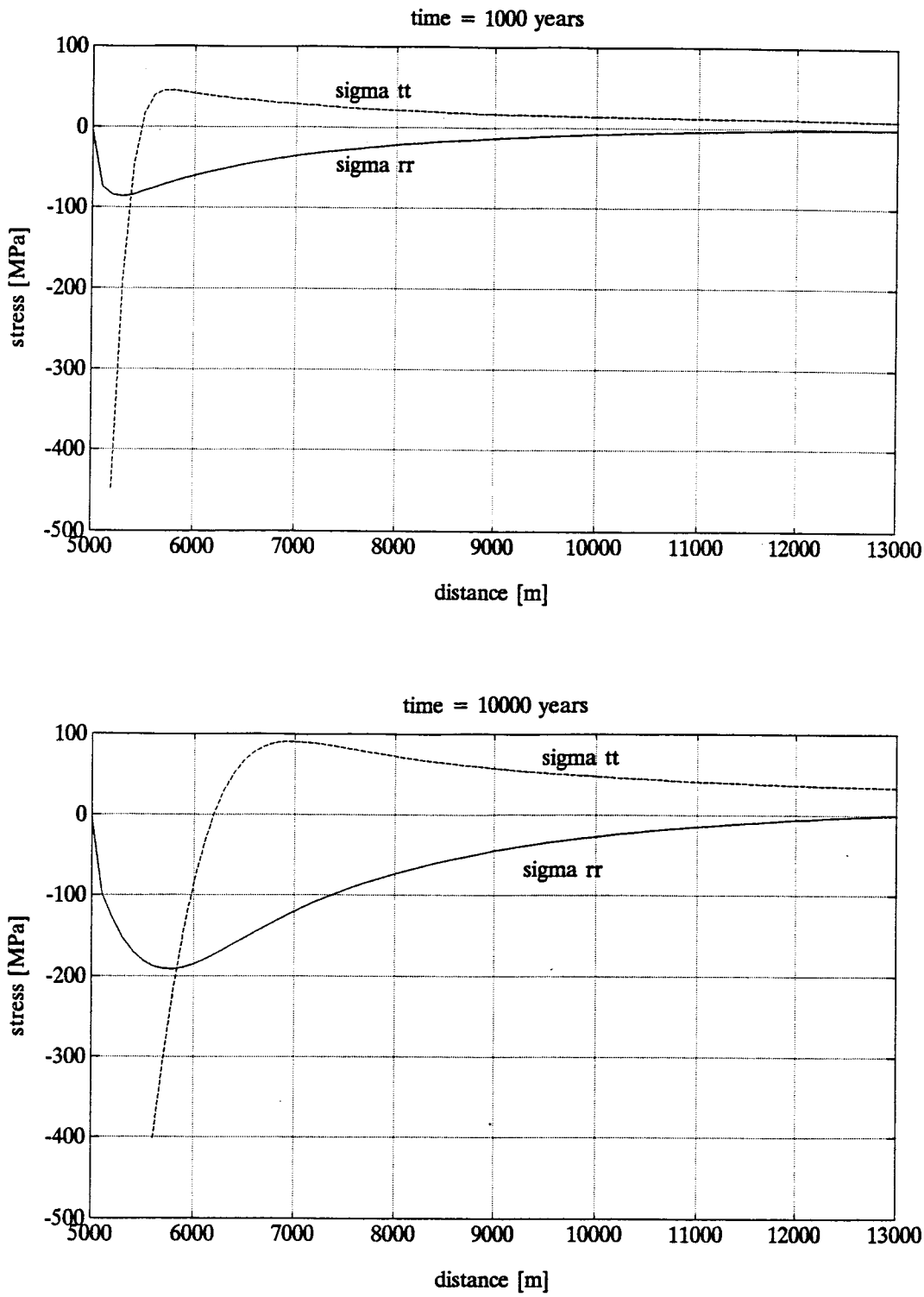

Fig. 3-1.6: Radial and tangential stress components as functions of distance calculated for two different times, t = 10^3 years and t = 10^4 years. 5000 m indicates the interface of magma and host rock and 13000 m represents the earth's surface since $\theta = 0^o$. For other variables see text.

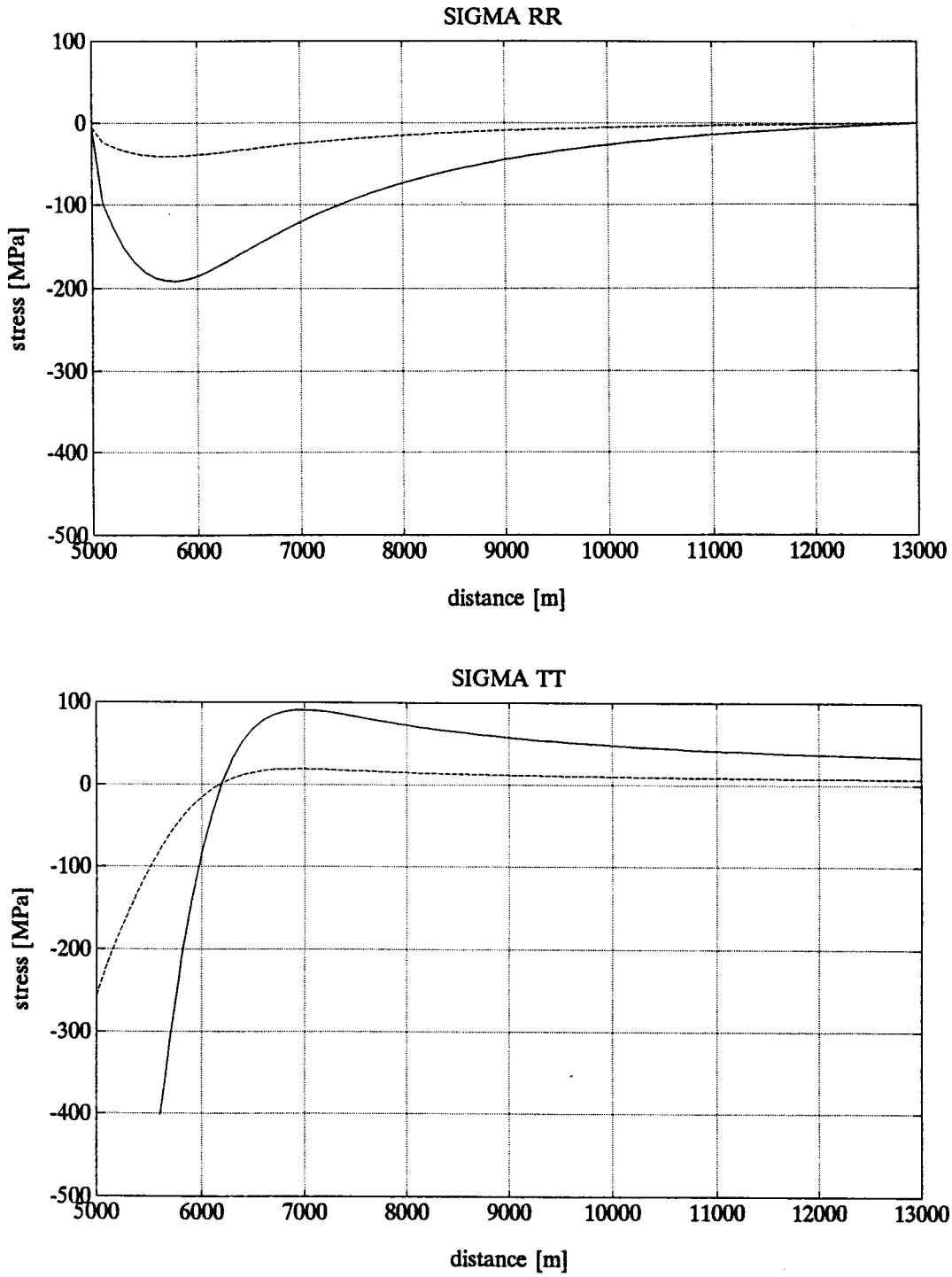

Fig. 3-1.7: The radial stress component versus distance. 5000 m indicates the interface of magma and host rock and 13000 m represents the earth's surface since $\theta = 0^{o}$. The solid curves are calculated for $E = 5x10^{10}$ Pa, $\alpha_T = 5x10^{-5}$ $K^{-1}$and for a time of 10^4 years (same as solid lines in Fig. 3-1.6). The dashed curves represent either the stress condition for $E = 5x10^{10}$ Pa and $\alpha_T = 1x10^{-5}$ K^{-1} or $E = 1x10^{10}$ Pa and $\alpha_T = 5x10^{-5}$ K^{-1}. The Poisson's ratio and the pressure inside the chamber is in both graphs kept constant at 0.25 and 5 MPa, respectively.

3.2 Magma Chamber Ascent

In the previous section we considered an expanding spherical magma chamber fixed at a particular location within the earth's crust. Now, we let the chamber ascend but keep its volume constant.

Important variables are the densities and viscosities of magma and host rock. We use equations from fluid mechanics involving these two variables to estimate magnitudes of three aspects of the geological situation,

(i) the ascent velocity of the magma body;
(ii) the flow field within and around the chamber;
(iii) the stress distribution within and around the chamber.

3.2.1 Magma as a Fluid Sphere

Consider a fluid sphere moving with a steady velocity U through an infinite incompressible, Newtonian fluid. Between the two immiscible fluids, interfacial tension tends to maintain a spherical shape against the shearing stresses that tend to deform it. As long as inertial effects do not affect distortion, and motion is sufficiently small, the moving fluid will be spherical (Happel and Brenner, 1965). For a creeping fluid, the Navier-Stokes equation for this system can be written as :

$$\nabla p = \eta \nabla^2 \mathbf{q} \qquad (3\text{-}2.1.1)$$

where $\nabla^2\mathbf{q}$ is the Laplacian of the velocities, η is the viscosity of the fluid, and ∇p is the pressure gradient. In orthogonal coordinates

$$\nabla = \mathbf{i}\frac{\partial}{\partial x} + \mathbf{j}\frac{\partial}{\partial y} + \mathbf{k}\frac{\partial}{\partial z}$$

and

$$\nabla^2 = \mathbf{i}\frac{\partial^2}{\partial x^2} + \mathbf{j}\frac{\partial^2}{\partial y^2} + \mathbf{k}\frac{\partial^2}{\partial z^2}$$

with **i**, **j**, **k** as the rectangular unit vectors. If the densities of both materials are invariant, the mass conservation equation is

$$\nabla \cdot \mathbf{q} = 0 \qquad (3\text{-}2.1.2)$$

Since the flow is axisymmetric about the direction of the velocity U, we choose spherical coordinates with the origin centered in the sphere and oriented with respect to the flow field at infinity according to Fig. 3-2.1. It is assumed that at the interface the radial velocity, u_r, is zero and the tangential velocity, u_θ, is continuous. The shear stress ,$\sigma_{r\theta}$, must be continuous across the interface. The boundary conditions of the flow are:

$$\begin{aligned}
u_r^{(o)} &= u_r^{(i)} = 0 && \text{at} \quad r = R \\
u_\theta^{(o)} &= u_\theta^{(i)} && \text{at} \quad r = R \\
\sigma_{r\theta}^{(o)} &= \sigma_{r\theta}^{(i)} && \text{at} \quad r = R \\
U &= \text{constant} && \text{as} \quad r \to \infty
\end{aligned}$$

where the superscripts i and o correspond to inside and outside the fluid sphere, respectively. The general solution of the stream functions for external and internal motion is given by Happel and Brenner (1965):

$$\psi^{(o)} = \sin^2\theta \left[\frac{1}{10}\mathcal{A} r^4 - \frac{1}{2}\mathcal{B} r + \mathcal{C} r^2 + \frac{\mathcal{D}}{r}\right] \qquad (3\text{-}2.1.4a)$$

$$\psi^{(i)} = \sin^2\theta \left[\frac{1}{10}\mathcal{E} r^4 - \frac{1}{2}\mathcal{F} r + \mathcal{G} r^2 + \frac{\mathcal{H}}{r}\right] \qquad (3\text{-}2.1.4b)$$

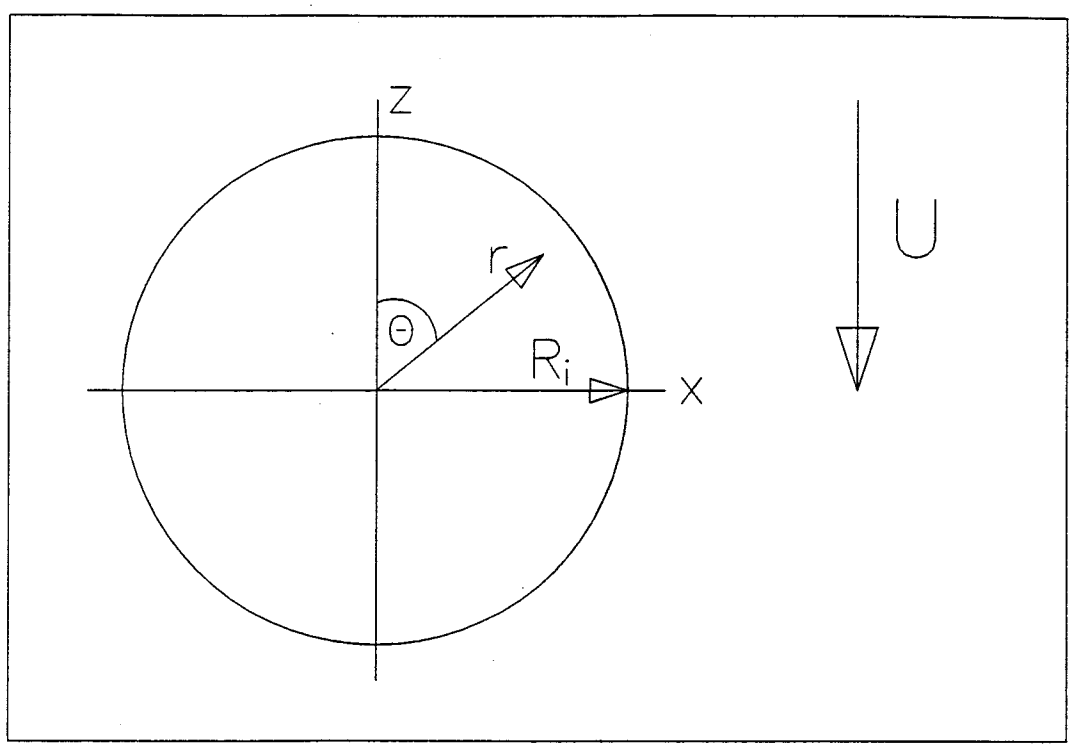

Fig. 3-2.1: The coordinate system of a spherical magma chamber with radius R_i embedded in an infinite viscous medium. The ascent of the sphere is considered by letting the surrounding material pass the fixed sphere in the negative z-direction. r is the position vector from the center of the sphere to any point within or outside the fluid sphere.

with

$$\mathcal{A} = 0 \qquad \mathcal{B} = U R_i \frac{(3 + 2\eta_{eff})}{2(1 + \eta_{eff})}$$

$$\mathcal{C} = \frac{1}{2} U \qquad \mathcal{D} = U R_i^3 \frac{1}{4(1 + \eta_{eff})}$$

$$\mathcal{E} = \frac{U}{R^2} \frac{5\eta_{eff}}{2(1 + \eta_{eff})} \qquad \mathcal{F} = 0$$

$$\mathcal{G} = - U \frac{\eta_{eff}}{4(1 + \eta_{eff})} \qquad \mathcal{H} = 0$$

$\eta_{eff} = \eta_h/\eta_m$ is defined as the ratio of viscosity outside ,η_h, and inside ,η_m, the fluid sphere. If the sphere rises due to gravity, then the constant velocity at infinity is

$$U = - \frac{2R_i^2 g \, \Delta\rho \, (1 + \eta_{eff})}{3\eta_h \, (3 + 2\eta_{eff})} \qquad (3\text{-}2.1.5)$$

where g is the acceleration due to gravity, and $\Delta\rho = \rho_m - \rho_h$ is the density difference of fluid inside (ρ_m) and outside (ρ_h) the sphere, respectively (Landau and Lifshitz, 1959).

Flow Field

The components of the velocity in spherical coordinates can be calculated in the following way (Happel and Brenner,1965):

$$u_r = - \frac{1}{r^2 \sin\theta} \frac{\partial\psi}{\partial\theta} \qquad (3\text{-}2.1.6a)$$

$$u_\theta = \frac{1}{r \sin\theta} \frac{\partial\psi}{\partial r} \qquad (3\text{-}2.1.6.b)$$

where r and θ are the spherical coordinates and u_r and u_θ the radial and tangential velocities. The velocity components inside the fluid sphere are then given by:

$$u_r^{(i)} = -\frac{1}{2} U \frac{\eta_{eff}}{1 + \eta_{eff}} \left[\frac{r^2}{R_i^2} - 1 \right] \cos\theta \qquad (3\text{-}2.1.7a)$$

$$u_\theta^{(i)} = \frac{1}{2} U \frac{\eta_{eff}}{1 + \eta_{eff}} \left[\frac{2\, r^2}{R_i^2} - 1 \right] \sin\theta \qquad (3\text{-}2.1.7b)$$

The velocity field outside the fluid sphere is given by:

$$u_r^{(o)} = -U \left[\frac{R_i^3}{2r^3 (1 + \eta_{eff})} - \frac{R_i (3 + 2\eta_{eff})}{2r (1 + \eta_{eff})} + 1 \right] \cos\theta \qquad (3\text{-}2.1.8a)$$

$$u_\theta^{(o)} = -U \left[\frac{R_i^3}{4r^3 (1 + \eta_{eff})} + \frac{R_i (3 + 2\eta_{eff})}{4r (1 + \eta_{eff})} - 1 \right] \sin\theta \qquad (3\text{-}2.1.8b)$$

A sketch of the velocity field of this flow is shown in Fig. 3-2.2. For mathematical analysis the reference system is fixed on the sphere and the fluid moves downwards. This downward motion far from the sphere corresponds directly to the rising sphere in a resting fluid.

Stress Field

The components of the stress tensor in an axisymmetric frame are given by Landau and Lifshitz (1959) and a definition sketch is shown in Fig. 3-2.3.

$$\sigma_{rr} = -p + 2\eta \frac{\partial u_r}{\partial r} \qquad (3\text{-}2.1.9a)$$

$$\sigma_{\theta\theta} = -p + 2\eta \left[\frac{1}{r} \frac{\partial u_\theta}{\partial \theta} + \frac{u_r}{r} \right] \qquad (3\text{-}2.1.9b)$$

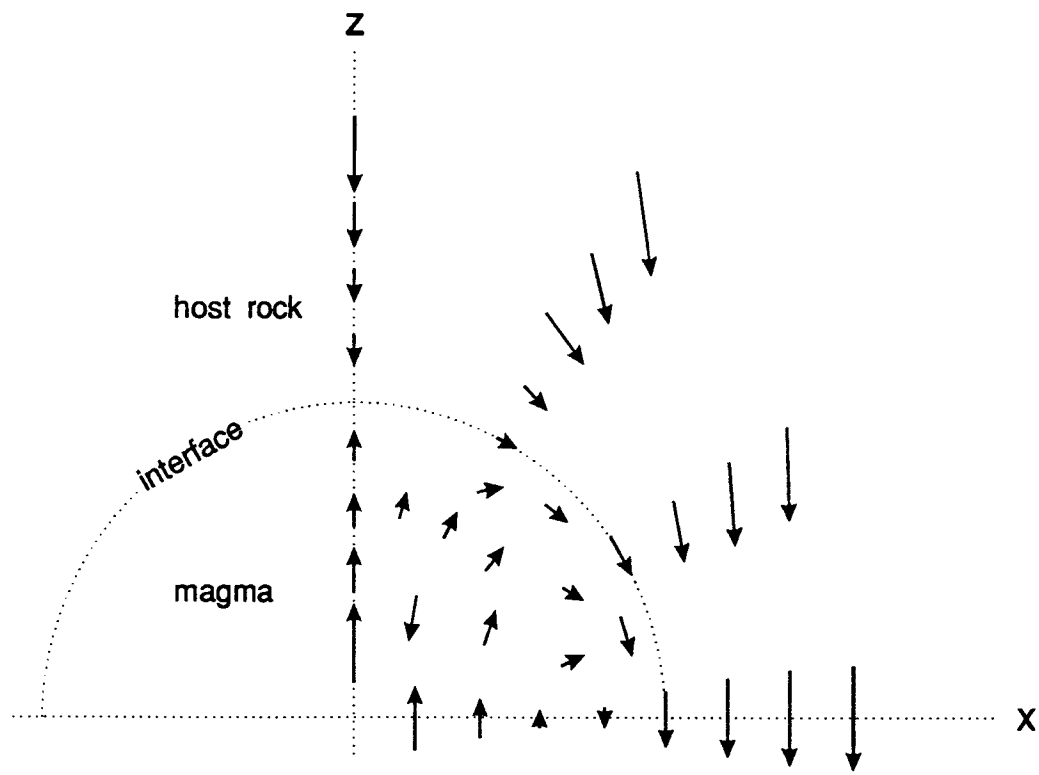

Fig. 3-2.2: Sketch of velocity field of Stokes flow inside and outside a fluid sphere.

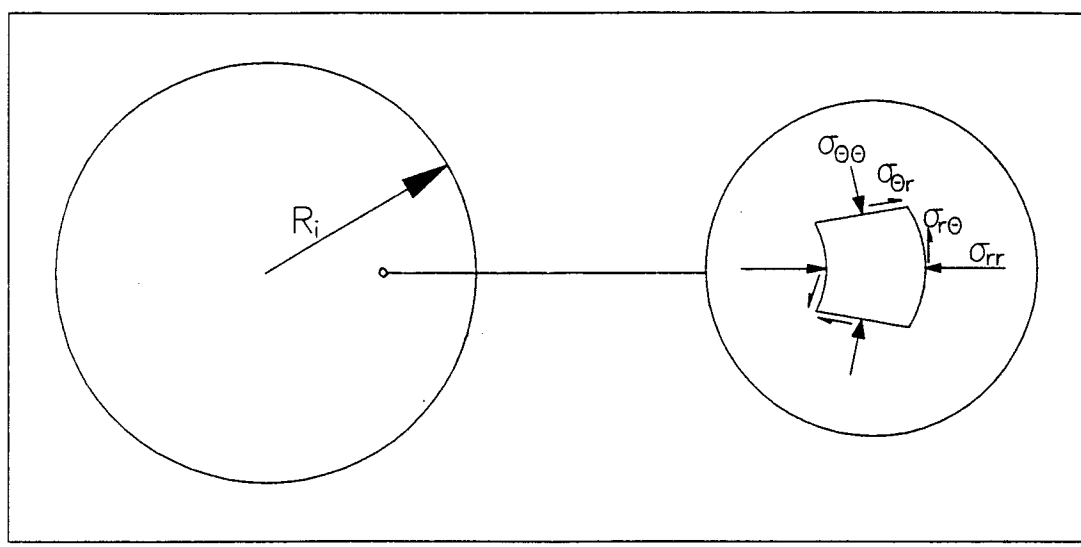

Fig. 3-2.3: Sketch defining the stress components within and around a magma chamber with radius R_i.

$$\sigma_{r\theta} = \eta \left[\frac{1}{r} \frac{\partial u_r}{\partial \theta} + \frac{\partial u_\theta}{\partial r} - \frac{u_\theta}{r} \right] \qquad (3\text{-}2.1.9c)$$

where p is the hydrostatic pressure. This term can be calculated by integrating the following equation:

$$dp = \frac{\partial p}{\partial r} dr + \frac{\partial p}{\partial \theta} d\theta \qquad (3\text{-}2.1.10)$$

with

$$\frac{\partial p}{\partial r} = - \frac{\eta}{r^2 \sin\theta} \frac{\partial}{\partial \theta} (f^2 \psi)$$

$$\frac{\partial p}{\partial \theta} = \frac{\eta}{\sin\theta} \frac{\partial}{\partial r} (f^2 \psi)$$

inside magma chamber: $f^2 \psi = \sin^2\theta \, (\mathcal{A} r^2 + \mathcal{B} / r)$

in the host rock: $f^2 \psi = \sin^2\theta \, (\mathcal{E} r^2 + \mathcal{F} / r)$

Evaluating equations (3-2.1.5), (3-2.1.7) and (3-2.1.10), then inserting into equation (3-2.1.9) and adding a buoyancy term of $\Delta\rho$ g r $\cos\theta$ to the radial and tangential stress components yields a stress description inside the fluid sphere:

$$\sigma_{rr}^{(i)} = \Delta\rho \, g \, r \left[1 - \frac{2}{(3 + 2\eta_{eff})} \right] \cos\theta \qquad (3\text{-}2.1.11a)$$

$$\sigma_{\theta\theta}^{(i)} = \Delta\rho \, g \, r \left[1 - \frac{4}{(3 + 2\eta_{eff})} \right] \cos\theta \qquad (3\text{-}2.1.11b)$$

$$\sigma_{r\theta}^{(i)} = - \frac{\Delta\rho \, g}{(3 + 2\eta_{eff})} \, r \sin\theta \qquad (3\text{-}2.1.11c)$$

The stress distribution outside the sphere is given by evaluating equations (3-2.1.5), (3-2.1.8), (3-2.1.10) and inserting into (3-2.1.9):

$$\sigma_{rr}^{(o)} = \Delta\rho\, g \left[\frac{R_i^3}{r^2} - \frac{2R_i^5}{r^4(3 + 2\eta_{eff})}\right] \cos\theta \qquad (3\text{-}2.1.12a)$$

$$\sigma_{\theta\theta}^{(o)} = \Delta\rho\, g \left[\frac{R_i^5}{r^4(3 + 2\eta_{eff})}\right] \cos\theta \qquad (3\text{-}2.1.12b)$$

$$\sigma_{r\theta}^{(o)} = -\Delta\rho\, g \left[\frac{R_i^5}{r^4 (3 + 2\eta_{eff})}\right] \sin\theta \qquad (3\text{-}2.1.12c)$$

When $\eta_{eff} \rightarrow \infty$, the results simplify to

$$\sigma_{rr}^{(o)} = \Delta\rho\, g \left[\frac{R_i^3}{r^2}\right] \cos\theta \qquad (3\text{-}2.1.13a)$$

$$\sigma_{\theta\theta}^{(o)} = \text{negligible} \qquad (3\text{-}2.1.13a)$$

$$\sigma_{r\theta}^{(o)} = \text{negligible} \qquad (3\text{-}2.1.13a)$$

3.2.2 Deformation Layer

The previous calculations were made under the assumption that the surrounding material is infinite in extent and Newtonian in behavior. In reality, the earth would be more like a power-law fluid and its behavior varies with depth. When magma rises through the earth's crust it encounters cooler, stiffer material. Eventually magma can only migrate if the surrounding rock fractures or becomes softer due to heating and water-weakening. In the latter case the magma body motion can be described as a fluid sphere that rises within a bigger spherical container, with a so-called deformation layer surrounding the magma reservoir. The radii of the inner and outer sphere are R_i and R_b, respectively. For the purpose of assembling equations, the inner sphere is assumed to remain at rest while the outer, rigid sphere moves in the negative z-direction with a constant velocity U as in Fig. 3-2.4. The solution for this problem is given by Happel and

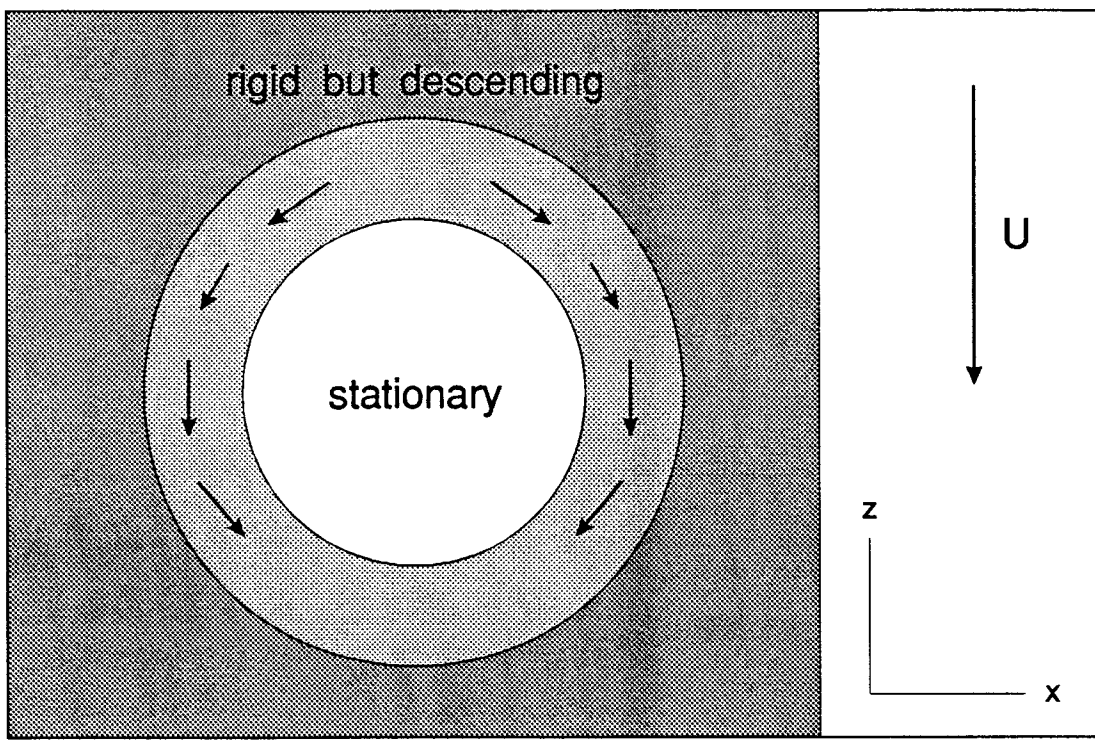

Fig. 3-2.4: Relative motion of a fluid sphere within a spherical container.

Brenner (1965). It reduces to the problem already discussed as R_b tends to infinite.

If the drag of the inner liquid sphere is equal to the gravity force the constant velocity U can be calculated:

$$U = -\frac{2 R_i^2 \Delta\rho\, g\, (1 + \eta_{eff})}{3\, \eta_h\, (3 + 2\eta_{eff})\, K_a} \qquad (3\text{-}2.2.1)$$

where η_{eff}, the viscosity ratio of external and internal viscosity (η_h/η_m), is a function of the temperature field. K_a is the wall correction factor defined by

$$K_a = \frac{\text{drag in the presence of outer sphere}}{\text{drag in infinite medium}}$$

$$K_a = \frac{1 - \dfrac{3(1 - \eta_{eff})\,\lambda^5}{(3 + 2\eta_{eff})}}{1 - \dfrac{3(3 + 2\eta_{eff})}{4(1 + \eta_{eff})}\lambda + \dfrac{5}{2(1 + \eta_{eff})}\lambda^3 - \dfrac{3(3 - 2\eta_{eff})}{4(1 + \eta_{eff})}\lambda^5 + \dfrac{(1 - \eta_{eff})}{(1 + \eta_{eff})}\lambda^6} \qquad (3\text{-}2.2.2)$$

with:

$$\lambda = \frac{R_i}{R_b} = \frac{\text{inner radius}}{\text{outer radius}}$$

Flow Field

The radial and tangential velocity components u_r and u_θ are given by Happel and Brenner (1965). Inside the fluid sphere they are:

$$u_r^{(i)} = -\frac{1}{2} U\, a\, \mathcal{E} \left[\frac{r^2}{R_i^2} - 1\right] \cos\theta \qquad (3\text{-}2.2.3a)$$

$$u_\theta^{(i)} = \frac{1}{2} U a \mathcal{E} \left[\frac{2 r^2}{R_i^2} - 1 \right] \sin\theta \qquad (3\text{-}2.2.3b)$$

where

$$a = \frac{1}{1 + \eta_{eff} - \frac{3}{2}\left[\frac{3}{2} + \eta_{eff}\right]\lambda + \frac{5}{2}\lambda^3 - \frac{3}{2}\left[\frac{3}{2} - \eta_{eff}\right]\lambda^5 + (1 - \eta_{eff})\lambda^6}$$

$$\mathcal{E} = 1 - \frac{5}{2}\lambda^3 + \frac{3}{2}\lambda^5$$

The velocity components of the deformation layer are

$$u_r^{(o)} = U a \left[\frac{r^2}{2R_i^2} \mathcal{A} + \frac{3 R_i}{2 r} \mathcal{B} - \mathcal{C} - \frac{R_i^3}{2 r^3} \mathcal{D} \right] \cos\theta \qquad (3\text{-}2.2.4a)$$

$$u_\theta^{(o)} = U a \left[-\frac{r^2}{R_i^2} \mathcal{A} - \frac{3 R_i}{4 r} \mathcal{B} + \mathcal{C} - \frac{R_i^3}{4 r^3} \mathcal{D} \right] \sin\theta \qquad (3\text{-}2.2.4b)$$

where

$$\mathcal{A} = \left[\frac{3}{2} + \eta_{eff}\right]\lambda^3 - \frac{3}{2}\lambda^5 \qquad \mathcal{B} = 1 + \frac{2}{3}\eta_{eff} - (1 - \eta_{eff})\lambda^5$$

$$\mathcal{C} = 1 + \eta_{eff} + \frac{5}{4}\lambda^3 - \frac{3}{2}\left[\frac{3}{2} - \eta_{eff}\right]\lambda^5 \qquad \mathcal{D} = 1 - (1 - \eta_{eff})\lambda^3$$

Stress Field

Within the deformation layer the stress field can be described as

$$\sigma_{rr}^{(o)} = \frac{2 a \Delta\rho g (1 + \eta_{eff})}{K_a (3 + 2\eta_{eff})} \left[r \mathcal{A} + \frac{3R_i^3}{2r^2} \mathcal{B} - \frac{R_i^5}{r^4} \mathcal{D} \right] \cos\theta \qquad (3\text{-}2.2.5a)$$

$$\sigma_{\theta\theta}^{(o)} = \frac{a \Delta\rho g (1 + \eta_{eff})}{K_a (3 + 2\eta_{eff})} \left[4r \mathcal{A} + \frac{R_i^5}{r^4} \mathcal{D} \right] \cos\theta \qquad (3\text{-}2.2.5b)$$

$$\sigma_{r\theta}^{(o)} = \frac{\alpha\,\Delta\rho\; g\,(1+\eta_{eff})}{K_a\,(3+2\eta_{eff})}\left[r\,\mathcal{A} - \frac{R_i^5}{r^4}\mathcal{B}\right]\sin\theta \qquad (3\text{-}2.2.5c)$$

Spera et al. (1982) pointed out that during boundary layer convection, viscous shear stress arises with a maximum at the interface of magma and wall rock, but the shear stress at the wall is low and reaches a magnitude of order 10^{-2} MPa.

Deformation Layer Thickness

The deformation layer thickness (δ_d) depends on the viscosity of host rock material that is able to flow. As a first approximation δ_d can be linked to the temperature distribution as described in chapter 2.2 (see Figs. 2-1.2 and 2-1.5). The idea is based on a critical temperature (T_{fl}) at which the material begins to flow. Tullis (1990) reported that a quartzo-feldspathic aggregate undergoes macroscopically ductile cataclastic flow at pressures of ~700 - 1500 MPa and temperatures of ~573 - 973 K. In this case, one can draw a horizontal line at 573 K in the temperature-distance diagram. The intersection of this horizontal line with the temperature distribution curve yields the deformation-layer thickness, δ_d. For example in Figure 2.1.5, after 300 years $\delta_d \cong 150$ m.

3.2.3 Example and Discussion

As a geological example consider a spherical liquid magma chamber with a radius of 5 km and a constant temperature of 1073 K at 8 km depth. Suppose its highly viscous surroundings is chemically identical. Let the temperature of the host rock be 483 K, and its density and viscosity be 2500 kg m^{-3} and 4×10^{17} Pas, respectively. The density of the magma can be calculated according to equation

(2-3.2.1) which results in a value of 2425 kg m^{-3} if its thermal expansion, α_T, is equal to $5x10^{-5}$ K^{-1}.

The ascent velocity, U, for an infinite surrounding medium can be calculated by using equation (3-2.1.5) or (3-2.2.1) by letting $R_b \rightarrow \infty$. With the variables above, U becomes 0.48 m a^{-1}. This value is only correct if the viscosity of the whole host rock is constant at $4x10^{17}$ Pa s. Now, consider a spherical magma chamber which rises within a deformation zone. Assume that the thickness of the deformation layer, δ_d, is given when the temperature of the material is $\approx$573 K. For a temperature profile after t = 300 years, δ_d becomes $\approx$150 m (see Fig. 2-1.5). Let the viscosity ratio of country rock and magma be infinite. The temperature dependent viscosity can be calculated by using equation (2-3.1.2). A temperature of 708 K gives a viscosity of $4x10^{17}$ Pa s. By letting the deformation layer thickness be 150 m, λ becomes 0.97 and K_a is equals 19400 ($\eta_{eff} \rightarrow \infty$). According to equation (3-2.2.1) the ascent velocity becomes $0.025x10^{-3}$ ma^{-1}. A deformation layer thickness of 500 m results in an ascent velocity of $0.82x10^{-3}$ m a^{-1}. Fig. 3-2.5 shows the variation of U versus temperature by combining equation (3-2.2.1) with (2-3.1.2). In this diagram, the deformation layer thickness is kept constant at 150 m. The ascent velocity is calculated as if the whole deformation layer has equal viscosity. In reality, the viscosity is not uniform across the deformation layer because the temperature varies with distance (see Fig. 2-1.5, for example). Therefore, the viscosity should be lower at the magma chamber's margin than further out. To come closer to the real ascent velocity we can use the model in which ascent occurs within a deformation layer of thickness equals 150 m and a temperature distribution after 300 years, for example (eqn. 2-1.4.3b). Then, an average temperature across the deformation layer can be evaluated. This approach assumes that the whole

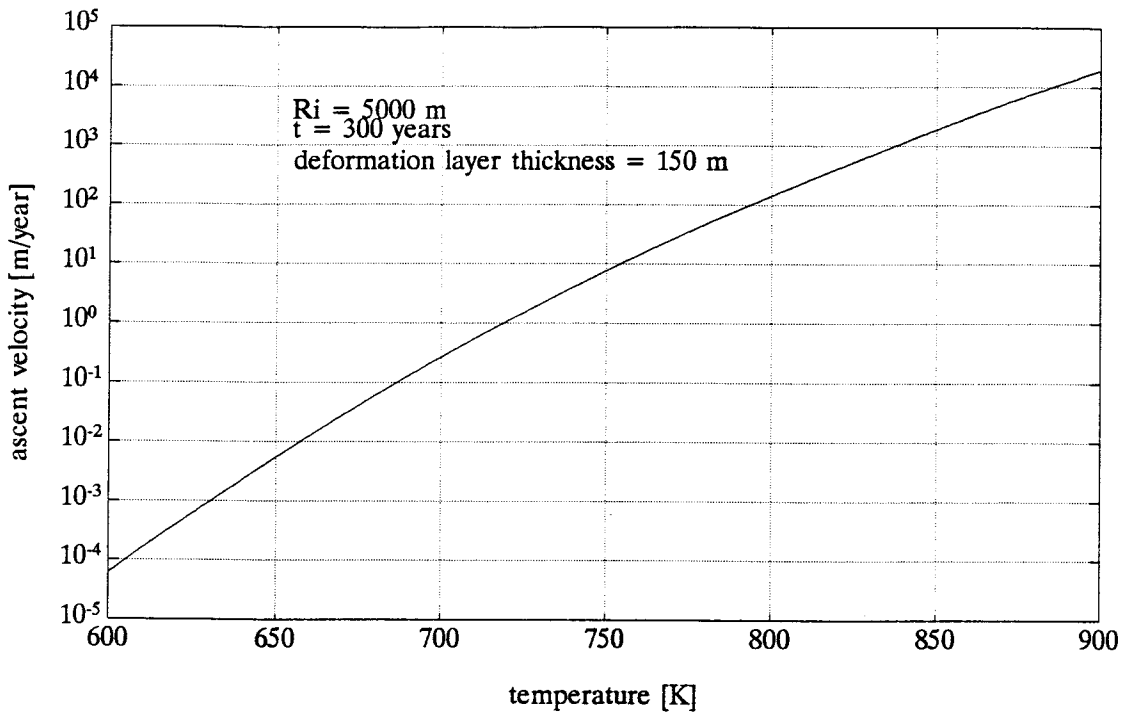

Fig. 3-2.5: Semi-logarithmic plot of ascent velocity versus temperature. The magma chamber rises within a bigger spherical container of radius R_b = 5150 m. A distance of 5000 m indicates the magma - host rock interface.

deformation layer has a uniform, average temperature of 711.4 K. The average viscosity then becomes 3.3×10^{17} Pa s and the ascent velocity results in 0.03×10^{-3} m a^{-1}. A more detailed study of the ascent velocity in a temperature varying host rock is written in Mahon et al. (1988). They report a decreasing ascent velocity as the chamber becomes closer to the earth's surface. This is because of the fact that the viscosity of the country rock increases with decreasing depth.

All the previous calculations about magma ascent assume a continuous velocity. This could be true since host rock is able to flow. But, if the magma chamber gets into a brittle medium, flow is only possible by fracturing material. In this case magma chamber ascent could be in a jerky manner. The chamber rests at a specific location for a certain amount of time, then, when the stress is sufficient enough to overcome the strength of the host rock the magma body rises a certain distance.

The stress distribution within and around the magma reservoir for different viscosity ratios, $\eta_{eff} = 1$, 5 and $\eta_{eff} \rightarrow \infty$, is demonstrated in Fig. 3-2.6. A distance of zero represents the magma chamber center, 5000 m indicates the interface of magma and host rock, and the earth's surface is at 13 km as in Fig. 3-1.2. The stress field is calculated for an infinite surroundings according to equations (3-2.1.11) and (3-2.1.12). Note that the stress components represent the deviation from the lithostatic pressure which increases linearly with depth. For σ_{rr} and $\sigma_{\theta\theta}$, the stress is maximal at $\theta = 0^o$ (up a vertical line) and $\sigma_{r\theta}$ at $\theta = 90^o$ (along a horizontal line). The radial and tangential stress components are zero if $\theta = 90^o$, and there is no shear stress if $\theta = 0^o$. Inside the reservoir all stress components increase linearly from zero at the center to the interface. With increasing viscosity ratio, the shear stress approaches zero. Both normal stress components, σ_{rr} and

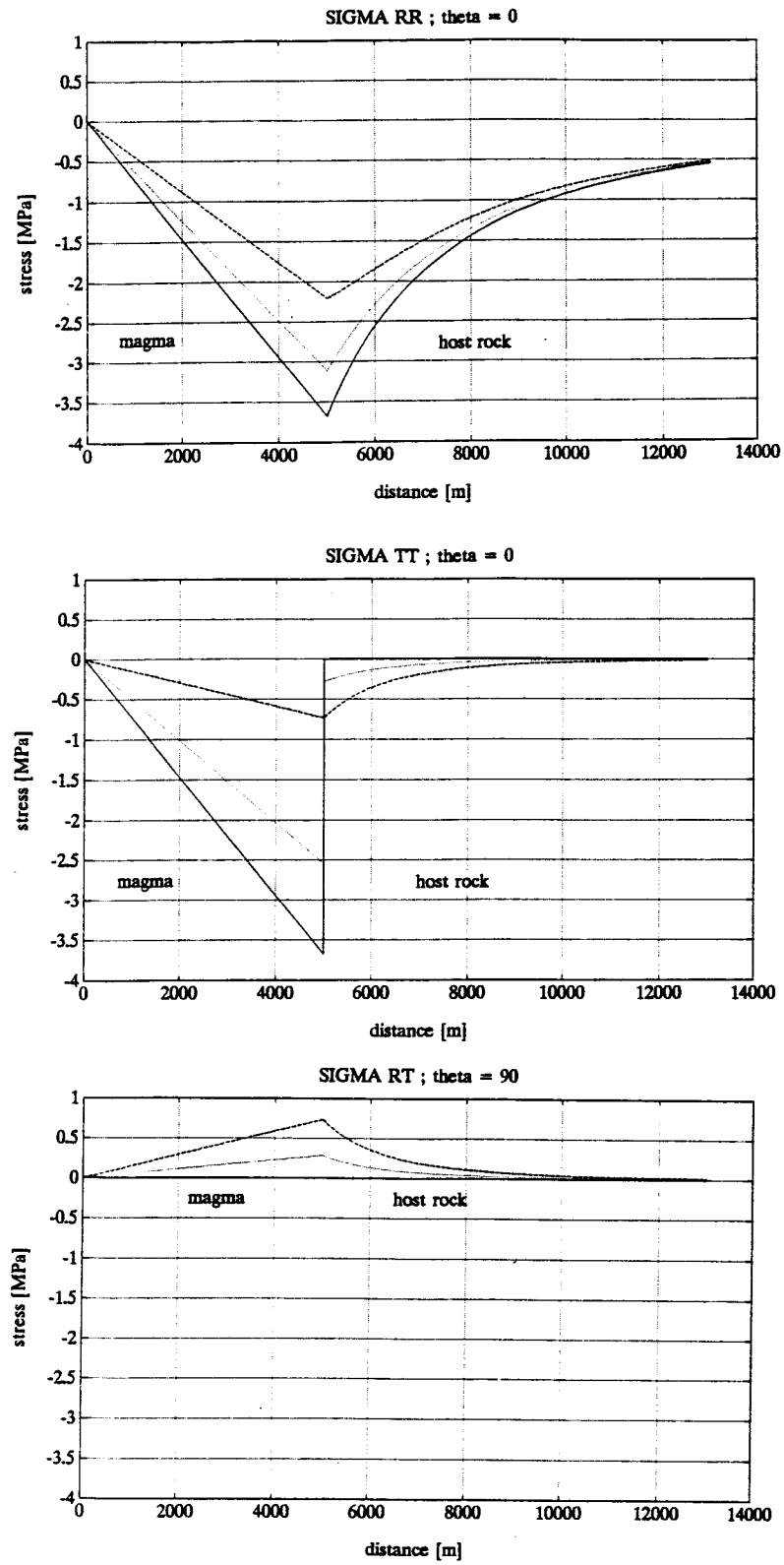

Fig. 3-2.6: The three stress components versus distance for different viscosity ratios: (___): $\eta_{eff} \rightarrow \infty$; (····): $\eta_{eff} = 5$, and (– – –): $\eta_{eff} = 1$. 5000 m indicates the interface of magma and host rock. The stresses are calculated for an infinite host rock. At an angle of zero degree, 13 km represents the earth's surface. SIGMA RR: radial normal stress component at $\theta = 0^{o}$, SIGMA TT: tangential normal stress component at $\theta = 0^{o}$, SIGMA RT: shear stress component at $\theta = 90^{o}$.

$\sigma_{\theta\theta}$, are compressive and approach the buoyancy term: $\Delta p\ g\ r\ \cos\theta \cong 3.7$ MPa. The friction due to flow can be neglected. Lowering the viscosity difference of host rock and magma effects a decrease in stress magnitudes. Across the interface, the shear stress and radial normal stress components are continuous and decrease in a non-linear manner towards the earth's surface. The tangential normal stress component is continuous across the interface only if there is zero viscosity difference between magma and host rock. The transition is discontinuous if the viscosities are not equal. The break at the interface increases with increasing host rock viscosity, and the tangential stress component approaches zero as the viscosity ratio increases. In a reasonable geological situation η_{eff} has values $>> 1$.

In Fig. 3-2.7 the variation of radial stress with density contrast is shown as an example ($\eta_{eff} >> 1$). The stress magnitude increases with increasing density contrast. A density that changes with time can be used as the compositional effect on the stress development. If magma differentiates during ascent, it becomes less dense and effects an increase in the country rock's stress magnitudes. Also, if magma rises into a denser material, the stress magnitudes in the host rock will increase.

The wall effect on the normal stress components is demonstrated in Fig. 3-2.8 by using equation (3-2.2.5) and letting R_o equal 6, 9, and 13 km, respectively ($\eta_{eff} \rightarrow \infty$). At the interface, the radial stress component is unaffected by the wall effect. The bigger R_o the more rapidly $\sigma_{rr}^{(o)}$ decreases towards the wall. For a viscosity ratio much bigger than 1 the tangential stress component cannot be neglected if the magma chamber ascent is considered as a flow within a bigger container with radius R_o. For example when R_o = 13 km, its magnitude increases

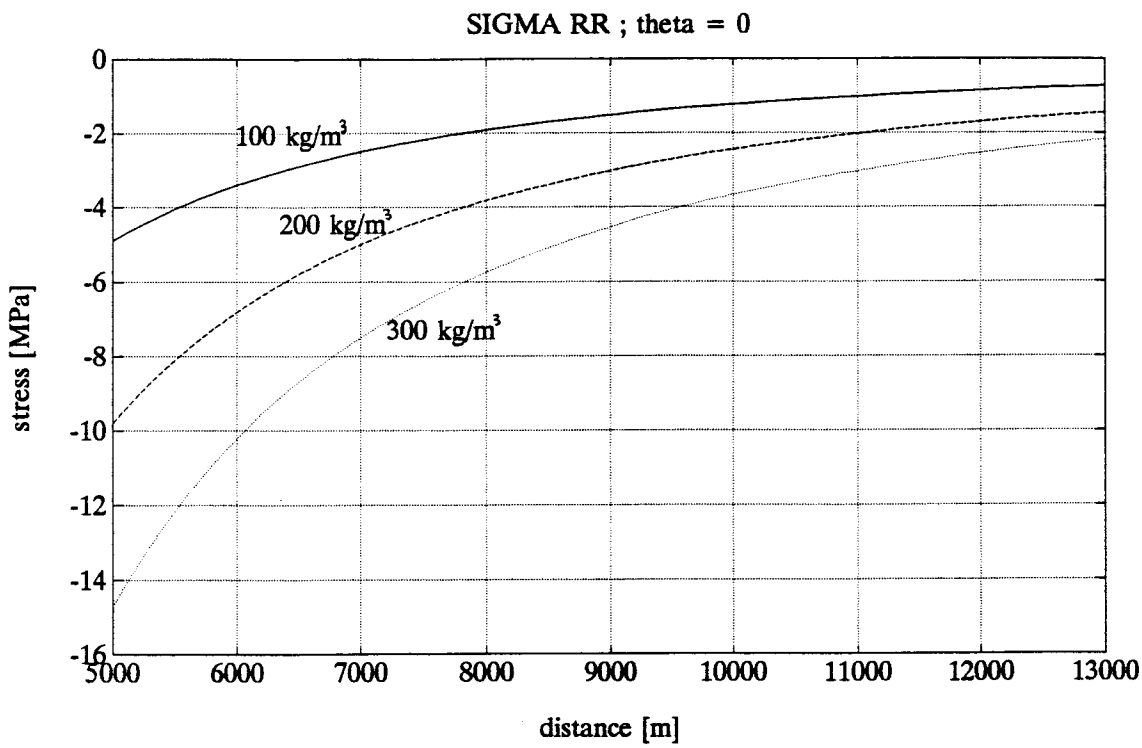

Fig. 3-2.7: The density effect on the radial normal stress component from the interface (5 km) to the earth's surface (13 km) at $\theta = 0^{o}$. The numbers indicate the density difference of magma and host rock in kg m^{-3}. A density contrast greater than 300 kg m^{-3} is abnormal; the only realistic way to increase σ_{rr} above the maximum value shown, with 15 MPa, would be to consider a taller magma chamber, more than 10 km from top to bottom. This would be abnormal for a well defined stock (multi-component batholiths are a different topic).

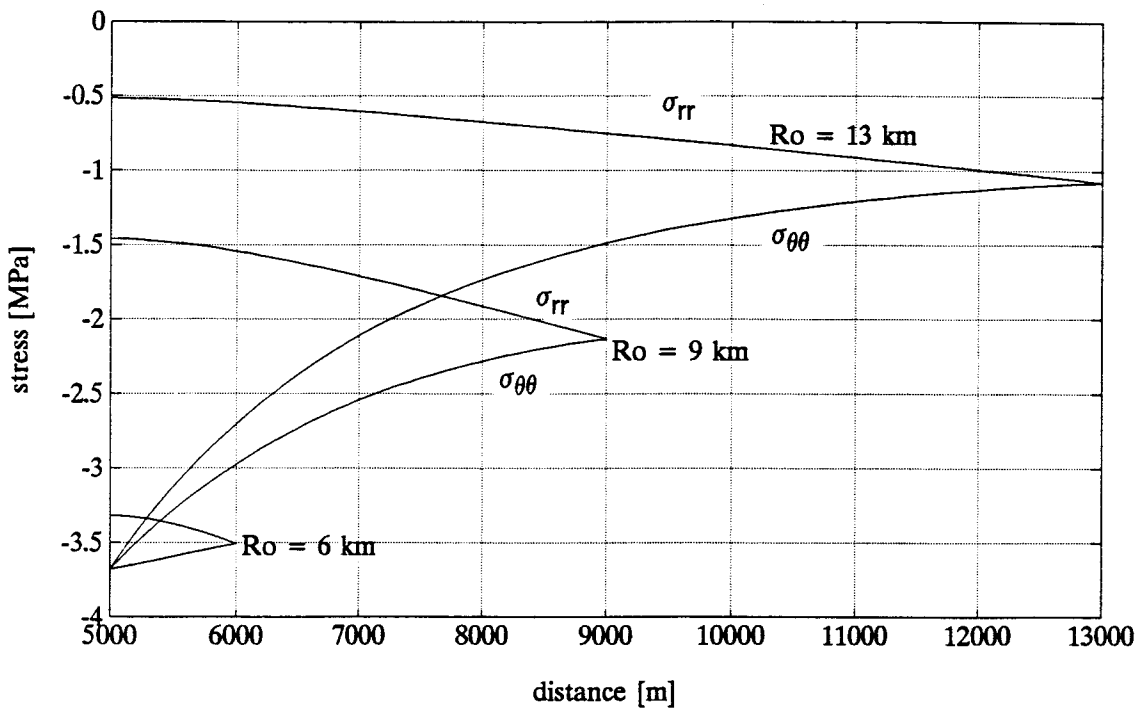

Fig. 3-2.8: The distribution of radial and tangential stress components in the host rock which is considered as a deformable shell of radii R_o = 6, 9, and 13 km inside an extensive rigid host as in Fig. 3-2.4. In each pair of curves the upper curve represents the radial stress and the lower curve represents the tangential stress component. 5 km distance indicates the interface, $\theta = 0^o$.

from 0.53 MPa at the interface to about 1.1 MPa at R_o. At R_o, both the radial and tangential stress components are equal ($\theta = 0^o$).

When a spherical magma chamber rises within a small deformation layer the stress state is close to hydrostatic and close to the magnitude of σ_{rr} (3.7 MPa) that buoyancy produces in an infinitely extended environment. The radial and tangential stress components are shown in Fig. 3-2.9 for a viscosity ratio $>> 1$.

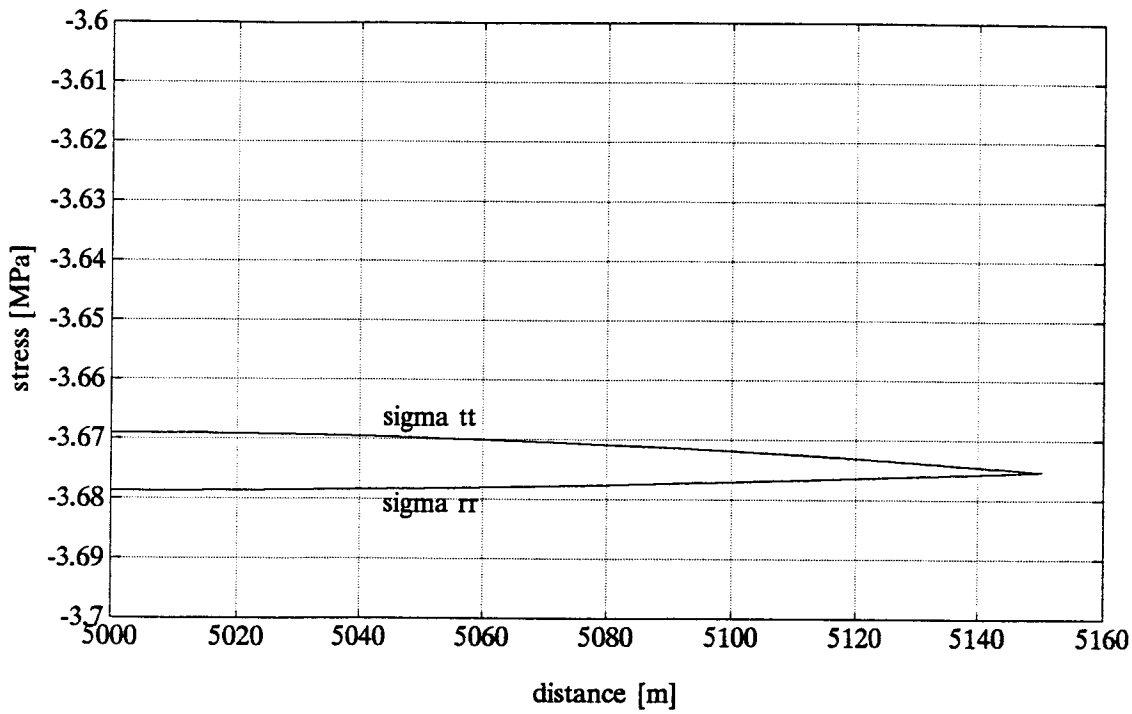

Fig. 3-2.9: The stress components, σ_{rr} and $\sigma_{\theta\theta}$, caused by magma ascent due to a thin viscous deformation layer with thickness 500 m, (θ = 0^{o}). 5 km indicates the interface and 5.5 km represents the outer border of the deformation layer.

3.3 Summary

This chapter has described magma pressures, thermal stresses in the host rock, and the stress field due to magma ascent. If a magma reservoir resides very deep inside the earth's crust its surroundings can be considered as infinite, but as the chamber becomes closer to the earth's surface, wall effects alter the stress field and should be included. In the previous calculation the influence of the earth's surface is included by considering the host rock as a thick shell whose radius is equal to depth as in Fig. 3-1.2.

The stress field within the host rock is calculated for two extreme cases (Fig. 3-3.1). Model 1 assumes a spherical magma body embedded in a medium that responds elastically when heat is transferred into it and when the magma chamber tries to expand due to water exsolution. In the other model (model 2) a spherical chamber with constant radius, R_i, is surrounded by viscous material. Table 3-2 compares the three stress components outside the magma body calculated under the assumption of an infinite host rock for both model 1 and model 2.

In model 1 the country rock is supposed to be elastic. The magnitudes of the thermal-elastic stresses are clearly proportional to α_T and E and could be smaller than in Fig. 3-1.6 (see Fig. 3-1.7). The highest stress magnitudes are reached when there is a strong temperature contrast between magma and host rock. The tangential stress at the interface is compressive and can theoretically reach magnitudes in the order of GPa. In model 2 only the buoyancy stresses with values of a few MPa have to be considered.

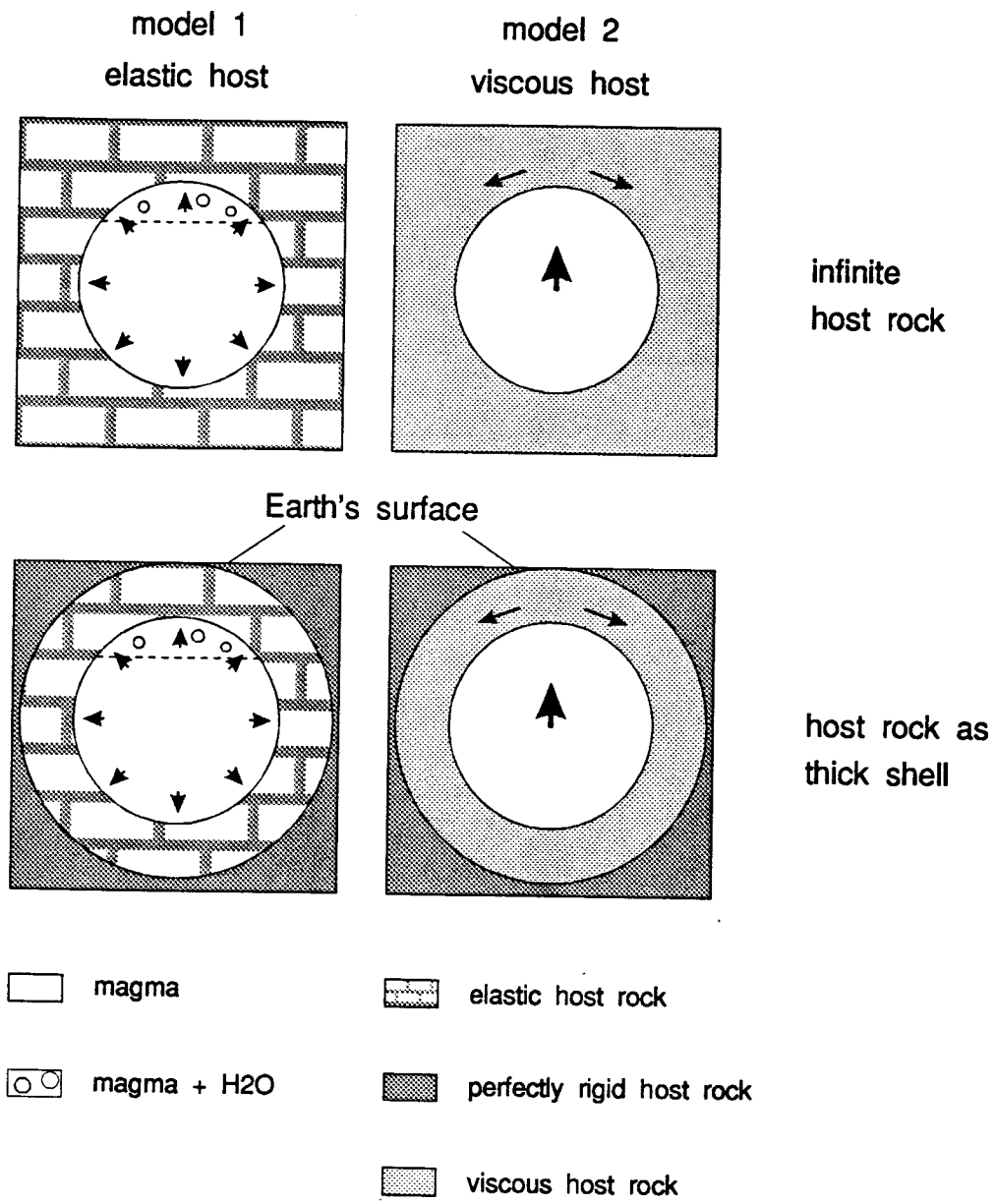

Fig. 3-3.1: Two models used for stress calculations. Model 1: Spherical magma body embedded in elastic host rock. Model 2: Viscous material surrounds a spherical magma chamber. Arrows indicate relative motion of material. For more details see text.

Table 3-2

	Model 1 : **elastic host rock** **with thermal effects**	**Model 2 :** **viscous host rock** **with buoyancy effects**
	$R_o \rightarrow \infty$	$\eta_{eff} \rightarrow \infty$, $\lambda = 0$
equation:	3-1.3.10	3-2.1.13
$\sigma_{rr}^{(o)}$	$-\frac{2\,\alpha_T\,E\,T^*_r}{(1-\nu)\,r^3} - \Delta p\,\frac{R_i^3}{r^3}$	$\Delta\rho\,g\,\frac{R_i^3}{r^2}\cos\theta$
$\sigma_{\theta\theta}^{(o)}$	$\frac{\alpha_T\,E}{(1-\nu)}\left[\frac{T^*_r}{r^3} - \Delta T\right] + \frac{1}{2}\Delta p\,\frac{R_i^3}{r^3}$	negligible
$\sigma_{r\theta}^{(o)}$	0	negligible

The overpressure, Δp, has a maximum value if the surrounding medium is perfectly rigid. In an elastic medium maximum values of Δp can be reached at about 1 km depth in order of tens of MPa depending on the material properties, volume of exsolved water, and temperature.

The next chapter weighs and combines the different kinds of stresses at different levels in the earth's crust and tries to suggest what could happen to the host rock at different conditions.

Chapter IV: Response of Country Rock

4.0 Introduction

This chapter uses the previous thoughts to come to a unified picture of the stress distribution within the country rock. First for a stationary magma body, the overall stress field in a perfectly thermal-elastic material is described. But usually, material has only a limited elastic behavior. When a certain stress is reached, material fractures or deforms permanently. A second model is presented in which the host rock is considered as an elasto-plastic material that shows cataclastic flow when a certain state of stress is overcome. Thirdly, the fluid pressure is considered, fourthly, the overpressure of the magma is taken into account, and fifthly, the mechanism of magma ascent in an elasto-plastic host rock is discussed.

4.1 Overall Stress Field in Thermal-elastic Medium

To learn more about the response of the country rock to an intruding magma chamber it is important to know the overall stress field. In this section the host rock is considered as a thermal-elastic medium that is not able to flow. The following stress terms have to be combined: lithostatic pressure due to the overburden, fluid pressure within a porous host rock, thermal stress, overpressure due to crystallization and buoyancy of the magma chamber. Mathematically, the overall stress field can be expressed by adding up the above stress terms. In any vertical plane through the sphere's center the stress field becomes:

effective $\sigma_{rr}^{(tot)}$ = lithostatic pressure - fluid pressure + thermal stress + overpressure + stress due to buoyancy

effective $\sigma_{\theta\theta}^{(tot)}$ = lithostatic pressure - fluid pressure + thermal stress + overpressure + (stress due to buoyancy = negligible)

$\sigma_{\theta r}^{(tot)} = \sigma_{r\theta}^{(tot)}$ = negligible

For a start the country rock is considered as an infinite, isotropic medium in which the effect of the earth's surface is neglected. To include this effect, see McTigue, 1987). In this model the magma body does not ascend, but its cooling is allowed for and this makes the entire stress field change with time.

Thermal Stress and Overpressure

From equation (3-1.3.4):

$$\sigma_{rr}^{(t)} = -\frac{2\,\alpha_T\,E}{(1-\nu)\,r^3}\int_{R_i}^{r}\Delta T(r,t)\,r^2\,dr - \Delta p_i\frac{R_i^3}{r^3} \qquad (4\text{-}1.1.1a)$$

$$\sigma_{\theta\theta}^{(t)} = \frac{\alpha_T\,E}{(1-\nu)\,r^3}\int_{R_i}^{r}\Delta T(r,t)\,r^2\,dr + \frac{1}{2}\Delta p_i\frac{R_i^3}{r^3} - \frac{\alpha_T\,E\,\Delta T(r,t)}{1-\nu} \qquad (4\text{-}1.1.1b)$$

where α_T is the linear thermal expansivity, E is the Young's modulus, ν is the Poisson's ratio, $\Delta T(r,t)$ is the time and position dependant temperature field (eqn. 2-2.4.1) minus the temperature of the host rock far away from the magma, r is the distance from the center of the chamber into the country rock, and R_i is the radius

of the magma body. Δp_i, the current pressure within the magma chamber (eqn. 3-1.4.3) minus lithostatic pressure, has a positive sign and is kept constant.

Buoyancy Component

From equation (3-2.1.13):

$$\sigma_{rr}^{(b)} = \Delta\rho\, g \frac{R_i^3}{r^2} \cos\theta \qquad (4.1.1.2)$$

in which $\Delta\rho$, the density difference of magma and country rock, has a negative sign, and g is the acceleration due to gravity. The angle θ is measured clockwise from a vertical line passing through the center of the magma reservoir.

Lithostatic and Fluid Pressure

The fluid pressure can be expressed as a fraction of the lithostatic pressure. If this fraction, Φ_f, is constant, the difference of lithostatic pressure and fluid pressure is given by

$$\sigma_{rr}^{(l)} = \sigma_{\theta\theta}^{(l)} = -\rho_h g\, (1 - \Phi_f)\, (R_o - r\cos\theta) \qquad (4\text{-}1.1.3)$$

where ρ_h is the density of the host rock and R_o is the vertical distance from magma chamber's center to the earth's surface.

The overall stress field up a vertical line for a temperature profile after 1000 years is shown in Fig. 4-1.1. The depth of the magma chamber's crest is taken as 4 km (R_o = 9 km). The other variables are: $\alpha_T = 5\text{x}10^{-5}$ K^{-1}, $E = 5\text{x}10^{10}$ Pa, ν = 0.25, T_m = 1073 K, T_h = 383 K, Δp_i = 5 MPa, R_i = 5 km, g = 10 m s^{-2}, Φ_f = 0.7. The temperature distribution is shown in Fig. 4-1.2.

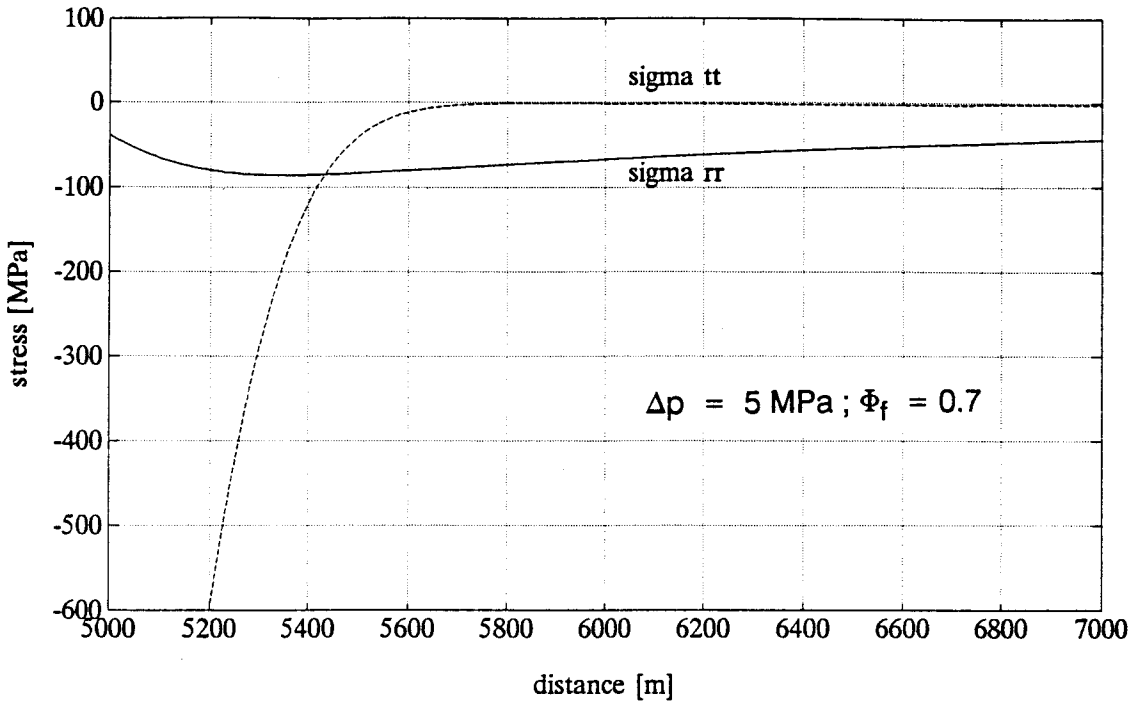

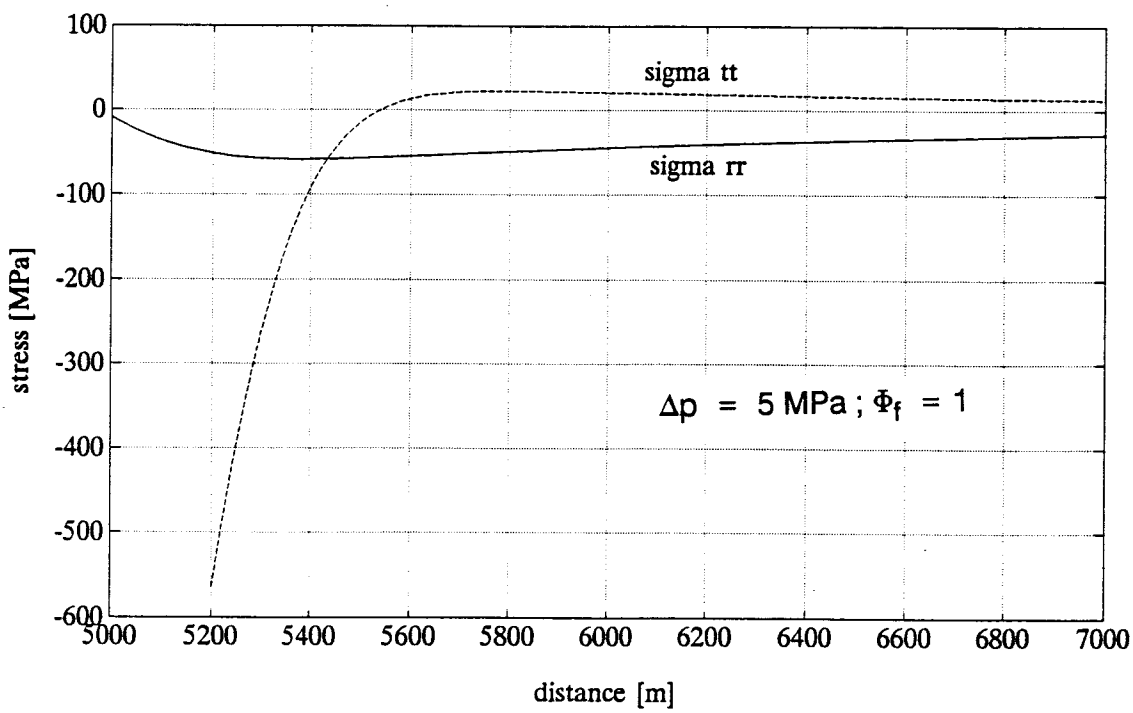

Fig. 4-1.1: Overall stress field in a thermal-elastic country rock after 1000 years after emplacement of a hot magma chamber. The upper plot is calculated with Δp = 5 MPa and Φ_f = 0.7; the lower diagram is calculated for Δp = 5 MPa and Φ_f = 1 (sigma t = $\sigma_{\theta\theta}$, sigma r = σ_{rr}, $\theta = 0^o$, R_o = 9 km, 5000 m distance indicates the interface of magma and host rock, other variables are explained in text).

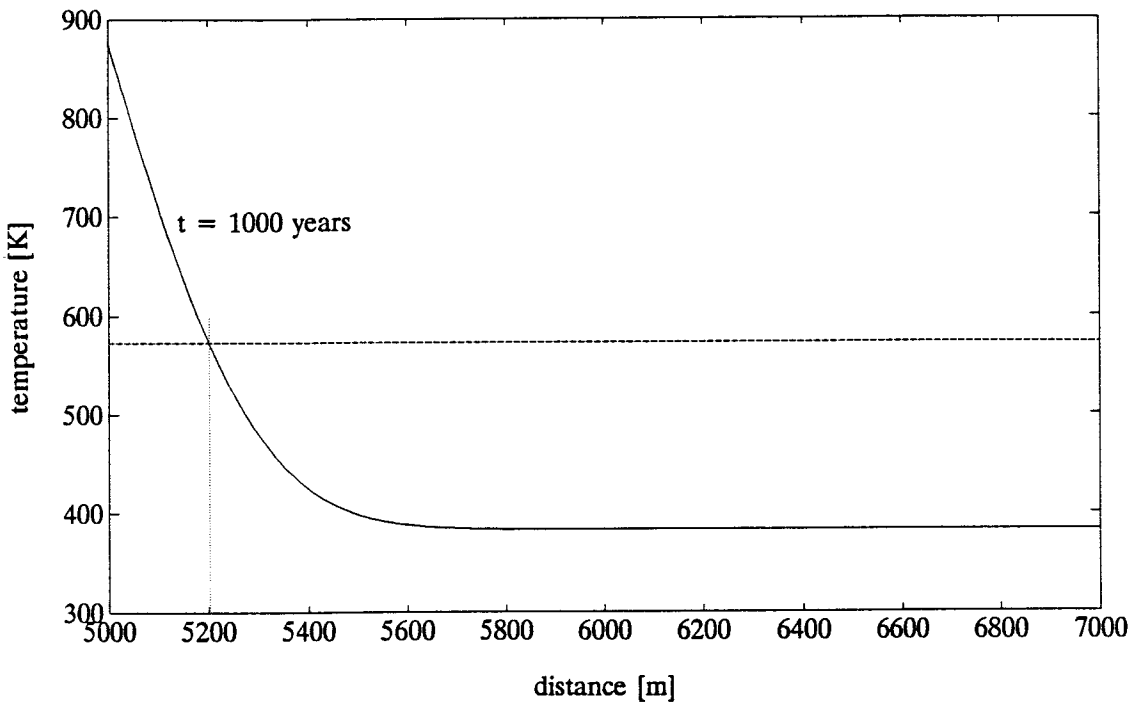

Fig. 4-1.2: Temperature field within the host rock for t = 1000 years used to calculate the total stress field. The horizontal and vertical lines are discussed in section 4.2 as follows.

4.2 Strength of Country Rock

The stress field described above is only correct if the host rock responds in a thermal-elastic manner. But, usually, this material will deform permanently or will fracture when a certain minimum stress or the strength of the rock is overcome. In which manner the host rock will deform or fracture depends on the material itself, temperature, strain rate, and water content. Granite, for example, begins to flow at confining pressures of ~700 - 1500 MPa and temperatures of 573 K (Tullis and Yund, 1977, Tullis, 1990, see horizontal line in Fig. 4-1.2). At lower temperatures it behaves in a brittle manner and fractures. The brittle-ductile transition of 'wet' granite takes place at lower stress magnitudes than that of 'dry' granite (Tullis and Yund, 1980). Paterson, 1978, reported the brittle-ductile transition of a rock decreases with increasing temperature but when the rock failures in a brittle manner, the behavior is affected very little by temperature.

Fig. 4-2.1 shows a sketch of representative stress-strain curves of rocks. The stress quantity in these diagrams is the stress difference of maximum and minimum principal stresses (σ_1 - σ_3). The left-hand figure represents brittle fracture. After a small reversible deformation ($\leq$5%) the rock fractures and the stress drops. The right-hand figure shows the other extreme, perfectly ductile behavior. When a certain yield stress is reached, the material deforms permanently and may accumulate large amounts of strain before it fractures. If the stress difference is constant during flow (horizontal curve) the behavior is called steady state flow. Strain hardening or softening gives a slope in this diagram. A positive slope represents strain hardening. The middle figure shows the transitional case. The same rock may be brittle under low confining pressure and temperatures, but ductile under high pressure and temperature.

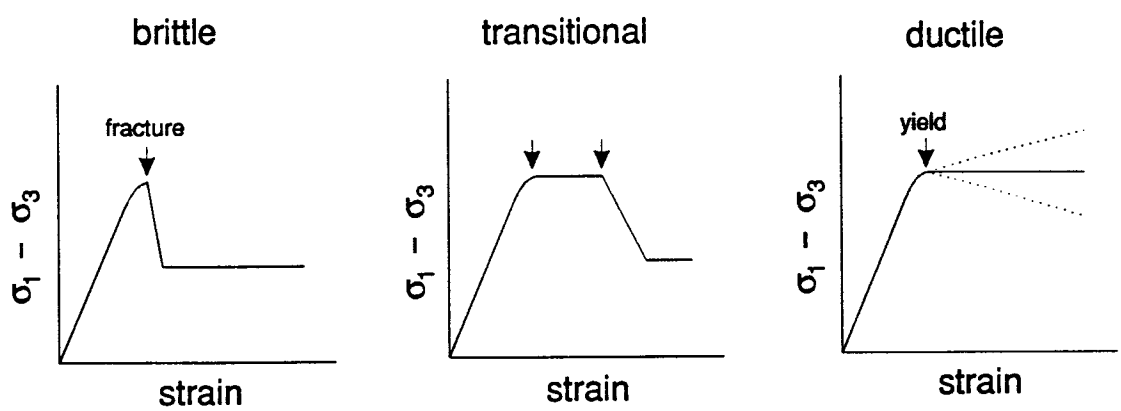

Fig. 4-2.1: Representative stress-strain curves for rocks.

4.2.1 Failure Criteria

The behavior of a rock is difficult to describe in mathematical equations. Therefore, I begin by discussing two extreme cases, brittle fracture and ideal plastic yielding. In the first, a rock fractures after a certain amount of thermal-elastic deformation depending on the stress magnitudes. In this case the temperature effect on the fracture strength is neglected. In a compression regime the Navier-Coulomb criterion is used, in a tensile regime a parabolic fracture envelope of Griffith type is used. In the second case, ideal plastic yielding, a rock deforms permanently if a certain critical shear stress is applied. If this kind of ductile failure occurs the Tresca criterion can be used. Equations for the three criteria follow.

Griffith Criterion

Rock fails if

$$\left[\frac{\sigma_1 - \sigma_3}{2}\right]^2 + 4T_o\frac{\sigma_1 + \sigma_3}{2} - 4T_o^2 > 0 \qquad (4\text{-}2.1.3)$$

where T_o is the tensile strength of a rock.

Navier-Coulomb Criterion

Rock fails if

$$\sigma_1 > C_o + \beta\,\sigma_3 \qquad (4\text{-}2.1.1)$$

with

$$\beta = \frac{1 + \sin\phi}{1 - \sin\phi} \qquad (4\text{-}2.1.2)$$

Here, σ_1 and σ_3 are the maximum and minimum principal stresses, respectively, C_o is the uniaxial compressive strength when unconfined, and ϕ is the angle of internal friction.

Tresca Criterion

$$\frac{\sigma_1 - \sigma_3}{2} = Y(T) \qquad (4\text{-}2.1.4)$$

where Y(T) is some constant dependent on temperature,T.

Fig. 4-2.2 shows schematically the different failure criteria used in this study in a Mohr diagram with normal stress along the horizontal and shear stress along the vertical axis. In this one diagram, a positive normal stress represents compression. Note that the failure criteria are simplifications. Real rocks follow a more curved envelope. The solid line represents the fracture strength of an intact rock, subdivided into Griffith (tension), Navier-Coulomb (compression), and Tresca type (ductile behavior). ϕ_i is the angle of internal friction of an intact rock, and S_o is its shear strength which can be related to the compressive strength, C_o:

$$S_o = \frac{C_o (1 - \sin \phi_i)}{2 \cos \phi_i} \qquad (4\text{-}2.1.5)$$

Failure occurs when the Mohr circle touches the envelope.

If the rock is already fractured sliding along preexisting fracture planes occurs when the rock's frictional strength is reached dashed line. Frictional sliding can be expressed by a criterion similar to the Navier-Coulomb criterion, but C_o is much lower and the angle of friction, ϕ, along preexisting faults is usually higher. At the point where the dashed line intersects the solid line, the rock begins to flow in form of a cataclastic flow. Within this brittle-ductile transition, a

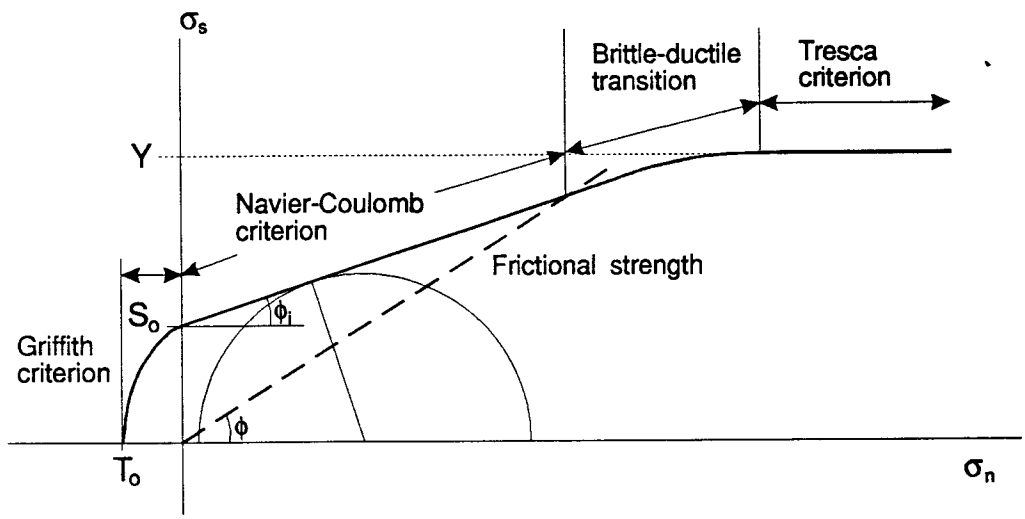

Fig. 4-2.2: Schematic failure envelope and frictional strength of rocks in Mohr diagram. T_O = tensile strength, S_O = shear strength, Y = yield stress, ϕ_i = angle of internal friction of intact rock, ϕ = angle of friction of cracked material.

rock will produce new fractures rather than moving along preexisting faults. When the yield strength, Y, is exceeded, the rock behaves in a ductile manner.

Fig. 4.2.3 shows a plot of mean stress versus maximum shear stress for the radial and tangential stress components in a thermal-elastic rock which is stressed due to an intruding magma chamber (see paragraph 4.1). The time after emplacement is 1000 years and $\theta = 0^o$ (solid lines). Numbers in meters labelling curves are distances away from the magma-host rock interface. In the two-dimensional case, the mean stress is defined as

$$\sigma_{mean} = \frac{\sigma_1 + \sigma_3}{2} \qquad (4\text{-}2.1.6)$$

and the maximum shear stress can be calculated according to

$$\sigma_s(max) = \frac{\sigma_1 - \sigma_3}{2} \qquad (4\text{-}2.1.7)$$

In this example where θ is equals to zero σ_{rr} and $\sigma_{\theta\theta}$ are the principal stresses, and the maximum shear stress is positive when $\sigma_{rr} > \sigma_{\theta\theta}$ and is negative when $\sigma_{\theta\theta} > \sigma_{rr}$. The dashed and dotted lines represent representative fracture and frictional strengths of a particular rock, respectively with the variables: C_o = 10 MPa for intact rock and C_o = 0 for frictional strength, $\phi_i = 27^o$, $\phi = 30^o$ This kind of diagram is similar to the Mohr diagram with the difference that failure does not occur when the Mohr circle touches the envelope, but takes place when its crest or the maximum shear stress is on the so called failure line (Bayly, 1992). Note, that the failure line is slightly displaced from the envelope. The diagrams clearly show intersections of the stress curves (solid lines) with the failure line and friction line. Rock would fracture; and because of the presence of fractures the stress

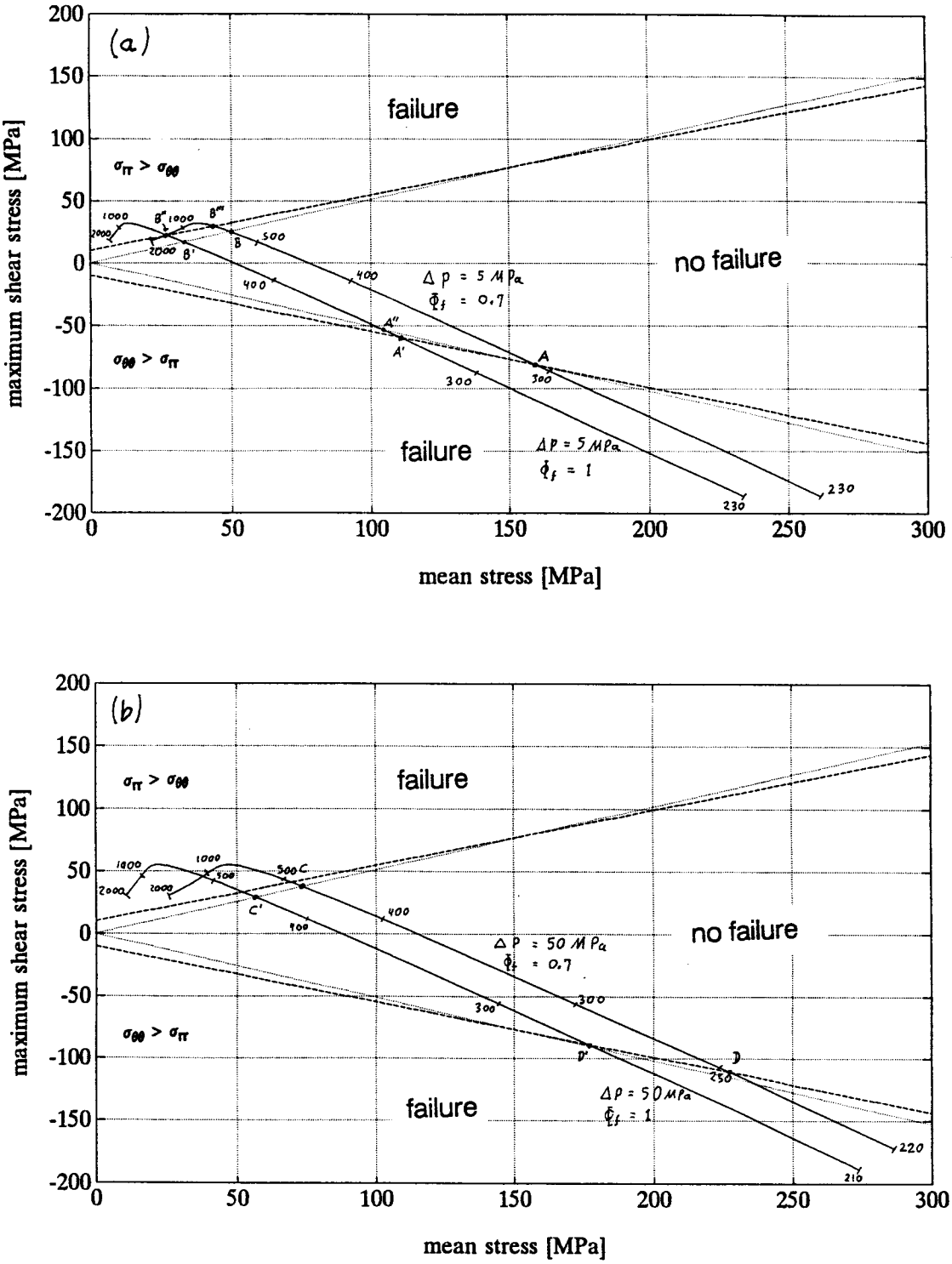

Fig. 4-2.3: Stress distribution within the thermal-elastic host rock represented as maximum shear stress versus mean stress after 1000 years after magma body emplacement. Dashed and dotted lines describe the failure- and friction line for a particular rock, respectively. Numbers labeling curves indicate the distance in meters from the magma - host rock interface into the host rock.

distribution within the host rock is different as described in chapters 3 and 4.1. An approximation of a more realistic model is explained below.

4.2.2 Country Rock as an Elasto-Plastic Medium

Consider a brittle thermal-elastic rock surrounding a hot magma reservoir. This problem is similar to that described in chapter 3.1.3 and 4.1. The difference now is that the material will fracture when a certain minimum stress is reached according to a Navier-Coulomb criterion. In this study two possible failure modes are described. First, the tangential stress, $\sigma_{\theta\theta}$, is bigger than the radial stress, σ_{rr}, that corresponds to the region adjacent to the magma body (region I). Within the failure-region further away $\sigma_{rr} > \sigma_{\theta\theta}$ (region III). Between these there is a region where failure is not expected, region II.

Region I (closer to magma chamber): failure with $\sigma_{\theta\theta} > \sigma_{rr}$

It is assumed that in the thermal-elastic region failure will occur when

$$\sigma_{\theta\theta}' = C_o + \beta\, \sigma_{rr}'$$

and that in the fractured region

$$\sigma_{\theta\theta}'' = C_o + \beta\, \sigma_{rr}'' \qquad (4\text{-}2.2.1)$$

where the superscripts ' and " indicate thermal-elastic region and fractured region respectively. If we look just at stresses superimposed on the lithostatic field the stresses are symmetric with respect to the spherical coordinates θ and ϕ, the equilibrium conditions for the fractured region reduce to

$$\frac{\partial \sigma_r''}{\partial r} = \frac{2}{r}(\sigma_\theta'' - \sigma_r'') + \rho_h\, g\, (1 - \Phi_f) \qquad (4\text{-}2.2.2)$$

As an approximation the stress field in the thermal-elastic region is taken from that described in chapter 4.1. In addition to the above equations, the following boundary conditions must be satisfied:

$$\begin{aligned}
\sigma_r'' &= \Delta\rho\, g\, R_i \cos\theta - \Delta p_i - \rho_h\, g\, (R_o - R_i)\,(1 - \Phi_f) && \text{at } r = R_i \\
\sigma_r'' &= \sigma_r' && \text{at } r = R_c \\
\sigma_\theta'' &= \sigma_\theta' && \text{at } r = R_c \\
\sigma_\theta' &= \sigma_r = 0 && \text{at } r = \infty
\end{aligned} \qquad (4\text{-}2.2.3)$$

where R_c is the radius of the boundary between the fractured and unfractured zones. Solving the above three sets of equations, the stress field within the fractured zone becomes:

$$\sigma_{rr}'' = \mathcal{A} \left[\frac{r}{R_i}\right]^{2(\beta - 1)} - \frac{\rho_h\, g\, r\,(1 - \Phi_f)}{(2\beta - 3)} - \frac{C_o}{\beta - 1} \qquad (4\text{-}2.2.4a)$$

$$\sigma_{\theta\theta}'' = \beta\, \mathcal{A} \left[\frac{r}{R_i}\right]^{2(\beta - 1)} - \frac{\beta\, \rho_h\, g\, r\,(1 - \Phi_f)}{(2\beta - 3)} - \frac{C_o}{\beta - 1} \qquad (4\text{-}2.2.4b)$$

with

$$\mathcal{A} = \Delta\rho\, g\, R_i \cos\theta - \Delta p_i + \frac{C_o}{\beta - 1} - \rho_h\, g\,(1 - \Phi_f) \left[R_o - R_i - \frac{Ri}{2\beta - 3}\right]$$

At the transition point between thermal-elastic and fractured zones, the equations for σ_{rr} and $\sigma_{\theta\theta}$ for both fractured and elastic equilibrium should be valid.

Region III (further out): failure with $\sigma_{rr} > \sigma_{\theta\theta}$

As in region I, within the fractured region, the equations to be satisfied are the equilibrium conditions and the Navier-Coulomb failure criterion or

$$\frac{\partial \sigma_r''}{\partial r} = \frac{2}{r}(\sigma_\theta'' - \sigma_r'') + \rho_h g (1 - \Phi_f) \qquad (4\text{-}2.2.5)$$

$$\sigma_{rr}'' = C_o + \beta \sigma_{\theta\theta}'' \qquad (4\text{-}2.2.6)$$

Using the same boundary condition as above the stress field within the fractured zone is given by

$$\sigma_{rr}'' = \not{A} \left[\frac{r}{R_i}\right]^{2(\beta - 1)/\beta} - \frac{\rho_h g r (1 - \Phi_f)}{(2/\beta - 3)} - \frac{C_o}{\beta - 1} \qquad (4\text{-}2.2.7a)$$

$$\sigma_{\theta\theta}'' = \frac{1}{f} \not{A} \left[\frac{r}{R_i}\right]^{2(\beta - 1)/\beta} - \frac{\rho_h g r (1 - \Phi_f)}{\beta (2/\beta - 3)} - \frac{C_o}{\beta (\beta + 1)} \qquad (4\text{-}2.2.7b)$$

with

$$\not{A} = \Delta\rho g R_i \cos\theta - \Delta p_i - \frac{C_o}{\beta + 1} - \rho_h g (1 - \Phi_f) \left[R_o - R_i - \frac{R_i}{2/\beta - 3}\right]$$

A stress-distance plot for both cases is shown in Fig. 4-2.4 with $\phi = 30^o$ and $C_o = 0$ MPa. The other variables are taken from the thermal-elastic example described above. This example supposes an already fractured rock ($C_o = 0$ MPa). This assumption can be made because of two reasons. First, there is a steady heat conduction from the magma into the host rock. As soon as the adjacent rock becomes heated, consequent thermal stresses are sufficient to fracture this material immediately or after a negligible period of time. Second, diapirs usually are in continuous ascending motion. A halo of fractured material would automatically migrate together with the magma chamber.

To come closer to the real stress distribution around a magma chamber, both fractured and thermal-elastic zones need to be combined. As shown in the

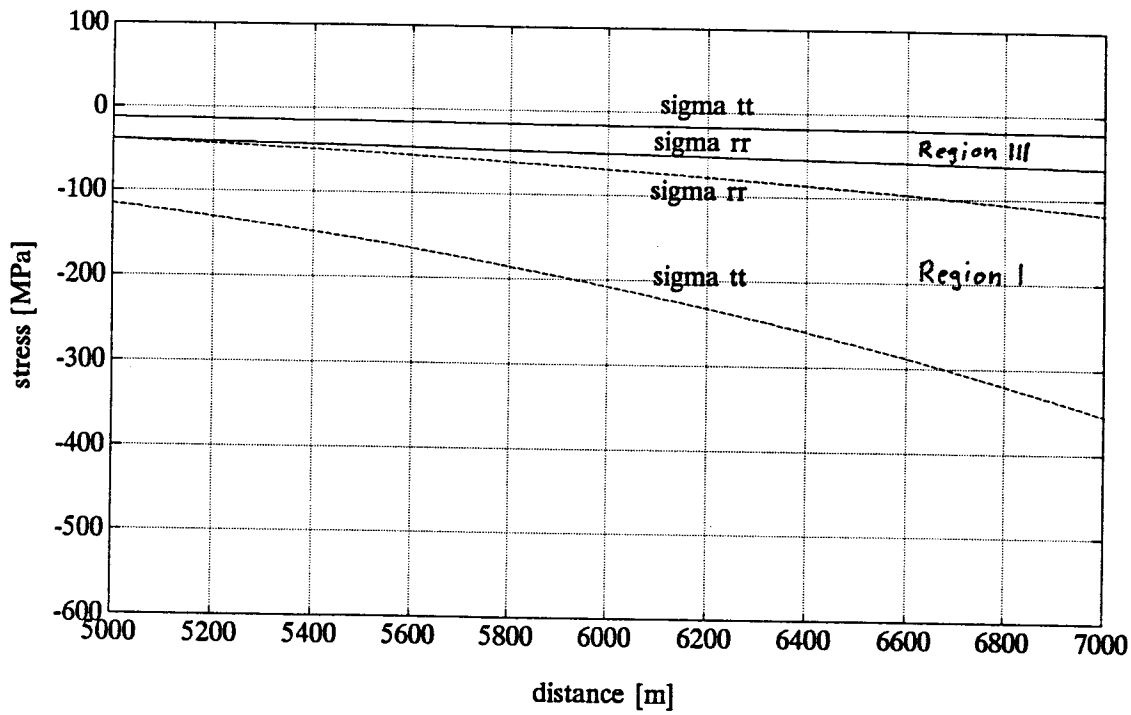

Fig. 4-2.4: Stress field in a fractured country rock. Solid lines: $\sigma_{rr} > \sigma_{\theta\theta}$, dashed lines: $\sigma_{\theta\theta} > \sigma_{rr}$. C_o = 0 MPa, ϕ = 30^o, Δp = 5 MPa, and Φ_f = 0.7. For other variable see text.

thermal-elastic stress-distance diagram (Fig. 4-1.1) there is a region around 5400 m distance at t = 1000 years in which the stresses would not be high enough to fracture the surroundings. Fig. 4.2.3 also confirms this statement. Consequently, the dashed lines in Fig. 4-2.4 should merge with an elastic stress field.

Fig. 4-2.5 shows the stress distribution in the host rock with distance by considering the above thoughts. Four regions can be distinguished which we call I, II, III and IV. A fractured region I is adjacent to the magma - host rock interface with $\sigma_{\theta\theta} > \sigma_{rr}$, further away an unfractured thermal-elastic zone II. Zone III shows fractures again but now $\sigma_{rr} > \sigma_{\theta\theta}$, the outer region IV behaves in an elastic manner (beyond the limit of Fig. 4-2.5). The stresses near the interface are considerably smaller for the fractured material than they are for a perfectly thermal-elastic material. The tangential stress outside the fractured regions should be larger than the tangential stress at the same distance for a perfectly elastic material (Coates, 1981). In other words the intersection of the tangential stress in Fig. 4-2.4 with the tangential stress in Fig. 4-1.1 is not the transition point of plastic and elastic region. This is because of the fact that the relaxed fractured zone remains intact and builds up sufficient back pressure.

When the temperature migrates outward with time, the stress profile should also move outward. If the rock was fractured before 1000 years, the elastic zones remain still elastic, but only their elastic properties should change (e.g. the Young's modulus becomes smaller). In region I the tangential stress, $\sigma_{\theta\theta}$ is always bigger than the radial stress. Two important effects can be found. First, when this region fractures, shear fractures are produced oriented with a low angle to the interface between magma and host rock. Second, a loose piece of rock should pop into the magma. In the elastic region II there is a particular location

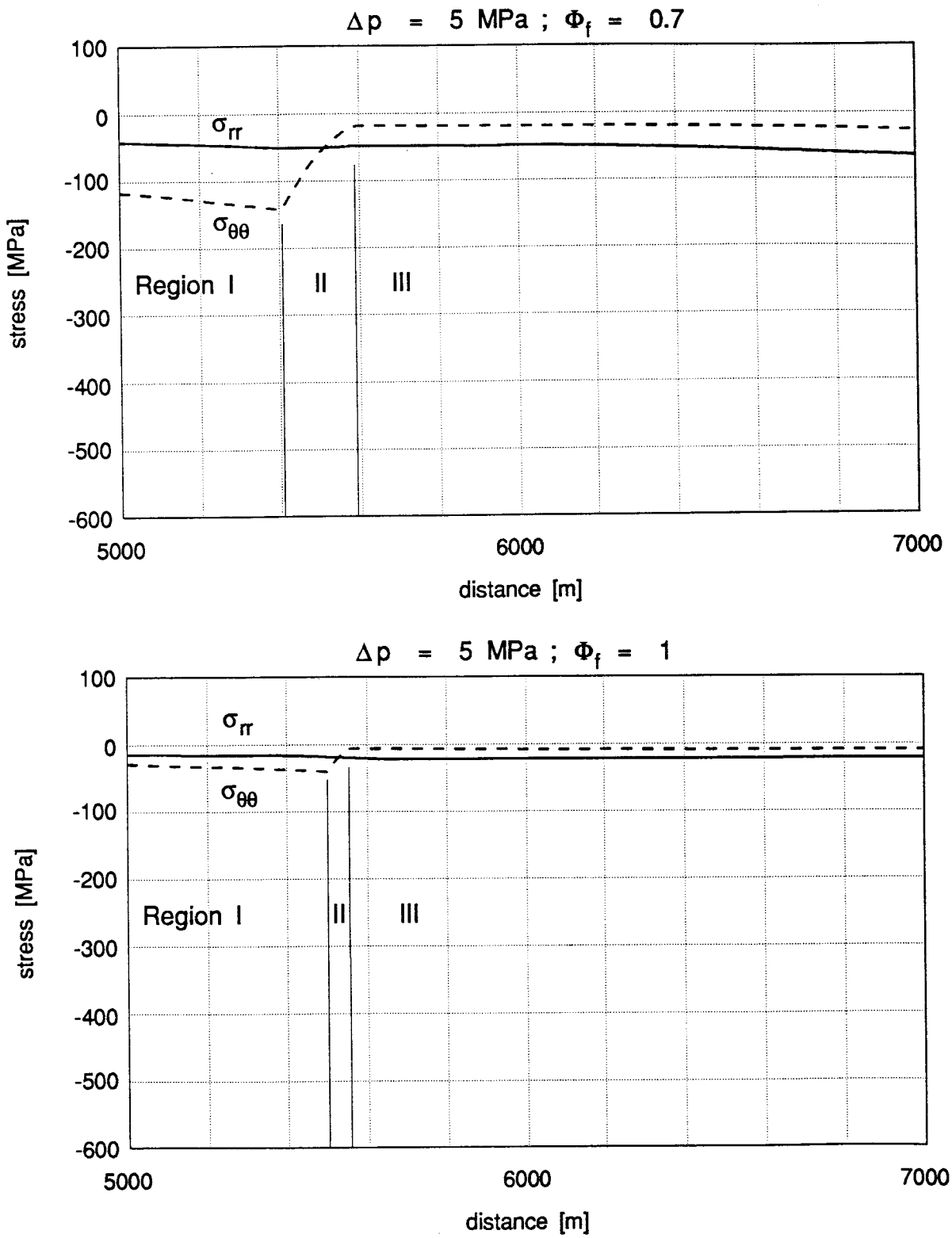

Fig. 4-2.5: Semi-quantitative stress distributions around magma body in elasto-plastic rock at 1000 years after magma intrusion. 5000 m distance indicates the country rock - magma interface.

(e.g. ≈5500 m distance in the upper Fig. 4-2.5) in which the stress field is hydrostatic ($\sigma_{rr} = \sigma_{\theta\theta}$), we call this the neutral zone of the stress field. The fractured region III develops fractures oriented with a high angle to the interface and material is elongated parallel to the chamber's wall. This is so because $\sigma_{rr} > \sigma_{\theta\theta}$. When the magma body ascends all four regions move together with the diapir. Initially unfractured, elastic regions II and IV soon turn into elastic zones showing preexisting cracks.

4.2.3 The Effect of Water within the Host Rock

The water content within the country rock effects a change of the stress pattern along the vertical axis in Fig. 4-2.4 and along the horizontal axis in Fig. 4-2.3. Consider Fig. 4-2.3.a in which the overpressure of the magma, Δp, is kept constant at 5 MPa. The solid lines represent the state of stress above the top of the magma chamber for $\Phi_f = 0.7$ (upper curve) and $\Phi_f = 1$ (lower curve). The upper curve with the lower fluid pressure intersects more or less with both the friction and failure line at ≈300 m distance away from the interface. According to Fig. 4-2.2, these fractures are close to the brittle-ductile transition. Host rock within this region I should flow in form of a cataclastic flow in which the material fractures and heals again. Within region I, the material just at the interface may deform in a ductile manner because of its high temperature, then turns into a more cataclastic behavior further away.

The upper stress curve in Fig. 4-2.3 intersects a second time with the failure or friction line at point B or B‴, respectively, depending on an intact or already fractured rock. The stress difference is high enough to overcome the strength of the rock again. The host rock fails and produces shear fractures now

oriented with a high angle to the border of the magma chamber (region III). At point B" the stress curve turns into the elastic field again (region IV). Note, that the distances (labelling numbers in Fig. 4-2.3) should be higher because of the back pressure.

An increase of the fluid pressure from 0.7 times lithostatic pressure to equal lithostatic pressure shifts the upper solid line to the left. Intersection points A and B move to A' or A" and B' or B"'. Region I extends when the fluid pressure rises and the elastic region II moves further out. Further increase of the fluid pressure may produces tensile fractures oriented perpendicular to the chamber's walls. An increase in fluid pressure works against the confining pressure. Therefore, the curves in Fig. 4-2.3 move to the left and the stress curves in Fig. 4-2.5 move up by an increase of the fluid pressure. A drier rock with less fluid pressure prevents the fracturing process of region III and reduces the extent of region I. After rock is fractured it is in a more relaxed state of stress (Fig. 4-2.5).

4.2.4 The Effect of Δp

The overpressure of the magma has two effects (compare Fig. 4-2.3a with 4-2.3b). First, Δp works against the fracture process adjacent to the wall rock (region I). The magma under pressure works in the same manner as a drilling fluid in a drill hole; it prevents fractured material from popping into the hole. The upper curve in Fig. 4-2.3a with Δp = 5 MPa moves to the right, point A moves to point D (Δp = 50 MPa, Fig. 4-2.3b), and region I becomes smaller. Second, Δp supports the fracturing process in region III. For example the upper curve in Fig. 4-2.3a fractures in region III at $\approx$680 m whereas when Δp is bigger (Fig. 4-2.3.b) the stress curve shows an intersection with the failure line at $\approx$500 m (point C).

Both effects are linked to the same fact that the overpressure of the magma tends to expand the chamber and stretches material parallel to the chamber's wall. It works against the stress due to heating of the wall which has the opposite effect. The overpressure reduces the probability that wall rock fractures in region I but increases the probability to fracture material in region III.

4.2.5 Ascent Mechanism

We consider a magma chamber fixed at a particular location within the earth's crust, say 4 km (chamber's top). As heat is transferred from the magma into the host rock, wall rock fractures mainly due to thermal stress. The cracking front (interface of region I and II) moves outward together with the isotherms. Most parts of region I are cataclastic in which material flows due to fracturing and healing. Here, internal cracking and re-arrangement takes place with an increase in volume, because rock becomes less well packed (e.g. Paterson, 1978). The Poisson's ratio may increase above 0.5. Mobile material flows from the surroundings and heals the open space. Water is highly mobile and flows rapidly from the surroundings into open space. Furthermore, it reinforces two important mechanisms: (i) it supports the crack propagation and (ii) it decreases the friction between slip planes. With an increasing number of cracks the elastic property, E, or the viscosity of the fractured rock should decrease because material is easier to deform. When a large number of cracks form, the result is probably reversed: rock would become highly porous, so that water escapes. This would strengthen the rock again.

The above assumes a fixed magma chamber that does not ascend. As soon as the fractured region I is created, loose material drops or stopes into the

magma. This gives room for the magma to stream in. The magma body ascends in a way in which denser host rock blocks sink into the less dense magma. The process is known as stoping (Daly, 1903, Marsh, 1982). On the way down, parts of the host rock material will be melted and will contaminate the magma (Furlong and Myers, 1985). Magma ascends because of material exchange, wall rock is replaced by magma and vice versa. There is a dynamic process zone in which wall rock fragments slowly descend, and just created open space is filled with magma. Suppose a loose rock fragment has disengaged from the wall and sinks downward. The temperature contrast of the just created magma - wall rock interface is high for a moment. Only after a certain time will enough heat be delivered into the host rock at this location to warm the rock up. This results in the thermal stress at this particular location being low. The strength of the wall rock can only be overcome when the pressure of the magma is high enough. If this occurs, a new crack is formed and propagates further outward as a dike. The dike will come into the neutral region of the stress field where $\sigma_{rr} \approx \sigma_{\theta\theta}$. Water rich magmas near the dike tip can accelerate the crack propagation and may induce tensile fractures. Two possible explanations for this phenomena exist. First, water, being a highly mobile phase, can escape into the host rock. This would increase the fluid pressure within the wall rock, while reducing the confining pressure. Secondly, water can be exsolved from the magma and would tend to increase the pressure within the magma (see section 3.1.4). If the magma does not solidify on its way up, the dike will reach the earth's surface.

4.3 Summary

This chapter has described the overall stress field in a thermal-elastic country rock when a magma chamber approaches. The main stress component

clearly is the thermal stress due to heating of the wall rock. The strength of the country rock is soon overcome. This results in fractures since the wall rock is brittle. Two fractured regions around the magma chamber can be distinguished. One zone is just at the interface between magma and host rock in which fault planes are oriented having a low angle to the border of the chamber ($\sigma_{\theta\theta} > \sigma_{rr}$). A second zone further out shows fault planes with high angles to the interface ($\sigma_{rr} > \sigma_{\theta\theta}$). The stress field in the fractured regions is much more relaxed. The fluid pressure within the country rock reinforces the fracturing process near the interface whereas the overpressure within the magma body works against it. One possible ascent mechanism is stoping in which fractured and disengaged wall rock fragments sink into the magma. Another transport of magma can occur within dikes. The latter mechanism can happen when magma is locally in contact with colder wall rock. The local stress field around a dike tip may becomes tensile due to a water rich magma.

Chapter V: Conclusions

This chapter summarizes the observations made in this study in form of a history of events at point X as a magma chamber approaches and leads to suggestions and proposals to be answered in further research.

To review and consolidate these ideas, let us consider a cubic meter of rock at a point X, say, 4 km beneath the earth's surface and a magma body ascending toward it. But while the magma body is still at depth, say, 10 km it has not yet had any effect on point X; conditions could be "normal crustal conditions" for such a depth, for example

temperature:	380 - 400 K
lithostatic pressure	100 - 120 MPa ($\sigma_{rr} \cong \sigma_{\theta\theta}$)
fluid pressure	60 - 90 MPa
effective stress:	30 - 40 MPa (σ_{rr} or $\sigma_{\theta\theta}$ minus fluid pressure)

As the magma body approaches, the first effect at point X is that the cubic meter of rock deforms elastically because $\sigma_{rr} > \sigma_{\theta\theta}$. It becomes elongated parallel to the border of the magma chamber and shortened perpendicular to it. The stress difference increases as the magma comes closer to point X. When the strength of the rock is overcome (depth of magma $\approx$ 6.5 km) shear fractures are produced with a low angle to a line from the chamber's center to this rock (radial line). The stress drops and rock X deforms by slipping along this fracture planes. The conditions are for example:

temperature:	400 K
fluid pressure	60 - 90 MPa
effective σ_{rr}:	55 - 65 MPa
effective $\sigma_{\theta\theta}$:	5 - 25 MPa

At a distance of about 600 m between magma and country rock the cubic meter of rock becomes heated. This results in a decrease of the tangential stress component and the rock turns into elastic behavior again. At about 500 m distance to the magma both stress components have equal magnitudes again. The temperature of the rock is approximately 500 K. When the piece of rock has a temperature of 580 K ($\approx$400 m distance to magma) the $\sigma_{\theta\theta}$ is high enough to overcome the friction between preexisting faults and the fracture strength of the rock. The material comes into the semi-brittle field and deforms permanently. The radial stress component is about 55 MPa and the tangential stress component is around 145 MPa. The rock fractures, re-arranges, and mobile material heals the open space at the same time. The material has a chaotic texture and flows in a cataclastic manner. Main fractures or a main foliation should have low angles to the border of the magma chamber. The volume of the rock increases because material is less well packed. This dilation may absorb water from the surroundings. The conditions of the rock X at 200 m away from the magma are for example:

temperature:	700 K
fluid pressure	90 - 100 MPa
effective σ_{rr}:	45 - 55 MPa
effective $\sigma_{\theta\theta}$:	130 - 150 MPa

The rock X at the contact to the magma has a temperature of about 880 K and may contains fissures filled with magma. Eventually, this rock becomes disengaged from its surroundings and sinks by its gravity into the magma.

The models derived in this study are based on many simplified assumptions. The principal assumption is that the host rock is modeled as an

isotropic, homogeneous material that responds in a thermal-elastic, viscous, or elasto-plastic manner. In reality, crustal material is stratified and much more complicated. Many rocks are anisotropic and change their behavior with changing temperature, pressure, water content, and strain rate. Experimental work and field work need to be done to gain a closer description of the real process at a particular location in the earth's crust when a magma body approaches.

Another important assumption used in this work is the temperature description within the country rock. The temperature field is important for evaluating the resulting thermal stresses. The thermal stress yields the highest magnitudes and has the strongest influence on the behavior of the material. In this study heat conduction is the only heat transfer mechanism used for the quantitative description of the temperature field. Other mechanisms, such as convection and stoping are important. They accelerate the heating process of the country rock, but they also effect a more rapid cooling and crystallization of the magma. Therefore, the thermal stresses calculated in this study are minimum estimates.

Finally, the overall stress field is calculated by adding up the different kinds of stresses. To evaluate a more exact stress field a set of complicated differential equations with variable material properties has to be solved simultaneously. This would require sophisticated computer modeling. This work dealt with best numerical estimates to come to a realistic preliminary picture of what could happen to a piece of rock as a magma body ascends toward it.

References

Anderson A.T., Newman S., Williams S.N.W., Druitt T.H., Skirius C. & Stolper E., 1989: H_2O, CO_2, Cl, and gas in plinian and ash-flow Bishop rhyolite.- Geology 17, 221 - 225.

Baker B.H. & McBirney A.R., 1985: Liquid fractionation. Part III: Geochemistry of zoned magmas and the compositional effects of liquid fractionation.- J. Volcanol. Geotherm. Res. 24, 55 - 81.

Bayly M.B., 1992: Mechanics in structural geology.- 253 p., Springer, New York.

Blake S., 1984: Volatile oversaturation during evolution of silicic magma chambers as an eruption trigger.- J. Geophys. Res. 89, 8237 - 8244.

Bottinga Y. & Weill D.F., 1972: The viscosity of magmatic silicate liquids: A model for calculation.- Am. J. Sci. 272, 438 - 475.

Brandeis G. & Jaupart C., 1986: On the interaction between convection and crystallization in cooling magma chambers.- Earth Planet. Sci. Lett. 77, 345 - 361.

Brandeis G., Jaupart C. & Allègre C.J., 1984: Nucleation, crystal growth and the thermal regime of cooling magmas.- J. Geophys. Res. 89, 10161 - 10177.

Burnham C.W., 1975: Water content and magmas: a mixing model.- Geochim. Cosmochim. Acta 39, 1077 - 1084.

Burnham C.W., 1979: The importance of volatile constituents. In: Yoder H.S.Jr (ed.): The evolution of the igneous rocks: Fiftieth anniversary perspectives.- p. 440 - 482, Princeton University Press.

Candela P.A., 1986: The evolution of aqueous vapor from silicate melts: effect on oxygen fugacity.-Geochim. Cosmochim. Acta, 50, 1205 - 1211.

Candela P.A., 1991: Physics of aqueous phase evolution in plutonic environments.- Am. Mineralogist 76, 1081 - 1091.

Carter N.L. & Tsenn M.C., 1987: Flow properties of continental lithosphere.- Tectonophys. 136, 27 - 63.

Clark S.P. (ed), 1966: Handbook of physical constants.- Geol. Soc. Amer. Mem. 97, 587 p..

Coates D.F., 1981: Rock mechanics principles.- CANMET Energy, Mines and Resources Canada, Monograph 874.

Daly R.A., 1903: The mechanics of igneous intrusion.- Am. J. Sci., 15, 269 - 298.

Dunbar N.W., Kyle P.R., 1992: Volatile contents of obsidian clasts in tephra from Taupo Volcanic Zone, New Zealand: Implications to eruptive processes.- J. Volcanol. Geotherm. Res. 49, 127 - 145.

Eckert E.R.G. & Drake R.M., 1972: Analysis of heat and mass transfer.- 806 p., McGraw-Hill, New York.

Ewy R.T. & Cook N.G.W., 1990: Deformation and fracture around cylindrical openings in Rock-II. Initiation, growth and interaction of fractures.- Int. J. Rock Mech. Min. Sci. & Geomech. Abstr. 27, 409 - 427.

Furlong K.P. & Myers J.D., 1985: Thermal-mechanical modeling of the role of thermal stresses and stoping in magma contamination.- J. Volcanol. Geotherm. Res. 24, 179 - 191.

Halbach H. & Chatterjee N.D., 1982: An empirical Redlich-Kwong-Type equation of state for water to 1,000 ^{o}C and 200 Kbar.- Contrib. Mineral. Petrol. 79, 337 - 345.

Happel J. & Brenner H., 1965: Low Reynolds number hydrodynamics.- 553 p., Perentice Hall, Englewood Cliffs, N.J..

Hamilton D.L., Burnham C.W. & Osborn E.F., 1964: The solubility of water and effects of oxygen fugacity and water content on crystallization in mafic magmas.- J. Petrol. 5, 21 - 39.

Harrison T.M. & McDougall I., 1980: Investigations of an intrusive contact, northwest Nelson, New Zealand - I. Thermal, chronological and isotopic constraints.- Geochim. Cosmochim. Acta 44, 1985 - 2003.

Hervig R.L., Dunbar N., Westrich H.R. & Kyle P., 1989: Pre-eruptive water content of rhyolitic magmas as determined by ion microprobe analysis of melt inclusions in phenocrysts.- J. Volcanol. Geotherm. Res. 36, 293 - 302.

Jaeger J.C., 1968: Cooling and solidification of igneous rocks. In: Hess H.H. (ed.): Basalts: The Poldervaart treatise on rock of basaltic composition.- 503 - 536, Wiley, New York.

Jambon A., 1982: Tracer diffusion in granitic melts: Experimental results for Na, K, Rb, Cs,Ca, Sr, Ba,Ce, Eu, to 1300^{o}C and a model of calculation.- J. Geophys. Res. 87, 10797 - 10810.

Kirby S.H., 1985: Rock mechanics observations pertinent to the rheology of the continental lithosphere and the localization of strain along shear zones.- Tectonophys. 119, 1 - 27.

Kushiro I., 1980: Viscosity, density, and structure of silicate melts at high pressures, and their petrological applications. In: Hargraves R.B. (ed.): Physics of magmatic processes.- 93 - 120, Princeton University Press.

Landau L.D. & Lifshitz E.M., 1959: Fluid mechanics. Course of theoretical physics, Vol. G.- 536 p., Pergamon, London.

Lasaga A.C., 1981: Implications of a concentration dependent growth rate on the boundary layer crystal-melt model.- Earth Planet. Sci. Lett. 56, 429 - 434.

Maaløe S. & Wyllie P.J., 1975: Water content of a granite magma deduced from the sequence of crystallization determined experimentally with water-undersaturated conditions.- Contrib. Mineral. Petrol. 52, 175 - 191.

Mahon K.I., Harrison T.M. & Drew D.A., 1988: Ascent of a granitoid diapir in a temperature varying medium.- J. Geophys. Res. 93, 1174 - 1188.

Marsh B.D., 1982: On the mechanics of igneous diapirism, stoping, and zone melting.- Am. J. Sci. 282, 808 - 855.

Marsh B.D., 1984: On the mechanics of caldera resurgence.- J. Geophys. Res. 89, 8245 - 8251.

McBirney A.R., Baker B.H. & Nilson R.H., 1985: Liquid fractionation. Part 1: Basic principles and experimental simulations.- J. Volcanol. Geotherm. Res.24, 1 - 24.

McBirney A.R. & Murase T., 1984: Rheological properties of magmas.- Ann. Rev. Earth Planet. Sci. 12, 337 - 357.

McMillan P., Peraudeau G., Holloway J. & Coutures J-P., 1986: Water solubility in a calcium aluminosilicate melt.- Contrib. Mineral. Petrol. 94, 178 - 182.

McTigue D.F., 1987: Elastic stress and deformation near a finite spherical magma body: Resolution of the point source paradox.- J. Geophys. Res. 92, 12931 - 12940.

Mogi K., 1971: Fracture and flow of rocks.- Tectonophys. 13, 541 - 568.

Murase T. & McBirney A.R., 1973: Properties of some common igneous rocks and their melts at high temperatures.- Geol. Soc. Am. Bull. 84, 3563 - 3592.

Obert L. & Duvall W.I., 1967: Rock mechanics and the design of structures in rock.- 650 p., Wiley, New York.

Paterson M.S., 1978: Experimental rock deformation - the brittle field.- 254 p., Springer, New York.

Phillips W.J., 1974: The dynamic emplacement of cone sheets.- Tectonophys. 24, 69 - 84.

Rutherford M.J., Sigurdsson H., Carey S. & Davis A., 1985: The May 18, 1980, Eruption of Mount St. Helens: 1. Melt composition and experimental phase equilibria.- J. Geophys. Res. 90, 2929 - 2947.

Saada A.S., 1974: Elasticity: Theory and applications.- 643 p., Pergamon, New York.

Sommer M.A., 1977: Volatiles H_2O, CO_2, and CO in silicate melt inclusions in quartz phenocrysts from the rhyolitic bandelier air-fall and ash-flow tuff, New Mexico.- J. Geol. 85, 423 - 432.

Sparks R.S.R, 1978: The dynamics of bubble formation and growth in magmas: A review and analysis.- J. Volcanol. Geotherm. Res. 3, 1 - 37.

Spera F.J., Yuen D.A. & Kirschvink S.J., 1982: Thermal boundary layer convection in silicic magma chambers: Effects of temperature-dependent rheology and implications for thermogravitational chemical fractionation.- J. Geophys. Res. 87, 8755 - 8767.

Tait S., Jaupart C. & Verniolle S., 1989: Pressure, gas content and eruption periodicity of a shallow, crystalizing magma chamber.- Earth Planet. Sci. Lett. 92, 107 - 123.

Taylor R.P., Strong D.F. & Fryer B.J., 1981: Volatile control of contrasting trace element distributions in peralkine granitic and volcanic rocks.- Contrib. Mineral. Petrol. 77, 267 - 271.

Trial A.F. & Spera F.J., 1990: Mechanisms for the generation of compositional heterogeneities in magma chambers.- Geol. Soc. Am. Bull. 102, 353 - 367.

Tritton D.J., 1989: Physical fluid dynamics.- 519 p., Oxford University Press, New York.

Tullis J.: 1990: Experimental studies of deformation mechanisms and microstructures in quartzo-feldspathic rocks. In: Barber D.J. & Meredith P.G. (eds.): Deformation processes in minerals, ceramics, and rocks.- Unwin Hyman, 190 - 227, London.

Tullis J. & Yund R.A., 1977: Experimental deformation of dry Westerly granite.- J. Geophys. Res. 82, 5705 - 5718.

Tullis J. & Yund R.A., 1980: Hydrolytic weakening of experimentally deformed Westerly granite and Hale albite rock.- J. Struct. Geol. 2, 439 - 451.

Wells P.R.A., 1980: Thermal models for the magmatic accretion and subsequent metamorphism of continental crust.- Earth Planet. Sci. Lett. 46, 253 - 265.

Whitney J.A., 1975: Vapor Generation in a quartz monzonite magma: A synthetic model with application to porphyry copper deposits.- Economic Geology 70, 346 - 358.